Untersuchung struktureller Konnektivität bei Menschen mit limbischer Enzephalitis

Inaugural-Dissertation

zur Erlangung des Doktorgrades

der Hohen Medizinischen Fakultät

der Rheinischen Friedrich-Wilhelms-Universität

Bonn

Tobias Bauer, geb. Stricker

aus Groß-Gerau

2022

Angefertigt mit der Genehmigung

der Medizinischen Fakultät der Universität Bonn

1. Gutachter: Priv.-Doz. Dr. med. Theodor Rüber
2. Gutachter: Prof. Dr. med. Ulrich Herrlinger

Tag der Mündlichen Prüfung: 21.09.2022

Aus der Klinik und Poliklinik für Epileptologie

Direktor: Prof. Dr. med. Rainer Surges, MHBA

Inhaltsverzeichnis

Abkürzungsverzeichnis

AMPAR	alpha-amino-3-hydroxy-5-methyl-4-isoxazolepropionic acid receptor
ANOVA	Analysis of variance, Varianzanalyse
CASPR2	contactin-associated protein-like 2
DTI	Diffusion Tensor Imaging, Diffusionstensorbildgebung
EPI	Echoplanar-Imaging
FC	Fiber cross-section, Faserdurchmesser
FD	Fiber density, Faserdichte
FDC	Fiber density and cross-section, Faserdichte und -durchmesser
FDR	false discovery rate, Falscherkennungsrate
FOD	fiber orientation distribution, Faserverteilungsfunktion
FSL	Functional Magnetic Resonance Imaging of the Brain Software Library
FWER	family-wise error rate
GABAA	gamma-aminobutyric acid A, gamma-Aminobuttersäure A
GABAB	gamma-aminobutyric acid B, gamma-Aminobuttersäure B
GAD65	Glutamic Acid Decarboxylase 65, Glutamat-Decarboxylase 65
HEK293	Human Embryonic Kidney 293
LE	Limbische Enzephalitis
LGI1	Leucine-rich glioma-inactivated 1
MPRAGE	magnetization-prepared rapid acquisition gradient echo
MRT	Magnetresonanztomographie
NMDAR	N-Methyl-D-Aspartat-Rezeptor
TE	echo time
TR	repetition time
VGKC	voltage-gated potassium channel, spannungsanhängiger Kaliumkanal

1. Deutsche Zusammenfassung

1.1 Einleitung

Die limbische Enzephalitis (LE) ist eine Autoimmunerkrankung des zentralen Nervensystems, die klinisch durch ein subakut auftretendes limbisches Syndrom bestehend aus der Trias Störung des Episodischen Gedächtnisses, epileptische Anfälle temporaler Semiologie sowie Affektstörungen charakterisiert ist (Bien und Elger, 2007; Dalmau und Graus, 2018; Dubey et al., 2018; Graus et al., 2016, 2010). Zwar tritt die LE gelegentlich im paraneoplastischen Kontext unter Nachweis intrazellulärer, onkoneuraler Antikörper auf (Dalmau und Rosenfeld, 2008; Graus et al., 2001; Gultekin et al., 2000; Hoffmann et al., 2008; Pittock et al., 2005), im Zentrum dieser Arbeit steht jedoch die nicht-paraneoplastische LE. Zu den am häufigsten assoziierten Autoantikörpern zählen Antikörper gegen das intrazelluläre Antigen Glutamat-Decarboxylase 65 (GAD65) (Malter et al., 2010), sowie Autoantikörper gegen die extrazellulären Antigene Leucine-rich glioma-inactivated 1 (LGI1) und contactin-associated protein-like 2 (CASPR2), die beide Bestandteile des Komplexes spannungsanhängiger Kaliumkanäle sind und vormals als solche zusammengefasst wurden (Binks et al., 2017; Irani et al., 2010; Lai et al., 2010; van Sonderen et al., 2017). Obgleich die Symptomtrias des limbischen Syndroms klinisch den gemeinsamen Nenner unabhängig von der Autoantikörperdiagnostik bildet, lassen sich dennoch deutliche Unterschiede hinsichtlich der Ausprägung einzelner Symptome in Abhängigkeit vom zugrundeliegenden Autoantikörper feststellen. So ist beispielsweise das Auftreten faziobrachialer dystoner Anfälle pathognomonisch für die LGI1-assoziierte LE (Irani et al., 2013, 2011), während das Spektrum der möglichen GAD65-assoziierten neurologischen Syndrome, unter anderem mit cerebellärer Ataxie und Stiff-Person-Syndrom, oftmals die Abgrenzung zur LE erschwert (Ariño et al., 2014; Dade et al., 2021; Honnorat et al., 2001; Pittock et al., 2006; Saiz et al., 2008). Bedenkt man zudem, dass Autoantikörper oftmals nicht verlässlich nachweisbar sind und außerdem auch bisher nicht beschriebene Autoantikörper ursächlich für das klinische Bild einer LE seien können (Dalmau und Vincent, 2017), kommt der Bildgebung mittels Magnetresonanztomographie (MRT) eine bedeutende Rolle in Diagnostik und Nachsorge zu. Auch hier gilt eine vergrößerte und signalgesteigerte Amygdala als gemeinsamer Nenner, darüber hinaus finden sich jedoch je nach zugrundeliegendem Autoantikörper weitere charakteristische Muster in der

strukturellen Bildgebung (Baumgartner et al., 2013; Ernst et al., 2019; Heine et al., 2015; Kotsenas et al., 2014; Plantone et al., 2013; Urbach et al., 2015; Wagner et al., 2015b, 2015a, 2013). Hieraus ist hervorzuheben, dass zuerst Wagner et al. (2016) weitgehende mikrostrukturelle Veränderungen der weißen Substanz bei GAD65-assoziierter LE mittels Diffusionstensorbildgebung (Diffusion Tensor Imaging, DTI) beschrieben.

Die DTI ist eine Bildgebungsmethode, bei der durch MRT die Diffusion freier Protonen gemessen wird. Nach anschließender Modellierung des Diffusionssignals sind so Rückschlüsse auf die mikrostrukturelle Integrität der weißen Substanz des Gehirns in vivo möglich. In der von Basser et al. (1994) vorgeschlagenen klassischen DTI wird das Diffusionssignal in jedem dreidimensionalen Bildpunkt (Voxel) als reelle, symmetrische 3 x 3-Tensormatrix modelliert. Die Diagonalelemente der Tensormatrix beschreiben die Diffusion entlang der Achsen eines beliebigen Orthogonalsystems, während paarweise Korrelationen zufälliger Bewegungen zwischen den Hauptachsen die Einträge jenseits der Diagonalen definieren. Definitionsgemäß ergibt die Diagonalisierung der Tensormatrix drei orthogonale Eigenvektoren mit zugehörigen Eigenwerten. Diese sind absteigend geordnet, womit das Modell wohldefiniert ist. Die Eigenwerte quantifizieren die Diffusion entlang der durch die zugehörigen Eigenvektoren beschriebenen Achsen, somit zeigt der erste Eigenvektor in Richtung der stärksten Diffusion. Eigenwerte und Eigenvektoren lassen sich als Ellipsoid visualisieren (siehe Abb. 1A), dessen geometrische Eigenschaften (fraktionelle Anisotropie, mittlere, axiale und radiale Diffusivität) als Maße für den Status der weißen Substanz gewertet werden. Dem liegt die Annahme zugrunde, dass die gemessene Diffusion entlang intakter mikroanatomischer Faserbündel, also entlang gesunder Axone, am stärksten ausgeprägt ist (Hagmann et al., 2006). Nachteil dieser Methode ist es, dass so lediglich ein skalarer Wert je Voxel verfügbar ist. In der Kenntnis, dass etwa 90 % aller Voxel weißer Substanz mehr als eine Faserpopulation höherer Komplexität (wie kreuzende, „fächernde“ oder „küssende“ Fasern) enthalten (Jeurissen et al., 2013), scheint dieses Modell nicht mehr tragfähig und gerät zunehmend in Kritik (Dell’Acqua und Tournier, 2018; Farquharson et al., 2013; Wheeler-Kingshott und Cercignani, 2009). Um dieser Entwicklung Rechnung zu tragen, haben wir uns zunächst für die neuere Fixel-basierte

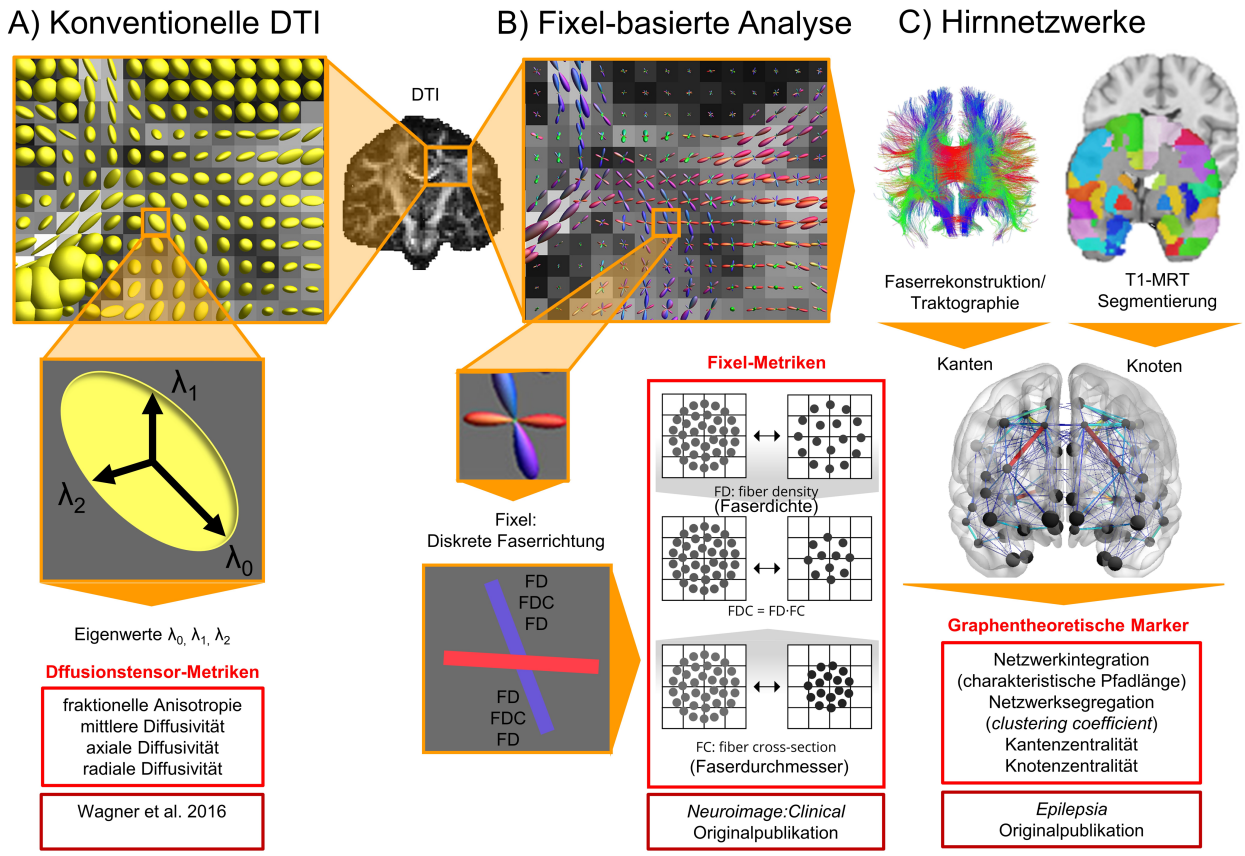

Abb. 1: Übersicht über die DTI-basierten Analysen, die in dieser Arbeit Anwendung finden. In den hellroten Kästen sind die zugehörigen Metriken aufgeführt, in den dunkelroten Kästen die entsprechende Publikation zur LE. A) Metriken der konventionellen Diffusionstensor-Analyse beruhen auf den geometrischen Eigenschaften des Tensorellipsoids, es ergibt sich je ein Wert für jedes Voxel. B) In der Fixel-basierten Analyse werden anhand der Faserverteilungsfunktion mehrere diskrete Faserpopulationen (Fixel) pro Voxel unterschieden und mit zugehörigen Metriken versehen. C) Der graphentheoretischen Analyse von Hirnnetzwerken liegen Graphen zugrunde, deren Knoten aus der automatisierten Segmentierung von T1-gewichteten MRT-Bildern bestehen und deren Kanten anhand der DTI-basierten Faserrekonstruktion berechnet werden. Eigene Darstellung, Teile aus der Originalpublikation in *Neuroimage:Clinical* sowie aus Dell'Acqua und Tournier (2018) entnommen.

Analyse entschieden (siehe Abb. 1B). Bei dieser ebenfalls DTI-basierten Methode werden Metriken nicht auf Voxel-Ebene bestimmt, sondern aus der geschätzten Faserorientierungsverteilung für jedes Voxel der weißen Substanz auf Fixel-Ebene abgeleitet (Raffelt et al., 2017, 2015). Unter einem Fixel versteht man dabei eine von potenziell mehreren diskreten Faserpopulationen je Voxel. Genauer werden zwei Metriken für jedes Fixel kombiniert: Der Faserquerschnitt (*fiber cross-section*, FC) beschreibt die makroskopischen Durchmesser eines Fasertraktes, während die Faserdichte (*fiber density*, FD) ein Maß für

die mikrostrukturelle Integrität darstellt. Durch das Zusammenführen von Informationen beider Skalen ergibt sich so ein weitaus detailreicheres Bild möglicher Veränderungen der weißen Substanz, was zunächst an Menschen mit Hippocampussklerose gezeigt wurde (Raffelt et al., 2017; Vaughan et al., 2017), nach Veröffentlichung unserer Studie über LE aber mittlerweile in mehr als 75 Publikationen über zahlreiche weitere Pathologien des zentralen Nervensystems bestätigt wurde (Dhollander et al., 2021).

Als treibender Fortschritt im Bereich der Neurobildgebung darf aktuell zweifelsohne die graphentheoretische Analyse von Hirnnetzwerken (im Englischen *connectomics*) gelten (Bassett und Bullmore, 2009; Bullmore und Sporns, 2009; Bullmore und Bassett, 2011; Fornito und Bullmore, 2015; Griffa et al., 2013; Park und Friston, 2013; Sporns et al., 2005). Dabei wird im Allgemeinen eine Auswahl an kortikalen Arealen sowie subkortikalen Strukturen als Knotenmenge eines Graphen aufgefasst. Diese Auswahl kann entweder Atlas-basiert (Desikan et al., 2006; Fischl et al., 2004; Tzourio-Mazoyer et al., 2002) oder datengetrieben (Wang et al., 2009; Wig et al., 2014; Yeo et al., 2011) erfolgen. Zur Definition der zugehörigen Kanten sind zahlreiche Paradigmen unter Nutzung von DTI (Jones et al., 2013; Smith et al., 2015), funktioneller Bildgebung (Biswal et al., 1997; Chen et al., 2015; Friston, 2011; van den Heuvel et al., 2008; van den Heuvel und Hulshoff Pol, 2010; Smitha et al., 2017; Zalesky et al., 2012) oder rein anhand strukturellen Bilddaten (Alexander-Bloch et al., 2013; Evans, 2013; He et al., 2007; Seidlitz et al., 2018) praktikabel. Ein häufig angewandter und gut untersuchter DTI-basierter Ansatz besteht darin, die Anzahl an Verbindungen der auf Ganzhirn-Ebene rekonstruierten Fasertrakte zur Modellierung der Kantenstärken heranzuziehen (Hagmann et al., 2008, 2007). Insbesondere sind hierfür neben strukturellen MRT-Daten lediglich konventionelle DTI-Daten erforderlich, wie auch für die zuvor skizzierte Fixel-basierte Analyse, womit diese Herangehensweise mit den uns retrospektiv vorliegenden Daten ohne Einschränkungen durchführbar war (siehe Abb. 1C). Die Vorteile der graphentheoretischen Analyse von Hirnnetzwerken liegen darin begründet, dass sich die funktionelle Relevanz struktureller Veränderungen bestimmter Hirnareale nicht erst durch Interpretation im Wissen um anatomisch-funktionelle Zusammenhänge ergibt, sondern die funktionelle Organisation des Hirnnetzwerkes selbst Gegenstand der Untersuchung ist. Mittels netzwerktheoretischer Marker lässt sich beispielsweise die Effizienz des Gesamtnetzwerkes (Netzwerkintegration), der Grad der Spezialisierung von Subnetzwerken (Netzwerksegregation) oder die Bedeutung einzelner

Knoten und Kanten für den Informationsaustausch quantifizieren (Bullmore und Sporns, 2009).

Fragestellung: Mittels aktuellster Methoden der Diffusionstensorbildgebung soll überprüft werden, inwiefern sich bei LE Beteilungen der weißen Substanz auf mikro- und makrostruktureller Ebene jenseits der mesiotemporalen Strukturen identifizieren lassen. Weiter sollen Veränderungen der Netzwerkstruktur unter Nutzung graphentheoretischer Marker untersucht und mit klinischen Verlaufsparametern in Zusammenhang gebracht werden, um so neue Einblicke in die Pathomechanismen, welche der LE zugrunde liegen, in einem weiteren Kontext zu erhalten.

1.2 Material und Methoden

In diese Arbeit wurden retrospektiv Menschen mit LE eingeschlossen, die zwischen April 2008 und November 2016 an der Klinik und Poliklinik für Epileptologie des Universitätsklinikums Bonn behandelt wurden. Die erforderlichen DTI-Daten waren bereits im Rahmen der Studie von Wagner et al. (2016) erhoben worden. Die Diagnose einer LE wurde anhand der Kriterien nach Graus et al. (2016) sowie der darauf basierenden Leitlinie der Deutschen Gesellschaft für Neurologie gestellt, zudem war ein positiver Antikörpernachweis notwendiges Einschlusskriterium. Insgesamt wurden 19 Menschen mit GAD65-assoziierter (mittleres Alter 35,9 Jahre, 11 weiblich), 4 Menschen mit LGI1-assoziierter, (mittleres Alter 63,3 Jahre, 2 weiblich) und 5 Menschen mit CASPR2-assoziierter LE (mittleres Alter 57,4 Jahre, keine weiblich) in die Studie eingeschlossen. Für die graphentheoretische Analyse mussten zwei Fälle von GAD65-assoziierter LE wieder ausgeschlossen werden, da die notwendige kortikale Segmentierung nicht den Qualitätsanforderungen entsprach. Daneben wurden als Kontrollgruppe 20 Menschen mit Temporallappenepilepsie und histologisch gesicherter Hippocampussklerose (mittleres Alter 38,8 Jahre, 11 weiblich) sowie gesunde Kontrollpersonen aus der Datenbank des Life&Brain-Instituts eingeschlossen. Weitere Details sind jeweils in Tabelle 1 der Originalpublikationen in *Neuroimage:Clinical* (Abschnitt 2.1) und *Epilepsia* (Abschnitt 2.3) nachzulesen. Alle Untersuchungen wurden auf Grundlage der revidierten Deklaration von Helsinki des

Weltärztebundes (1983), eines vorliegenden Ethikvotums der Ethikkommission der Medizinischen Fakultät Bonn und den geltenden gesetzlichen Bestimmungen durchgeführt.

Antikörpertestungen aus Serum und Liquor erfolgten an der Klinik für Neuropathologie des Universitätsklinikums Bonn oder wurde von dort an unten benannte Labore versandt. Ab 2014 erfolgte das Screening auf onkoneuronale Antikörper mittels semiquantitativer Immunoblots (EUROLINE PNS 12, Euroimmun, DL 1111-1601-7 G), welche mit rekombinantem Antigen oder Antigenfragmenten beschichtet waren. Serum wurde 1:100 verdünnt, Liquor 1:1. Darüber hinaus wurden mittels Immunzytochemie mit HEK293-Zellen (Human Embryonic Kidney 293) mit Expression von Antigenen auf der Zelloberfläche NMDAR-, CASPR2-, LGI1-, GABAA-, GABAB-, AMPAR- und GAD65-Autoantikörper nachgewiesen, Serum 1:10 verdünnt, Liquor 1:1 (IIFT: Autoimmun-Enzephalitis-Mosaik1, Euroimmun, FA 1120-1005-1; GAD65-IIFT, Euroimmun, FA 1022-1005-50). Vor 2014 erfolgte der Nachweis von GAD-Antikörpern im Serum mit einem Anti-125 I-GAD-Radioimmunopräzipitationstest (Normwert ≤1 U/ml; Weatherall Institute, Oxford, UK, oder Euroimmun, Lübeck, Deutschland). VGKC-Komplex-Antikörper wurden mittels Radioimmunpräzipitationstest nachgewiesen (Normwerte < 100 pM; Weatherall Institute oder Euroimmun). Antikörper gegen LGI1 und CASPR2 wurden durch indirekte Immunfluoreszenz mit formalinfixierten HEK293-Zellen nachgewiesen, die membrangebundenes LGI1 oder CASPR2 enthielten (Normwerte <1:10, Euroimmun).

Neuropsychologische Untersuchungen wurden berücksichtigt, wenn eine Testung in einem Abstand von höchstens 100 Tagen zum MRT-Scan erfolgt war. Als Testung für das Figuralgedächtnis wurde das revidierte *Diagnosticum für Cerebralschädigung* verwendet (Helmstaedter et al., 1991), die Testung des Verbalgedächtnisses erfolgte mittels verbalem Lern- und Merkfähigkeitstest (Helmstaedter und Durwen, 1990). Die Gedächtnisleistung wurde alterskorrigiert und relativ zu einem Normkollektiv aus 488 kognitiv unauffälligen Personen betrachtet (Mittelwert 100, Standardabweichung 10).

Alle MRT-Daten wurden im Life&Brain-Institut in Bonn an einem 3-Tesla-Magnetresonanztomographen (Magnetom Trio, Siemens Healthineers, Erlangen, Deutschland) erhoben. Aufgrund eines Scanner-Updates Anfang 2014 mussten zwei verschiedene Messprotokolle verwendet werden. Die DTI-Daten wurden mittels einer *Echoplanar-Imaging* (EPI) Sequenz aufgenommen. Die Messparameter vor dem Update waren:

Voxelgröße = 1,72 mm × 1,72 mm × 1,7 mm, Matrix = 128 × 128 Pixel, *repetition time* (TR) = 12 s, *echo time* (TE) = 100 ms, die Messung erfolgte mittels Achtkanal-Kopfspule. Die Messparameter nach dem Update waren: Voxelgröße = 1,72 mm × 1,72 mm × 1,7 mm, Matrix = 128 × 128 Pixel, TR = 9 s, TE = 87 ms, die Messung erfolgte mittels 32-Kanal-Kopfspule. Bei beiden Sequenzen war die Diffusionswichtung isotrop in 60 Richtungen mit b = 1000 s·mm^{-2} verteilt, zu Beginn und nach jeder Serie von zehn diffusionsgewichteten Bildern wurden sechs Bilder mit b = 0 aufgenommen. Strukturelle T1-gewichtete Bilddaten wurden mittels einer *magnetization-prepared rapid acquisition gradient echo* (MPRAGE) Sequenz aufgenommen Die Messparameter vor dem Update waren: Voxelgröße = 1 mm × 1 mm × 1 mm, Matrix = 256 × 256 Pixel, TR = 1,57 s, TE = 3,42 ms, *flip angle* = 15°, die Messung erfolgte mittels 32-Kanal-Kopfspule. Die Messparameter nach dem Update waren: Voxelgröße = 0,8 mm × 0,8 mm × 0,8 mm, Matrix = 320 × 320 Pixel, TR = 1,66 s, TE = 2,54 ms, *flip angle* = 9°, die Messung erfolgte mittels 32-Kanal-Kopfspule. Der anzunehmende Effekt durch das veränderte Messprotokoll wurde in den statistischen Modellen berücksichtigt.

Die Vorverarbeitung der DTI-Daten mit Hilfe der *FMRIB Software Library* (FSL), Version 5.0 (Jenkinson et al., 2012), umfasste das *denoising* (Veraart et al., 2016), eine Korrektur für Verzerrungen durch Bewegung und durch Wirbelströme (*motion and eddy current distortion correction)* (Andersson et al., 2003; Andersson und Sotiropoulos, 2016) und des *N4 bias field* (Tustison et al., 2011). Die Vorverarbeitung, Oberflächenrekonstruktion und volumetrische Segmentierung der strukturellen T1-gewichteten Daten erfolgte mit der Software *FreeSurfer*, Version 6.0 (Fischl, 2012). Alle Registrierungen, Segmentierungen und Oberflächenrekonstruktionen wurden einer visuellen Qualitätskontrolle unterzogen. Da aktuell diskutiert wird, inwiefern LE eine primär lateralisierte Pathologie ist (Ernst et al., 2019; Navarro et al., 2016), definierten wir entweder die linke, die rechte oder beide Hemisphären als primär betroffene Hemisphären. Dazu verwendeten wir ein zweistufiges Schema in Anlehnung an Ernst et al. (2019): Sofern iktale oder interiktale elektroenzephalographische Ableitungen aus dem selben Krankenhausaufenthalt wie die MRT-Daten vorhanden waren, entsprach die Lateralisierung den elektroenzephalographischen Auffälligkeiten. Falls diese nicht verfügbar oder unauffällig waren, nutzten wir das rechts/links-

Verhältnis $2 \cdot (V_R - V_L) \cdot (V_R + V_L)^{-1}$ des Amygdalavolumens (V). War dies im unteren Quartil des Kontrollkollektivs, betrachteten wir die linke Hemisphäre als primär betroffen. War dies im oberen Quartil des Kontrollkollektivs, betrachteten wir die rechte Hemisphäre als primär betroffen. Dazwischen sahen wir beide Hemisphären als primär betroffen an. Sofern wir nur die rechte Hemisphäre als primär betroffen ansahen, spiegelten wir die MRT-Daten entlang der links-rechts-Achse. Nach dieser Reorientierung finden sich damit auf der linken Bildseite lediglich primär betroffene Hemisphären, während auf der rechten Bildseite sowohl primär mitbetroffene wie auch mutmaßlich unbetroffene Hemisphären zu finden sind, weshalb wir hierfür die Bezeichnung kontralateral verwenden.

Die Fixel-basierte Analyse wurde anhand der vorverarbeiteten DTI-Daten mit der Toolbox *MRtrix3* durchgeführt (Raffelt et al., 2017; Tournier et al., 2019). Zunächst führten wir auf Gruppenebene eine Normalisierung der Intensitäten auf das mediane Signal der weißen Substanz bei $b = 0$ durch. Wir passten die Voxelgröße auf 1,3 mm × 1,3 mm × 1,3 mm an, um die anschließenden Verarbeitungsschritte zu optimieren. Anhand der auf Gruppenebene bestimmten durchschnittlichen Antwortfunktion der weißen Substanz (Tournier et al., 2013) führten wir eine *constrained spherical deconvolution* (Jeurissen et al., 2014) durch, um die Faserverteilungsfunktion (*fiber orientation distribution*, FOD) in jedem Voxel zu schätzen. Aus einer Untergruppe von 45 repräsentativen Bildern erstellten wir ein FOD-Gruppentemplate, auf das alle FOD-Bilder registriert wurden. Die probabilistischen FOD-Bilder wurden in diskrete Faserverteilungsrichtungen (Fixel) segmentiert (Smith et al., 2013), für die die Metriken Faserdichte (*fiber density,* FD) (Raffelt et al., 2012) und Faserdurchmesser *(fiber cross-section*, FC) (Raffelt et al., 2017) sowie daraus abgeleitet FDC = FD · FC und ln(FC) berechnet wurden. Ziel des Logarithmierens war es, eine um Null zentrierte Normalverteilung der Daten zu erreichen. Abb. 1B zeigt eine Skizze zur Verdeutlichung der Bedeutung der vorgenannten Metriken. Wir führten eine probabilistische Traktographie des gesamten Gehirns basierend auf dem FOD-Gruppentemplate durch und wählten $20 \cdot 10^6$ rekonstruierte Fasern mit einer Länge zwischen 10 und 250 mm und einem maximalen Winkel von 22,5° aus. Um mögliche Verzerrungen in der Traktographie zu korrigieren, führten wir das *spherical deconvolution informed filtering* durch (Smith et al., 2013) und reduzierten die Anzahl der Fasern auf $2 \cdot 10^6$. Eine graphische Zusammenfassung der Bildverarbeitungsschritte findet sich in Abb. 1 der Originalpublikation in *Neuroimage:Clinical* (Abschnitt 2.1). Der statistische Vergleich aller

Gruppen auf Ganzhirnebene erfolgte mittels *connectivity-based fixel enhancement* (Raffelt et al., 2015) und nicht-parametrischer Permutationstestung (5000 Permutationen) zur Korrektur der f*amily-wise error rate* (FWER). Anschließend extrahierten und mittelten wir die Fixel-Werte signifikanter Bereiche der Ganzhirnanalyse. Die Testung auf Gruppenunterschiede über alle Gruppen erfolgte mittels einfacher Varianzanalyse (*analysis of variance*, ANOVA), die post-hoc Testung auf paarweise Gruppenunterschiede erfolgte mittels Tukey-Kramer Tests. Als Maß für die Stärke des Zusammenhangs von Fixel-Werten mit klinischen Verlaufsmarkern verwendeten wir den Pearson-Korrelationskoeffizient sowie darüber hinaus lineare Regressionsmodelle. Zur Korrektur der *false discovery rate* (FDR) bei multiplem Testen verwendeten wir die Holm-Bonferroni-Methode.

Die Erstellung der Netzwerkgraphen basierend auf den vorverarbeiteten DTI- und T1-gewichteten Daten erfolgte ebenfalls mit der Toolbox *MRtrix3* (Tournier et al., 2019). Als Knotenmenge verwendeten wir alle 84 kortikalen und subkortikalen Areale des Desikan-Killiany Atlas aus der *FreeSurfer*-Segmentierung (Desikan et al., 2006). Anhand der DTI-Daten bestimmten wir für jeden Probanden eine durchschnittliche Antwortfunktion der weißen Substanz (Tournier et al., 2013) und schätzten die Faserverteilungsfunktion (*fiber orientation distribution*, FOD) in jedem Voxel mittels *constrained spherical deconvolution* (Jeurissen et al., 2014). Anders als bei der Fixel-basierten Analyse, wie im vorherigen Absatz beschrieben, ist für den netzwerkbasierten Ansatz keine Normalisierung auf ein Gruppentemplate erforderlich. Anhand der FOD-Daten rekonstruierten wir mittels probabilistischer Traktographie $10 \cdot 10^6$ Fasern mit einer Länge zwischen 10 und 250 mm und einem maximalen Winkel von 22,5°. Um etwaige Verzerrungen in der Traktographie zu korrigieren, führten wir auch hier das *spherical deconvolution informed filtering* durch (Smith et al., 2013) und reduzierten die Anzahl der Fasern auf $5 \cdot 10^6$. Die Kantenstärken wurden anhand der Anzahl rekonstruierter Fasern zwischen den Knoten bestimmt (Smith et al., 2015). Die symmetrischen, gewichteten Netzwerkmatrizen wurden schließlich auf das Intervall [0,1] skaliert und mit Hilfe der *Brain Connectivity Toolbox* graphentheoretisch untersucht (Rubinov und Sporns, 2010). Als Maß für die Effizienz des Netzwerkes in einer Umgebung einzelner Knoten berechneten wir den *clustering coefficient* (Onnela et al., 2005), die mittlere Pfadlänge (charakteristische Pfadlänge) zwischen allen Knotenpaaren diente als Maß für die globale Effizienz des Netzwerkes (Rubinov und Sporns, 2010). Da die Voraussetzungen der einfachen ANOVA nicht in allen Subgruppen gegeben war,

verglichen wir die Netzwerkmarker lediglich zwischen den Gruppen mit GAD65-assoziierter LE, Hippocampussklerose und der Kontrollgruppe mittels einfacher ANOVA und paarweisen Tukey-Kramer post-hoc Tests. Zusätzlich erfolgte der Vergleich über alle Gruppen mittels nicht-parametrischem Kruskal-Wallis-Test und paarweisen post-hoc Dunn-Tests. Zur Korrektur der FDR bei multiplem Testen verwendeten wir die Benjamini-Hochberg-Methode. Weiterhin verwendeten wir lineare Regressionsmodelle mit den unabhängigen Variablen charakteristische Pfadlänge respektive *clustering coefficient*, Alter bei Scan, Sequenz-Update, Autoantikörper, um die abhängigen Variablen Amygdalavolumen der primär betroffenen Hemisphäre und Gedächtnismarker zu erklären. Der Vergleich aller Kantenstärken auf Ganzhirn-Ebene erfolgte im Rahmen von *network-based statistics* (Zalesky et al., 2010) mittels ungepaarter *t*-Tests und nicht-parametrischer Permutationstestung (5000 Permutationen) zur Korrektur der FWER.

1.3 Ergebnisse

Im Vergleich der Gruppen mit LE waren Menschen mit GAD65-assoziierter LE jünger bei Erkrankungsbeginn und bei der MRT-Untersuchung als Menschen mit CASPR2- und LGI1-assoziierter LE (jeweils Tukey-Kramer $p < 0{,}001$). Zudem lag in allen Serogruppen das Alter bei Erkrankungsbeginn höher und die Krankheitsdauer war kürzer als bei Menschen mit Hippocampussklerose (jeweils Tukey-Kramer $p < 0{,}001$). Hinsichtlich Verbalgedächtnisleistung (ANOVA $F(5, 50) = 2{,}23$, $p = 0{,}065$) und Figuralgedächtnisleistung (ANOVA $F(5, 50) = 0{,}74$, $p = 0{,}60$) fanden wir keine Gruppenunterschiede.

Der Vergleich aller Fixel-Metriken FD, ln(FC) und FDC auf Ganzhirn-Ebene zeigte keine Gruppenunterschiede zwischen Menschen mit CASPR2-assoziierter LE und Kontrollpersonen sowie zwischen Menschen mit LGI1-assoziierter LE und Kontrollpersonen (jeweils $p_{min} > 0{,}05$, FWER-korrigiert). Im Vergleich von Menschen mit GAD65-assoziierter LE zu Kontrollpersonen fanden sich drei Regionen (siehe Abb. 2A) mit signifikant reduzierter FDC: Erstens und zweitens im fasciculus longitudinalis superior um im Mittel -5,4% in der primär betroffenen ($t_{max} = 4{,}57$, $p_{min} = 0{,}036$, FWER-korrigiert) wie auch um im Mittel -5,0% in der kontralateralen Hemisphäre ($t_{max} = 5{,}25$, $p_{min} = 0{,}002$, FWER-korrigiert),

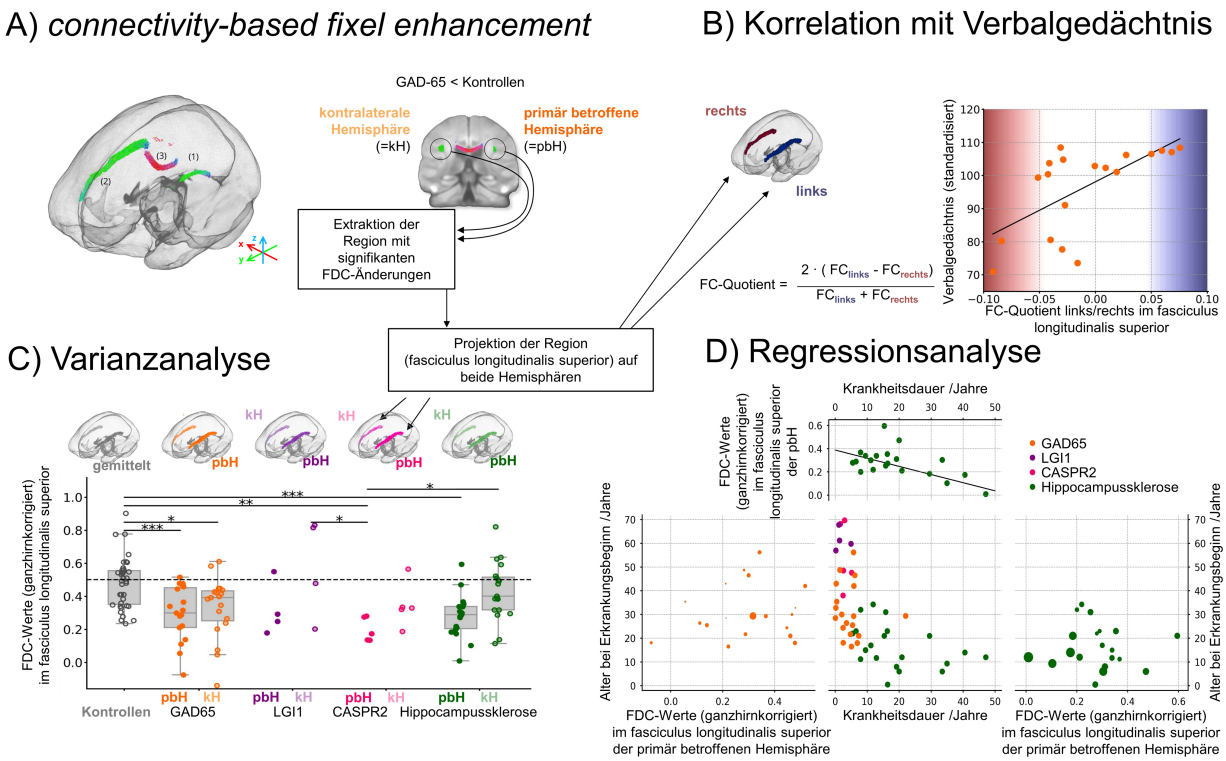

Abb. 2: Übersicht über die Ergebnisse der Fixel-basierten Analyse. A) Gruppenunterschiede auf Ganzhirnebene im Vergleich von Menschen mit GAD65-assoziierter LE mit Kontrollpersonen: (1) fasciculus longitudinalis superior der kontralateralen Hemisphäre, (2) fasciculus longitudinalis superior der primär betroffenen Hemisphäre, (3) Isthmus des corpus callosum. B) Korrelation des FC-Quotienten links/rechts mit der Verbalgedächtnisleistung in der Gruppe mit GAD65-assoziierter LE. C) Varianzanalyse zum Vergleich der FDC-Werte im fasciculus longitudinalis superior über alle Gruppen. D) Regressionsanalysen der extrahierten FDC-Werte mit dem Alter bei Erkrankungsbeginn und der Krankheitsdauer. */**/***: post-hoc Tukey-Kramer Test $p < 0{,}05$/$p < 0{,}01$/$p < 0{,}001$. pbH: Primär betroffene Hemisphäre. kH: Kontralaterale Hemisphäre. Modifiziert nach der Originalpublikation in *Neuroimage:Clinical*.

drittens im Isthmus des corpus callosum (t_{max} = 4,88, p_{min} = 0,012, FWER-korrigiert). In allen Regionen setzte sich die Reduktion von FDC aus einer Reduktion sowohl von FD wie auch FC zusammen. In einem zweiten Schritt projizierten wir die dem fasciculus longitudinalis superior entsprechende Region auf beide Hemisphären (siehe Abb. 2C) und fanden darin signifikante Gruppenunterschiede der FDC-Werte (ANOVA $F(9, 152) = 6{,}57$, $p < 0{,}001$). Bei Menschen mit GAD65-assoziierter LE fanden wir niedrigere FDC-Werte im Vergleich zu Kontrollpersonen sowohl in der primär betroffenen (Tukey-Kramer-Test $p < 0{,}001$) wie auch in der kontralateralen Hemisphäre (Tukey-Kramer-Test $p = 0{,}029$). Bei Menschen mit CASPR2-assoziierter LE fanden wir reduzierte FDC-Werte in der

primär betroffenen Hemisphäre im Vergleich zu Kontrollpersonen (Tukey-Kramer-Test $p = 0{,}003$), der kontralateralen Hemisphäre bei Menschen mit LGI1-assoziierter LE (Tukey-Kramer-Test $p = 0{,}015$) und der kontralateralen Hemisphäre bei Menschen mit Hippocampussklerose (Tukey-Kramer-Test $p = 0{,}042$). Eine Korrelationsanalyse zwischen den Fixel-Metriken FD, ln(FC) und FDC innerhalb des fasciculus longitudinalis superior und den Resultaten der neuropsychologischen Testungen zeigte eine signifikante Korrelation zwischen dem Quotienten der FC-Werte links/rechts sowie dem Verbalgedächtnis ($R = 0{,}64$, $p = 0{,}048$, Holm-Bonferroni FDR-korrigiert) bei Menschen mit GAD65-assoziierter LE (siehe Abb. 2B). Zudem untersuchten wir lineare Regressionsmodelle mit Alter bei Krankheitsbeginn und Krankheitsdauer als unabhängigen Variablen (siehe Abb. 2D). Bei Menschen mit Hippocampussklerose konnten FDC-Werte im fasciculus longitudinalis superior der betroffenen Hemisphäre als abhängige Variable mittels eines solchen Modells erklärt werden (globaler *F*-Test $F(2, 17) = 5{,}23$, $p = 0.017$, $R^2 = 0{,}38$), dabei war der Regressor Krankheitsdauer signifikant (*t*-Test des Regressionskoeffizienten $t = -3{,}22$, $p = 0{,}004$), der Regressor Alter bei Krankheitsbeginn hingegen war nicht signifikant (*t*-Test des Regressionskoeffizienten $t = -1{,}55$, $p = 0{,}14$). Bei Menschen mit GAD65-assoziierter LE war das Regressionsmodell weder mit den FDC-Werten im fasciculus longitudinalis superior der primär betroffenen Hemisphäre (globaler *F*-Test $F(2, 16) = 0{,}48$, $p = 0{,}63$), noch den gemittelten FDC-Werten über beide Hemisphären als abhängige Variablen signifikant (globaler *F*-Test $F(2, 16) = 0{,}82$, $p = 0{,}45$). Für die Gruppen mit CASPR2- und LGI1-assoziierter LE führten wir die Regressionsanalyse aufgrund zu kleiner Gruppengröße nicht durch.

Die Analyse der Hirnnetzwerke zeigte signifikante Gruppenunterschiede auf Ganzhirn-Ebene zwischen Menschen mit GAD65-assoziierter LE, Hippocampussklerose und Kontrollpersonen hinsichtlich der charakteristischen Pfadlänge als Maß für die Netzwerkintegration (ANOVA $F(4, 58) = 3{,}66$, $p = 0{,}010$) sowie des *clustering coefficient* als Maß für die Netzwerksegregation (ANOVA $F(4, 58) = 4{,}98$, $p = 0{,}002$). Dies fand sich ebenso im nicht-parametrischen Pendant über alle Gruppen (charakteristische Pfadlänge: Kruskal-Wallis-Test $\chi^2(4) = 10{,}83$, $p = 0{,}03$, *clustering coefficient*: Kruskal-Wallis-Test $\chi^2(4) = 15{,}78$, $p = 0{,}003$) (siehe Abb. 3A und 3B). Paarweise durchgeführte post-hoc Tests zeigten lediglich eine signifikant erhöhte charakteristische Pfadlänge sowie eine

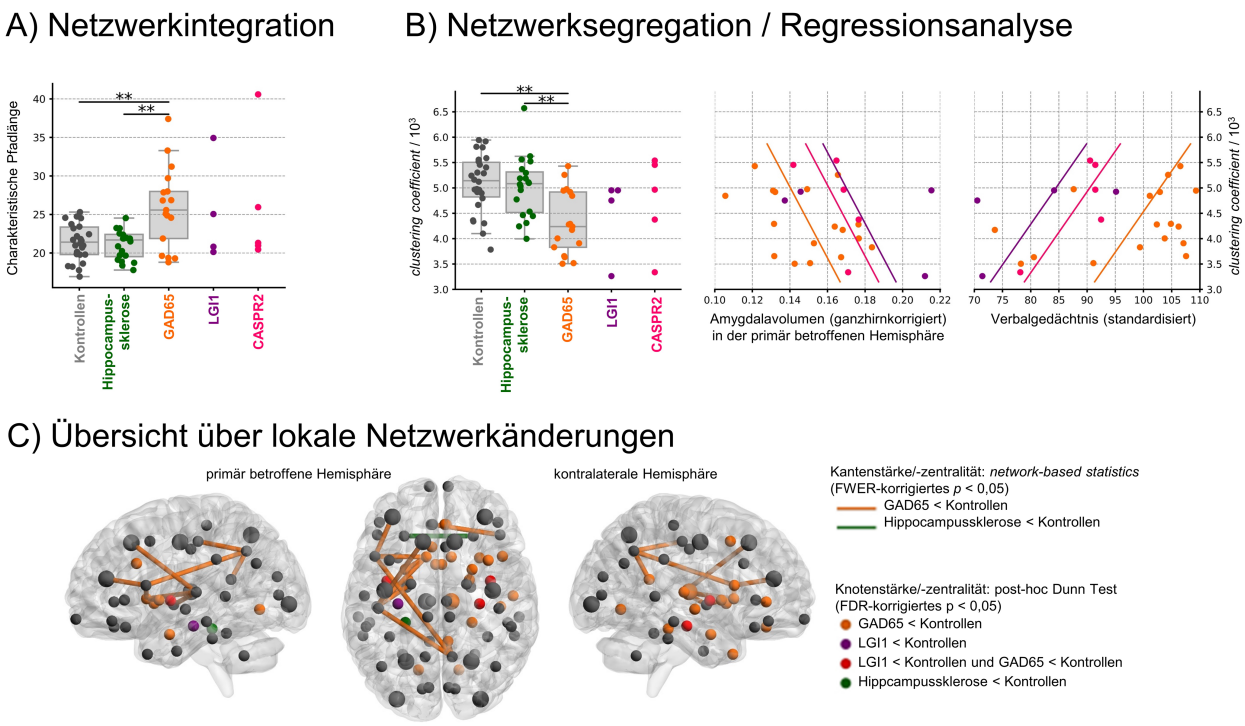

Abb. 3: Übersicht über die Ergebnisse der Netzwerkanalysen. A) Vergleich der charakteristischen Pfadlänge als Marker für die Netzwerkintegration über alle Serogruppen. B) Vergleich des *clustering coefficient* als Maß für die Netzwerksegregation über alle Gruppen, daneben Korrelationsanalyse mit dem Amygdalavolumen der primär betroffenen Hemisphäre und dem Verbalgedächtnis. C) Übersicht über die lokalen Netzwerkänderungen hinsichtlich Knoten- und Kantenzentralität. **: post-hoc Tukey-Kramer-/Dunn-Test 0,001< p < 0,01. Modifiziert nach der Originalpublikation in *Epilepsia*.

signifikant erniedrigten *clustering coefficient* im Vergleich zu Kontrollpersonen und Menschen mit Hippocampussklerose (jeweils Tukey-Kramer-Test und Dunn-Test p < 0,01). Mittels linearer Regressionsmodelle (siehe Abb. 3B) fanden wir einen Zusammenhang sowohl zwischen dem Amygdalavolumen in der primär betroffenen Hemisphäre als abhängigen Variable (globaler F-Test $F(4, 21) = 3.09$, p = 0,038, R^2 = 0,31) sowie dem Verbalgedächtnis als abhängigen Variable (globaler F-Test $F(4, 21) = 4,39$, p = 0,010, R^2 = 0,45) und jeweils dem Regressor *clustering coefficient* (t-Test des Regressionskoeffizienten jeweils p < 0,05). Lineare Regressionsmodelle mit dem Amygdalavolumen auf der kontralateralen Hemisphäre, dem über beide Hemisphären gemittelte Amygdalavolumen und dem Figuralgedächtnis als abhängige Variablen waren nicht signifikant im globalen F-Test (p > 0,05). Im Vergleich der Kantenstärken mittels *network-based statistics*

fanden wir elf Verbindungen mit signifikant reduzierter Kantenstärke bei Menschen mit GAD65-assoziierter LE im Vergleich zu Kontrollpersonen ($p < 0,05$ FWER-korrigiert) (siehe Abb. 3C für eine Übersicht, Details siehe Abb. 1C der Originalpublikation in *Epilepsia*, Abschnitt 2.3). Bei Menschen mit Hippocampussklerose zeigte die interhemisphärische Verbindung zwischen den orbitofrontalen Gyri eine reduzierte Kantenstärke im Vergleich zu Kontrollpersonen ($p < 0,05$ FWER-korrigiert). In allen anderen paarweisen Gruppenvergleichen war das FWER-korrigierte $p > 0,05$ für alle Kanten. Bei Betrachtung der Knotenzentralität fanden wir Gruppenunterschiede der Knotenstärken in 18 Knoten (jeweils $p < 0,05$ Benjamini-Hochberg FDR-korrigiert) (siehe Abb. 3C für eine Übersicht, Details siehe Abb. S4C im Supplementary Material der Originalpublikation in *Epilepsia*, Abschnitt 2.4).

1.4 Diskussion

Die klinischen Merkmale der einzelnen LE-Serogruppen unserer Kohorte entsprechen den Charakteristika, die zuvor in zahlreichen Studien beschrieben wurden (Bien et al., 2007; Dalmau und Graus, 2018; Graus et al., 2016; Malter et al., 2010). Insbesondere war der Anteil Frauen in der Gruppe der GAD65-assoziierten LE signifikant größer als in den anderen Serogruppen (Graus et al., 2016). Menschen mit GAD65-assoziierter LE waren zudem signifikant jünger bei Krankheitsbeginn als Menschen mit LGI1- oder CASPR2-assoziierter LE, dennoch lag der Erkrankungsbeginn aller von LE Betroffenen im Erwachsenenalter, während Menschen mit Hippocampussklerose bereits erste Symptome im Kindesalter zeigten (Bien et al., 2007; Bien und Elger, 2007; Malter et al., 2010). Die Leistung des Verbal- und Figuralgedächtnisses war, wie erwartet, in allen Gruppen eingeschränkt (Elger et al., 2004; Finke et al., 2017; Frisch et al., 2013; Griffith et al., 2020; Hermann et al., 2006; Witt und Helmstaedter, 2021).

Bei Menschen mit GAD65-assoziierter LE sind mittels konventioneller DTI weitreichende Änderungen der weißen Substanz beobachtet worden (Wagner et al., 2016). Diese Änderungen konnten wir erstens mit Hilfe der Fixel-basierten Analyse auf distinkte Fasertrakte eingrenzen, und zweitens mittels eines netzwerkbasierten Ansatzes funktionell interpretierbar kontextualisieren. Änderungen der Diffusivitätsparameter im corpus

callosum, wie wir sie auch in der Fixel-basierten Analyse in der Gruppe mit GAD65-assoziierter LE fanden, wurden bereits bei Temporallappenepilepsie beobachtet (Caligiuri et al., 2016; Whelan et al., 2015). Gegenstand der Diskussion ist diesbezüglich insbesondere die Frage, ob es sich hierbei um eine Folge von epileptischen Anfällen, ein Bestandteil der Pathologie oder eine genetische Komponente handelt (Vaughan et al., 2017). Auch die FDC-Reduktion des fasciculus longitudinalis superior in der betroffenen Hemisphäre wurde bereits bei Menschen mit Temporallappenepilepsie beobachtet (Raffelt et al., 2017; Smith et al., 2013; Vaughan et al., 2017), was unsere Daten nun erneut an Menschen mit Hippocampussklerose bestätigen. Neu hingegen ist die Beobachtung, dass diese Änderungen auch bei Menschen mit GAD65-assoziierter LE bilateral zu finden sind. Auch dies kann auf zwei Weisen interpretiert werden: Entweder als sekundärer axonaler Schaden durch epileptische Anfälle, die nicht zwangsläufig auf die primär betroffene Hemisphäre beschränkt sind, sondern sich über ein bilaterales Netzwerk ausbreiten (Ahmadi et al., 2009; Campos et al., 2015; Otte et al., 2012), oder aber als Bestandteil der autoimmunen Pathologie. Zwar fanden wir bei Menschen mit Hippocampussklerose einen zeitlichen Zusammenhang zwischen der Reduktion der FDC-Werte und der Krankheitsdauer, was prinzipiell eher für einen Sekundärschaden spricht. Allerdings lässt sich dies aufgrund des unterschiedlichen Erkrankungsalters nicht ohne Weiteres auf Menschen mit LE übertragen, da sich diese signifikant im Alter bei Erkrankungsbeginn unterscheiden und dies bekanntermaßen die Anfälligkeit des Gehirns für Anfälle und das Potenzial für Neuroplastizität maßgeblich beeinflusst (Ben-Ari und Holmes, 2006; Berg et al., 2012).

Hinsichtlich der Pathogenese von LGI1-assoziierter LE wird aktuell ein unilateraler Krankheitsbeginn diskutiert (Ernst et al., 2019; Navarro et al., 2016). Im Gegensatz dazu zeigen unsere Ergebnisse lediglich einen Trend in Richtung asymmetrischer Veränderungen mit niedrigeren FDC-Werten in der primär betroffenen Hemisphäre in dieser Gruppe. Dies könnte darauf zurückzuführen sein, dass nicht alle Menschen mit LGI1-assoziierter LE in unserer Kohorte unmittelbar bei Beginn der Erkrankung der MRT-Untersuchung unterzogen wurden. Bemerkenswert ist dennoch, dass in der Gruppe mit CASPR2-assoziierter LE trotz des geringen Stichprobenumfangs signifikant reduzierte FDC-Werte lediglich in der primär betroffenen Hemisphäre zu finden sind.

Das Verbalgedächtnis darf als wichtiger klinischer Verlaufsparameter der Temporallappenepilepsie, sowohl mit Hippocampussklerose als auch autoimmuner Ätiologie, gelten (Elger et al., 2004; Griffith et al., 2020; Hermann et al., 2006; Loane et al., 2019; Witt und Helmstaedter, 2021). Zudem ist bekannt, dass der fasciculus longitudinalis superior essentieller Bestandteil von Netzwerken zur Sprachverarbeitung ist und darin insbesondere zwischen Sprachfunktion und Gedächtnis vermittelt (Baddeley, 2000; Bernal und Ardila, 2009; Maldonado et al., 2011; Smits et al., 2014). Der Zusammenhang zwischen dem Verbalgedächtnis und der Asymmetrie von FC-Werten im fasciculus longitudinalis superior mit größeren Werten zu Gunsten der linken Hemisphäre korrespondiert mit den Resultaten zahlreicher Studien mit konventioneller DTI-Analyse (Catani et al., 2007; Thiebaut de Schotten et al., 2011; Vernooij et al., 2007). Darüber hinaus konnten wir zeigen, dass mit dem *clustering coefficient* die Netzwerkorganisation auf Ganzhirnebene mit dem Ausmaß der Verbalgedächtnisverlusts bei LE in Verbindung steht. Beides zusammengenommen untermauert das Konzept, dass das Verbalgedächtnis als wichtiger klinischer Verlaufsparameter der LE weniger durch die Funktion einzelner Komponenten alleine, sondern vielmehr durch die Integrität der zur Sprachverarbeitung relevanten Netzwerke im Gesamten bestimmt wird (Catani et al., 2007; Loane et al., 2019).

Darüber hinaus konnten wir zeigen, dass der *clustering coefficient* als Marker für die Netzwerksegregation neben dem Verbalgedächtnis mit dem Ausmaß der für LE charakteristischen Amygdalavergrößerung in Zusammenhang steht (Ernst et al., 2019; Wagner et al., 2015b). Hierbei ist von besonderem Interesse, dass dies lediglich für das Volumen in der primär betroffenen Hemisphäre gilt, nicht jedoch für das Amygdalavolumen in der kontralateralen Hemisphäre. Diese Beobachtung unterstreicht die Seitenspezifität der Amygdalavergrößerung hinsichtlich der Änderungen auf Netzwerkebene, was als Hinweis auf eine mögliche Lateralisierung des Krankheitsprozesses verstanden werden kann. Umgekehrt demonstriert dieser Zusammenhang die Relevanz der graphentheoretischen *in-silico* Metriken für die klinische Praxis.

Mit Blick auf die Netzwerkorganisation auf lokaler Ebene beschrieben bisherige Studien mittels funktioneller Bildgebung insbesondere eine reduzierte interhippocampale und hippocampo-kortikale Konnektivität bei Menschen mit LGI1-assoziierter LE (Heine et al., 2018; Loane et al., 2019). Dies konnten wir durch eine reduzierte Knotenzentralität des

Hippocampus bei Menschen mit LGI1- und GAD65-assoziierter LE unter Nutzung DTI-basierter Netzwerke bestätigen. Darüber hinaus fanden wir in diesen beiden Serogruppen zudem eine reduzierte Knotenzentralität des insulären Kortex, was bisher nicht auf Netzwerkebene reproduziert wurde, indes aber elektroklinisch, mittels konventioneller Bildgebung und mittels Positronen-Emissions-Tomographie beobachtet wurde (Bose et al., 2019; Falip et al., 2019; Li et al., 2018).

Im Vergleich zu Menschen mit Hippocampussklerose waren die Netzwerkänderungen bei Menschen mit GAD65-assoziierter LE zum einen wesentlich ausgedehnter, zum anderen weniger lateralisiert zu beobachten. Während sich Knoten mit reduzierter Zentralität bei Menschen mit Hippocampussklerose ausschließlich in der betroffenen Hemisphäre fanden, sahen wir bei Menschen mit GAD65-assoziierter LE eine reduzierte Knotenzentralität insbesondere bilateral in den Basalganglien. Dies verstehen wir als graphentheoretisches Korrelat des zuvor bereits beschriebenen Hypermetabolismus (Tripathi et al., 2018).

Insgesamt demonstrieren unsere Resultate, dass es sich bei der GAD65-assoziierten LE um eine Entität autoimmuner LE handelt, die mit deutlichen bilateralen Veränderungen entlang des gesamten Spektrums von mikro- bis makrostrukturellen sowie nicht zuletzt netzwerkbezogenen Bildgebungsmarkern einher geht. Im Gegensatz dazu fanden wir auf Ganzhirnebene keine mikro- und makrostrukturellen Veränderungen der weißen Substanz und allenfalls lokale Netzwerkänderungen in LGI1- und CASPR2-assoziierter LE, was dem in der Literatur gezeichneten Bild dieser Erkrankungen entspricht (Heine et al., 2015; Wagner et al., 2016). Nicht zuletzt spiegelt sich diese Gegenüberstellung innerhalb des Spektrums der LE in den typischen klinischen Verläufen wieder: Während Menschen mit LGI1- und CASPR2-assoziierter LE häufig ein gutes Ansprechen auf Immuntherapie zeigen (Bien, 2021; Dubey et al., 2020; Graus et al., 2016; Rodriguez et al., 2022; Shin et al., 2013; Toledano et al., 2014; Witt und Helmstaedter, 2021), sind chronische Langzeitverläufe mit mäßigem Ansprechen auf Immuntherapie und wiederholten akuten Krankheitsphasen typisch für GAD65-assoziierte LE (Bien, 2021; Frisch et al., 2013; Graus et al., 2016; Malter et al., 2010; Witt und Helmstaedter, 2021).

Im Wesentlichen schränken drei Aspekte die Aussagekraft dieser Arbeit ein. Erstens eignet sich ein transversales Studiendesign, wie es anhand der retrospektiv vorliegenden

Daten unumgänglich war, nur bedingt zur Untersuchung von Erkrankungen mit komplexen Langzeitverläufen. Insbesondere können verschiedene Therapieregime Einfluss auf die Daten haben (Foster et al., 2020; Het et al., 2005; Witt und Helmstaedter, 2017), was aufgrund der individuellen klinischen Verläufe statistisch nicht zu kontrollieren ist. Zweitens sind kleine und heterogene Stichproben statistisch herausfordernd, was in dieser Arbeit besonders die Gruppen mit LGI1- und CASPR2-assoziierte LE betrifft und die Teststärke erheblich mindert. Drittens und letztens können über die histopathologischen Zusammenhänge zwischen DTI-basierten und besonders netzwerkbezogenen Bildgebungsmarkern aktuell nur Mutmaßungen angestellt werden. Da dieser Aspekt die Bildgebungsforschung im Gesamten betrifft, profitiert diese im Besonderen von der Kontextualisierung ihrer Resultate mit etablierten klinischen Parametern, wie es nicht zuletzt diese Arbeit demonstriert.

1.5 Zusammenfassung

Bisher lag der Fokus der Bildgebungsforschung zur LE auf den mesiotemporalen Strukturen. Mittels Fixel-basierter Analyse und einem netzwerkbasierten Ansatz demonstriert diese Arbeit, dass auch extratemporale Strukturen der weißen Substanz von der Erkrankung betroffen sind. Zum einen hängt das genaue Muster und das Ausmaß dieser Veränderungen von dem zugrundeliegenden Autoantikörper ab, wobei diese bei GAD65-assoziierter LE bilateral und deutlich weitreichender sind als bei LGI1- und CASPR2-assoziierter LE. Zum anderen lassen sich die veränderten Bildgebungsmarker mit der Verbalgedächtnisleistung und dem Amygdalavolumen der primär betroffenen Hemisphäre in Zusammenhang bringen, die beide als klinisch etablierte Verlaufsparameter der LE gelten und damit die Relevanz dieser *in silico*-Metriken für die klinische Praxis untermauern.

1.6 Literaturverzeichnis

Ahmadi ME, Hagler DJ, McDonald CR, Tecoma ES, Iragui VJ, Dale AM, Halgren E. Side matters: Diffusion tensor imaging tractography in left and right temporal lobe epilepsy. AJNR Am J Neuroradio 2009; 30: 1740–1747

Alexander-Bloch A, Giedd JN, Bullmore ET. Imaging structural co-variance between human brain regions. Nat Rev Neurosci 2013; 14: 322–336

Andersson JLR, Skare S, Ashburner J. How to correct susceptibility distortions in spin-echo echo-planar images: Application to diffusion tensor imaging. Neuroimage 2003; 20: 870–888

Andersson JLR, Sotiropoulos SN. An integrated approach to correction for off-resonance effects and subject movement in diffusion MR imaging. Neuroimage 2016; 125: 1063–1078

Ariño H, Gresa-Arribas N, Blanco Y, Martínez-Hernández E, Sabater L, Petit-Pedrol M, Rouco I, Bataller L, Dalmau JO, Saiz A, Graus F. Cerebellar ataxia and glutamic acid decarboxylase antibodies: immunologic profile and long-term effect of immunotherapy. JAMA Neurol 2014; 71: 1009–1016

Baddeley A. The episodic buffer: a new component of working memory? Trends Cogn Sci 2000; 4: 417–423

Basser PJ, Mattiello J, LeBihan D. Estimation of the effective self-diffusion tensor from the NMR spin echo. J Magn Reson B 1994; 103: 247–254

Bassett DS, Bullmore ET. Human brain networks in health and disease. Curr Opin Neurol 2009; 22: 340–347

Baumgartner A, Rauer S, Mader I, Meyer PT. Cerebral FDG-PET and MRI findings in autoimmune limbic encephalitis: correlation with autoantibody types. J Neurol 2013; 260: 2744–2753

Ben-Ari Y, Holmes GL. Effects of seizures on developmental processes in the immature brain. Lancet Neurol 2006; 5: 1055–1063

Berg AT, Zelko FA, Levy SR, Testa FM. Age at onset of epilepsy, pharmacoresistance, and cognitive outcomes: A prospective cohort study. Neurology 2012; 79: 1384–1391

Bernal B, Ardila A. The role of the arcuate fasciculus in conduction aphasia. Brain 2009; 132: 2309–2316

Bien CG. Management of autoimmune encephalitis. Curr Opin Neurol 2021; 34: 166–171

Bien CG, Elger CE. Limbic encephalitis: A cause of temporal lobe epilepsy with onset in adult life. Epilepsy Behav 2007; 10: 529–538

Bien CG, Urbach H, Schramm J, Soeder BM, Becker AJ, Voltz R, Vincent A, Elger CE. Limbic encephalitis as a precipitating event in adult-onset temporal lobe epilepsy. Neurology 2007; 69: 1236–1244

Binks SNM, Klein CJ, Waters P, Pittock SJ, Irani SR. LGI1, CASPR2 and related antibodies: a molecular evolution of the phenotypes. J Neurol Neurosurg Psychiatry 2017; 89: 526–534

Biswal BB, Van Kylen J, Hyde JS. Simultaneous assessment of flow and BOLD signals in resting-state functional connectivity maps. NMR Biomed 1997; 10: 165–170

Bose G, Zwicker JC, Sitwell LD, Osman N, Fantaneanu TA. Anti-LGI1 Limbic Encephalitis Presenting as an Expanding Insular Lesion. Can J Neurol Sci 2019; 46: 770–772

Bullmore E, Sporns O. Complex brain networks: Graph theoretical analysis of structural and functional systems. Nat Rev Neurosci 2009; 10: 186–198

Bullmore ET, Bassett DS. Brain graphs: graphical models of the human brain connectome. Annu Rev Clin Psychol 2011; 7: 113–140

Caligiuri ME, Labate A, Cherubini A, Mumoli L, Ferlazzo E, Aguglia U, Quattrone A, Gambardella A. Integrity of the corpus callosum in patients with benign temporal lobe epilepsy. Epilepsia 2016; 57: 590–596

Campos BM, Coan AC, Beltramini GC, Liu M, Yassuda CL, Ghizoni E, Beaulieu C, Gross DW, Cendes F. White matter abnormalities associate with type and localization of focal epileptogenic lesions. Epilepsia 2015; 56: 125–132

Catani M, Allin MPG, Husain M, Pugliese L, Mesulam MM, Murray RM, Jones DK. Symmetries in human brain language pathways correlate with verbal recall. Proc Natl Acad Sci U S A 2007; 104: 17163–17168

Chen JJ, Jann K, Wang DJJ. Characterizing Resting-State Brain Function Using Arterial Spin Labeling. Brain Connect 2015; 5: 527–542

Dade M, Giry M, Berzero G, Benazra M, Huberfeld G, Leclercq D, Navarro V, Delattre J-Y, Psimaras D, Alentorn A. Quantitative brain imaging analysis of neurological syndromes associated with anti-GAD antibodies. Neuroimage Clin 2021; 32: 102826

Dalmau J, Graus F. Antibody-Mediated Encephalitis. N Engl J Med 2018; 378: 840–851

Dalmau J, Rosenfeld MR. Paraneoplastic syndromes of the CNS. Lancet Neurol 2008; 7: 327–340

Dalmau J, Vincent A. Do we need to measure specific antibodies in patients with limbic encephalitis? Neurology 2017; 88: 508–509

Dell'Acqua F, Tournier JD. Modelling white matter with spherical deconvolution: How and why? NMR Biomed 2018: 1–18

Desikan RS, Segonne F, Fischl B, Quinn BT, Dickerson BC, Blacker D, Buckner RL, Dale AM, Maguire RP, Hyman BT, Albert MS, Killiany RJ. An automated labeling system for subdividing the human cerebral cortex on MRI scans into gyral based regions of interest. Neuroimage 2006; 31: 968–980

Dhollander T, Clemente A, Singh M, Boonstra F, Civier O, Duque JD, Egorova N, Enticott P, Fuelscher I, Gajamange S, Genc S, Gottlieb E, Hyde C, Imms P, Kelly C, Kirkovski M, Kolbe S, Liang X, Malhotra A, Mito R, Poudel G, Silk TJ, Vaughan DN, Zanin J, Raffelt D, Caeyenberghs K. Fixel-based Analysis of Diffusion MRI: Methods, Applications, Challenges and Opportunities. Neuroimage 2021; 241: 118417

Dubey D, Britton J, McKeon A, Gadoth A, Zekeridou A, Lopez Chiriboga SA, Devine M, Cerhan JH, Dunlay K, Sagen J, Ramberger M, Waters P, Irani SR, Pittock SJ. Randomized Placebo-Controlled Trial of Intravenous Immunoglobulin in Autoimmune LGI1/CASPR2 Epilepsy. Ann Neurol 2020; 87: 313–323

Dubey D, Pittock SJ, Kelly CR, McKeon A, Lopez-Chiriboga AS, Lennon VA, Gadoth A, Smith CY, Bryant SC, Klein CJ, Aksamit AJ, Toledano M, Boeve BF, Tillema JM, Flanagan EP. Autoimmune encephalitis epidemiology and a comparison to infectious encephalitis. Ann Neurol 2018; 83: 166–177

Elger CE, Helmstaedter C, Kurthen M. Chronic epilepsy and cognition. Lancet Neurol 2004; 3: 663–672

Ernst L, David B, Gaubatz J, Domínguez-Narciso I, Lüchters G, Becker AJ, Weber B, Hattingen E, Elger CE, Rüber T. Volumetry of Mesiotemporal Structures Reflects Serostatus in Patients with Limbic Encephalitis. AJNR Am J Neuroradiol 2019; 40: 2081–2089

Evans AC. Networks of anatomical covariance. Neuroimage 2013; 80: 489–504

Falip M, Rodriguez-Bel L, Castañer S, Sala-Padró J, Miro J, Jaraba S, Casasnovas C, Morandeira F, Berdejo J, Carreño M. Hippocampus and Insula Are Targets in Epileptic Patients With Glutamic Acid Decarboxylase Antibodies. Front Neurol 2019; 9: 1143

Farquharson S, Tournier J-D, Calamante F, Fabinyi G, Schneider-Kolsky M, Jackson GD, Connelly A. White matter fiber tractography: why we need to move beyond DTI. J Neurosurg 2013; 118: 1367–1377

Finke C, Prüss H, Heine J, Reuter S, Kopp UA, Wegner F, Bergh FT, Koch S, Jansen O, Münte T, Deuschl G, Ruprecht K, Stöcker W, Klaus-Peterwandinger KP, Paul F, Bartsch T. Evaluation of cognitive deficits and structural hippocampal damage in encephalitis with leucine-rich, glioma-inactivated 1 antibodies. JAMA Neurol 2017; 74: 50–59

Fischl B. FreeSurfer. Neuroimage 2012; 62: 774–781

Fischl B, van der Kouwe A, Destrieux C, Halgren E, Segonne F, Salat DH, Busa E, Seidman LJ, Goldstein J, Kennedy D, Caviness V, Makris N, Rosen B, Dale AM. Automatically parcellating the human cerebral cortex. Cereb Cortex 2004; 14: 11–22

Fornito A, Bullmore ET. Connectomics: a new paradigm for understanding brain disease. Eur Neuropsychopharmacol J Eur Coll Neuropsychopharmacol 2015; 25: 733–748

Foster E, Malpas CB, Ye K, Johnstone B, Carney PW, Velakoulis D, O'Brien TJ, Kwan P. Antiepileptic drugs are not independently associated with cognitive dysfunction. Neurology 2020; 94: e1051–e1061

Frisch C, Malter MP, Elger CE, Helmstaedter C. Neuropsychological course of voltage-gated potassium channel and glutamic acid decarboxylase antibody related limbic encephalitis. Eur J Neurol 2013; 20: 1297–1304

Friston KJ. Functional and effective connectivity: a review. Brain Connect 2011; 1: 13–36

Graus F, Keime-Guibert F, Reñe R, Benyahia B, Ribalta T, Ascaso C, Escaramis G, Delattre JY. Anti-Hu-associated paraneoplastic encephalomyelitis: analysis of 200 patients. Brain 2001; 124: 1138–1148

Graus F, Saiz A, Dalmau J. Antibodies and neuronal autoimmune disorders of the CNS. J Neurol 2010; 257: 509–517

Graus F, Titulaer MJ, Balu R, Benseler S, Bien CG, Cellucci T, Cortese I, Dale RC, Gelfand JM, Geschwind M, Glaser CA, Honnorat J, Höftberger R, Iizuka T, Irani SR, Lancaster E, Leypoldt F, Prüss H, Rae-Grant A, Reindl M, Rosenfeld MR, Rostásy K, Saiz A, Venkatesan A, Vincent A, Wandinger K-P, Waters P, Dalmau J. A clinical approach to diagnosis of autoimmune encephalitis. Lancet Neurol 2016; 15: 391–404

Griffa A, Baumann PS, Thiran J-P, Hagmann P. Structural connectomics in brain diseases. Neuroimage 2013; 80: 515–526

Griffith SP, Malpas CB, Alpitsis R, O'Brien TJ, Monif M. The neuropsychological spectrum of anti-LGI1 antibody mediated autoimmune encephalitis. J Neuroimmunol 2020; 345: 577271

Gultekin SH, Rosenfeld MR, Voltz R, Eichen J, Posner JB, Dalmau J. Paraneoplastic limbic encephalitis: neurological symptoms, immunological findings and tumour association in 50 patients. Brain 2000; 123: 1481–1494

Hagmann P, Cammoun L, Gigandet X, Meuli R, Honey CJ, Van Wedeen J, Sporns O. Mapping the structural core of human cerebral cortex. PLoS Biol 2008; 6: 1479–1493

Hagmann P, Jonasson L, Maeder P, Thiran J-P, Wedeen VJ, Meuli R. Understanding diffusion MR imaging techniques: from scalar diffusion-weighted imaging to diffusion tensor imaging and beyond. Radiographics 2006; 26: S205-S223

Hagmann P, Kurant M, Gigandet X, Thiran P, Wedeen VJ, Meuli R, Thiran J-P. Mapping Human Whole-Brain Structural Networks with Diffusion MRI. PLoS One 2007; 2: e597

He Y, Chen ZJ, Evans AC. Small-world anatomical networks in the human brain revealed by cortical thickness from MRI. Cereb Cortex 2007; 17: 2407–2419

Heine J, Prüss H, Bartsch T, Ploner CJ, Paul F, Finke C. Imaging of autoimmune encephalitis - Relevance for clinical practice and hippocampal function. Neuroscience 2015; 309: 68–83

Heine J, Prüss H, Kopp UA, Wegner F, Then Bergh F, Münte T, Wandinger KP, Paul F, Bartsch T, Finke C. Beyond the limbic system: Disruption and functional compensation of large-scale brain networks in patients with anti-LGI1 encephalitis. J Neurol Neurosurg Psychiatry 2018: 1191–1199

Helmstaedter C, Durwen HF. VLMT: Verbaler Lern- und Merkfähigkeitstest: Ein praktikables und differenziertes Instrumentarium zur Prüfung der verbalen Gedächtnisleistungen. Schweiz Arch Neurol Neurochir Psychiatr 1990; 141: 21–30

Helmstaedter C, Pohl C, Hufnagel A, Elger CE. Visual Learning Deficits in Nonresected Patients with Right Temporal Lobe Epilepsy. Cortex 1991; 27: 547–555

Hermann BP, Seidenberg M, Dow C, Jones J, Rutecki P, Bhattacharya A, Bell B. Cognitive prognosis in chronic temporal lobe epilepsy. Ann Neurol 2006; 60: 80–87

Het S, Ramlow G, Wolf OT. A meta-analytic review of the effects of acute cortisol administration on human memory. Psychoneuroendocrinology 2005; 30: 771–784

van den Heuvel MP, Hulshoff Pol HE. Exploring the brain network: a review on resting-state fMRI functional connectivity. Eur Neuropsychopharmacol 2010; 20: 519–534

van den Heuvel MP, Stam CJ, Boersma M, Hulshoff Pol HE. Small-world and scale-free organization of voxel-based resting-state functional connectivity in the human brain. Neuroimage 2008; 43: 528–539

Hoffmann LA, Jarius S, Pellkofer HL, Schueller M, Krumbholz M, Koenig F, Johannis W, la Fougere C, Newman T, Vincent A, Voltz R. Anti-Ma and anti-Ta associated paraneoplastic neurological syndromes: 22 newly diagnosed patients and review of previous cases. J Neurol Neurosurg Psychiatry 2008; 79: 767–773

Honnorat J, Saiz A, Giometto B, Vincent A, Brieva L, de Andres C, Maestre J, Fabien N, Vighetto A, Casamitjana R, Thivolet C, Tavolato B, Antoine JC, Trouillas P, Graus F. Cerebellar Ataxia With Anti–Glutamic Acid Decarboxylase Antibodies: Study of 14 Patients. Arch Neurol 2001; 58: 225–230.

Irani SR, Alexander S, Waters P, Kleopa KA, Pettingill P, Zuliani L, Peles E, Buckley C, Lang B, Vincent A. Antibodies to Kv1 potassium channel-complex proteins leucine-rich, glioma inactivated 1 protein and contactin-associated protein-2 in limbic encephalitis, Morvan's syndrome and acquired neuromyotonia. Brain 2010; 133: 2734–2748

Irani SR, Michell AW, Lang B, Pettingill P, Waters P, Johnson MR, Schott JM, Armstrong RJE, S. Zagami A, Bleasel A, Somerville ER, Smith SMJ, Vincent A. Faciobrachial dystonic seizures precede Lgi1 antibody limbic encephalitis. Ann Neurol 2011; 69: 892–900

Irani SR, Stagg CJ, Schott JM, Rosenthal CR, Schneider SA, Pettingill P, Pettingill R, Waters P, Thomas A, Voets NL, Cardoso MJ, Cash DM, Manning EN, Lang B, Smith SJM, Vincent A, Johnson MR. Faciobrachial dystonic seizures: The influence of immunotherapy on seizure control and prevention of cognitive impairment in a broadening phenotype. Brain 2013; 136: 3151–3162

Jenkinson M, Beckmann CF, Behrens TEJ, Woolrich MW, Smith SM. FSL. Neuroimage 2012; 62: 782–790

Jeurissen B, Leemans A, Tournier JD, Jones DK, Sijbers J. Investigating the prevalence of complex fiber configurations in white matter tissue with diffusion magnetic resonance imaging. Hum Brain Mapp 2013; 34: 2747–2766

Jeurissen B, Tournier JD, Dhollander T, Connelly A, Sijbers J. Multi-tissue constrained spherical deconvolution for improved analysis of multi-shell diffusion MRI data. Neuroimage 2014; 103: 411–426

Jones DK, Knösche TR, Turner R. White matter integrity, fiber count, and other fallacies: The do's and don'ts of diffusion MRI. Neuroimage 2013; 73: 239–254

Kotsenas AL, Watson RE, Pittock SJ, Britton JW, Hoye SL, Quek AML, Shin C, Klein CJ. MRI Findings in Autoimmune Voltage-Gated Potassium Channel Complex Encephalitis with Seizures: One Potential Etiology for Mesial Temporal Sclerosis. AJNR Am J Neuroradiol 2014; 35: 84–89

Lai M, Huijbers MG, Lancaster E, Graus F, Bataller L, Balice-Gordon R, Cowell JK, Dalmau J. Investigation of LGI1 as the antigen in limbic encephalitis previously attributed to potassium channels: a case series. Lancet Neurol 2010; 9: 776–785

Li W, Wu S, Meng Q, Zhang X, Guo Y, Cong L, Cong S, Zheng D. Clinical characteristics and short-term prognosis of LGI1 antibody encephalitis: a retrospective case study. BMC Neurol 2018; 18: 96

Loane C, Argyropoulos GPD, Roca-Fernández A, Lage C, Sheerin F, Ahmed S, Zamboni G, Mackay C, Irani SR, Butler CR. Hippocampal network abnormalities explain amnesia after VGKCC-Ab related autoimmune limbic encephalitis. J Neurol Neurosurg Psychiatry 2019: 1–10

Maldonado IL, Moritz-Gasser S, Duffau H. Does the left superior longitudinal fascicle subserve language semantics? A brain electrostimulation study. Brain Struct Funct 2011; 216: 263–274

Malter MP, Helmstaedter C, Urbach H, Vincent A, Bien CG. Antibodies to glutamic acid decarboxylase define a form of limbic encephalitis. Ann Neurol 2010; 67: 470–478

Navarro V, Kas A, Apartis E, Chami L, Rogemond V, Levy P, Psimaras D, Habert M-O, Baulac M, Delattre J-Y, Honnorat J, Collaborators. Motor cortex and hippocampus are the two main cortical targets in LGI1-antibody encephalitis. Brain 2016; 139: 1079–1093

Onnela J-P, Saramäki J, Kertész J, Kaski K. Intensity and coherence of motifs in weighted complex networks. Phys Rev E 2005; 71: 065103

Otte WM, Van Eijsden P, Sander JW, Duncan JS, Dijkhuizen RM, Braun KPJ. A meta-analysis of white matter changes in temporal lobe epilepsy as studied with diffusion tensor imaging. Epilepsia 2012; 53: 659–667

Park H-J, Friston K. Structural and functional brain networks: from connections to cognition. Science 2013; 342: 1238411

Pittock SJ, Lucchinetti CF, Parisi JE, Benarroch EE, Mokri B, Stephan CL, Kim K-K, Kilimann MW, Lennon VA. Amphiphysin autoimmunity: paraneoplastic accompaniments. Ann Neurol 2005; 58: 96–107

Pittock SJ, Yoshikawa H, Ahlskog JE, Tisch SH, Benarroch EE, Kryzer TJ, Lennon VA. Glutamic acid decarboxylase autoimmunity with brainstem, extrapyramidal, and spinal cord dysfunction. Mayo Clin Proc 2006; 81: 1207–1214

Plantone D, Renna R, Grossi D, Plantone F, Iorio R. Teaching NeuroImages: Basal ganglia involvement in facio-brachial dystonic seizures associated with LGI1 antibodies. Neurology 2013; 80: e183–e184

Raffelt D, Tournier JD, Rose S, Ridgway GR, Henderson R, Crozier S, Salvado O, Connelly A. Apparent Fibre Density: A novel measure for the analysis of diffusion-weighted magnetic resonance images. Neuroimage 2012; 59: 3976–3994

Raffelt DA, Smith RE, Ridgway GR, Tournier JD, Vaughan DN, Rose S, Henderson R, Connelly A. Connectivity-based fixel enhancement: Whole-brain statistical analysis of diffusion MRI measures in the presence of crossing fibres. Neuroimage 2015; 117: 40–55

Raffelt DA, Tournier JD, Smith RE, Vaughan DN, Jackson G, Ridgway GR, Connelly A. Investigating white matter fibre density and morphology using fixel-based analysis. Neuroimage 2017; 144: 58–73

Rodriguez A, Klein CJ, Sechi E, Alden E, Basso MR, Pudumjee S, Pittock SJ, McKeon A, Britton JW, Lopez-Chiriboga AS, Zekeridou A, Zalewski NL, Boeve BF, Day GS, Gadoth A, Burkholder D, Toledano M, Dubey D, Flanagan EP. LGI1 antibody encephalitis: acute treatment comparisons and outcome. J Neurol Neurosurg Psychiatry 2022; 93: 309–315

Rubinov M, Sporns O. Complex network measures of brain connectivity: Uses and interpretations. Neuroimage 2010; 52: 1059–1069

Saiz A, Blanco Y, Sabater L, González F, Bataller L, Casamitjana R, Ramió-Torrentà L, Graus F. Spectrum of neurological syndromes associated with glutamic acid decarboxylase antibodies: diagnostic clues for this association. Brain 2008; 131: 2553–2563

Seidlitz J, Váša F, Shinn M, Romero-Garcia R, Whitaker KJ, Vértes PE, Wagstyl K, Kirkpatrick Reardon P, Clasen L, Liu S, Messinger A, Leopold DA, Fonagy P, Dolan RJ, Jones PB, Goodyer IM, NSPN Consortium, Raznahan A, Bullmore ET. Morphometric Similarity Networks Detect Microscale Cortical Organization and Predict Inter-Individual Cognitive Variation. Neuron 2018; 97: 231-247

Shin Y-W, Lee S-T, Shin J-W, Moon J, Lim J-A, Byun J-I, Kim T-J, Lee K-J, Kim Y-S, Park K-I, Jung K-H, Lee SK, Chu K. VGKC-complex/LGI1-antibody encephalitis: clinical manifestations and response to immunotherapy. J Neuroimmunol 2013; 265: 75–81

Smith RE, Tournier J-D, Calamante F, Connelly A. The effects of SIFT on the reproducibility and biological accuracy of the structural connectome. Neuroimage 2015; 104: 253–265

Smith RE, Tournier JD, Calamante F, Connelly A. SIFT: Spherical-deconvolution informed filtering of tractograms. Neuroimage 2013; 67: 298–312

Smitha K, Akhil Raja K, Arun K, Rajesh P, Thomas B, Kapilamoorthy T, Kesavadas C. Resting state fMRI: A review on methods in resting state connectivity analysis and resting state networks. Neuroradiol J 2017; 30: 305–317

Smits M, Jiskoot LC, Papma JM. White Matter Tracts of Speech and Language. Semin Ultrasound CT MR 2014; 35: 504–516

van Sonderen A, Petit-Pedrol M, Dalmau J, Titulaer MJ. The value of LGI1, Caspr2 and voltage-gated potassium channel antibodies in encephalitis. Nat Rev Neurol 2017; 13: 290–301

Sporns O, Tononi G, Kötter R. The Human Connectome: A Structural Description of the Human Brain. PLoS Comput Biol 2005; 1: e42

Thiebaut de Schotten M, ffytche DH, Bizzi A, Dell'Acqua F, Allin M, Walshe M, Murray R, Williams SC, Murphy DGM, Catani M. Atlasing location, asymmetry and inter-subject variability of white matter tracts in the human brain with MR diffusion tractography. Neuroimage 2011; 54: 49–59

Toledano M, Britton JW, McKeon A, Shin C, Lennon VA, Quek AML, So E, Worrell GA, Cascino GD, Klein CJ, Lagerlund TD, Wirrell EC, Nickels KC, Pittock SJ. Utility of an immunotherapy trial in evaluating patients with presumed autoimmune epilepsy. Neurology 2014; 82: 1578–1586

Tournier JD, Calamante F, Connelly A. Determination of the appropriate b value and number of gradient directions for high-angular-resolution diffusion-weighted imaging. NMR Biomed 2013; 26: 1775–1786

Tournier J-D, Smith R, Raffelt D, Tabbara R, Dhollander T, Pietsch M, Christiaens D, Jeurissen B, Yeh C-H, Connelly A. MRtrix3: A fast, flexible and open software framework for medical image processing and visualisation. Neuroimage 2019; 202: 116137

Tripathi Madhavi, Tripathi Manjari, Roy SG, Parida GK, Ihtisham K, Dash D, Damle N, Shamim SA, Bal C. Metabolic topography of autoimmune non-paraneoplastic encephalitis. Neuroradiology 2018; 60: 189–198

Tustison NJ, Cook PA, Gee JC. N4ITK: Improved N3 Bias Correction. IEEE Trans Med Imaging 2011; 29: 1310–1320

Tzourio-Mazoyer N, Landeau B, Papathanassiou D, Crivello F, Etard O, Delcroix N, Mazoyer B, Joliot M. Automated anatomical labeling of activations in SPM using a macroscopic anatomical parcellation of the MNI MRI single-subject brain. Neuroimage 2002; 15: 273–289

Urbach H, Rauer S, Mader I, Paus S, Wagner J, Malter MP, Prüss H, Lewerenz J, Kassubek J, Hegen H, Auer M, Deisenhammer F, Ufer F, Bien CG, Baumgartner A. Supratentorial white matter blurring associated with voltage-gated potassium channel-complex limbic encephalitis. Neuroradiology 2015; 57: 1203–1209.

Vaughan DN, Raffelt D, Curwood E, Tsai MH, Tournier JD, Connelly A, Jackson GD. Tract-specific atrophy in focal epilepsy: Disease, genetics, or seizures? Ann Neurol 2017; 81: 240–250

Veraart J, Fieremans E, Novikov DS. Diffusion MRI noise mapping using random matrix theory. Magn Reson Med 2016; 76: 1582–1593

Vernooij MW, Smits M, Wielopolski PA, Houston GC, Krestin GP, van der Lugt A. Fiber density asymmetry of the arcuate fasciculus in relation to functional hemispheric language lateralization in both right- and left-handed healthy subjects: A combined fMRI and DTI study. Neuroimage 2007; 35: 1064–1076

Wagner J, Schoene-Bake J-C, Malter MP, Urbach H, Huppertz H-J, Elger CE, Weber B. Quantitative FLAIR analysis indicates predominant affection of the amygdala in antibody-associated limbic encephalitis. Epilepsia 2013; 54: 1679–1687

Wagner J, Schoene-Bake JC, Witt JA, Helmstaedter C, Malter MP, Stoecker W, Probst C, Weber B, Elger CE. Distinct white matter integrity in glutamic acid decarboxylase and voltage-gated potassium channel-complex antibody-associated limbic encephalitis. Epilepsia 2016; 57: 475–483

Wagner J, Weber B, Elger CE. Early and chronic gray matter volume changes in limbic encephalitis revealed by voxel-based morphometry. Epilepsia 2015a; 56: 754–761

Wagner J, Witt J-A, Helmstaedter C, Malter MP, Weber B, Elger CE. Automated volumetry of the mesiotemporal structures in antibody-associated limbic encephalitis. J Neurol Neurosurg Psychiatry 2015b; 86: 735–742

Wang J, Wang L, Zang Y, Yang H, Tang H, Gong Q, Chen Z, Zhu C, He Y. Parcellation-dependent small-world brain functional networks: a resting-state fMRI study. Hum Brain Mapp 2009; 30: 1511–1523

Wheeler-Kingshott CAM, Cercignani M. About „axial“ and „radial“ diffusivities. Magn Reson Med 2009; 61: 1255–1260

Whelan CD, Alhusaini S, O'Hanlon E, Cheung M, Iyer PM, Meaney JF, Fagan AJ, Boyle G, Delanty N, Doherty CP, Cavalleri GL. White matter alterations in patients with MRI-negative temporal lobe epilepsy and their asymptomatic siblings. Epilepsia 2015; 56: 1551–1561

Wig GS, Laumann TO, Cohen AL, Power JD, Nelson SM, Glasser MF, Miezin FM, Snyder AZ, Schlaggar BL, Petersen SE. Parcellating an Individual Subject's Cortical and Subcortical Brain Structures Using Snowball Sampling of Resting-State Correlations. Cereb Cortex 2014; 24: 2036–2054

Witt J-A, Helmstaedter C. Neuropsychological Evaluations in Limbic Encephalitis. Brain Sci 2021; 11: 576

Witt J-A, Helmstaedter C. How can we overcome neuropsychological adverse effects of antiepileptic drugs? Expert Opin Pharmacother 2017; 18: 551–554

Yeo BT, Krienen FM, Sepulcre J, Sabuncu MR, Lashkari D, Hollinshead M, Roffman JL, Smoller JW, Zollei L, Polimeni JR, Fischl B, Liu H, Buckner RL. The organization of the human cerebral cortex estimated by intrinsic functional connectivity. J Neurophysiol 2011; 106: 1125–1165

Zalesky A, Fornito A, Bullmore ET. On the use of correlation as a measure of network connectivity. Neuroimage 2012; 60: 2096–2106

Zalesky A, Fornito A, Bullmore ET. Network-based statistic: Identifying differences in brain networks. Neuroimage 2010; 53: 1197–1207

2. Veröffentlichungen

2.1 Originalpublikation in *Neuroimage:Clinical*

NeuroImage: Clinical 27 (2020) 102289

Contents lists available at ScienceDirect

NeuroImage: Clinical

journal homepage: www.elsevier.com/locate/ynicl

Fixel-based analysis links white matter characteristics, serostatus and clinical features in limbic encephalitis

Tobias Bauer[a,1], Leon Ernst[a,1], Bastian David[a], Albert J. Becker[b], Jan Wagner[c], Juri-Alexander Witt[a], Christoph Helmstaedter[a], Bernd Weber[d], Elke Hattingen[e], Christian E. Elger[a], Rainer Surges[a], Theodor Rüber[a,f,g,*]

[a] Department of Epileptology, University Hospital Bonn, Venusberg-Campus 1, 53127 Bonn, Germany
[b] Department of Neuropathology, University Hospital Bonn, Venusberg-Campus 1, 53127 Bonn, Germany
[c] Department of Neurology, University of Ulm and Universitäts- and Rehabilitationskliniken, 89070 Ulm, Germany
[d] Institute of Experimental Epileptology and Cognition Research, University Hospital Bonn, Venusberg-Campus 1, 53127 Bonn, Germany
[e] Department of Neuroradiology, Goethe University Frankfurt, Schleusenweg 2, 60528 Frankfurt, Germany
[f] Epilepsy Center Frankfurt Rhine-Main, Department of Neurology, Goethe University Frankfurt, Schleusenweg 2, 60528 Frankfurt, Germany
[g] Center for Personalized Translational Epilepsy Research (CePTER), Goethe University Frankfurt, Schleusenweg 2, 60528 Frankfurt, Germany

A B S T R A C T

Limbic encephalitis (LE) is an autoimmune syndrome often associated with temporal lobe epilepsy. Recent research suggests that particular structural changes in LE depend on the type of the associated antibody and occur in both mesiotemporal gray matter and white matter regions. However, it remains questionable to what degree conventional diffusion tensor imaging (DTI)-methods reflect alterations in white matter microstructure, since these methods do not account for crossing fibers. To address this methodological shortcoming, we applied fixel-based analysis as a novel technique modeling distinct fiber populations. For our study, 19 patients with LE associated with autoantibodies against glutamic acid decarboxylase 65 (GAD-LE, mean age = 35.9 years, 11 females), 4 patients with LE associated with autoantibodies against leucine-rich glioma-inactivated 1 (LGI1-LE, mean age = 63.3 years, 2 females), 5 patients with LE associated with contactin-associated protein-like 2 (CASPR2, mean age = 57.4, 0 females), 20 age- and gender-matched control patients with hippocampal sclerosis (19 GAD-LE control patients: mean age = 35.1 years, 11 females; 4 LGI1-LE control patients: mean age = 52.6 years, 2 females; 5 CASPR2-LE control patients: mean age = 42.7 years, 0 females; 10 patients are included in more than one group) and 33 age- and gender-matched healthy control subjects (19 GAD-LE healthy controls: mean age = 34.6 years, 11 females; 8 LGI1-LE healthy controls: mean age = 57.0 years, 4 females, 10 CASPR2-LE healthy controls: mean age = 57.2 years, 0 females; 4 subjects are included in more than one group) underwent structural imaging and DTI at 3 T and neuropsychological testing. Patient images were oriented according to lateralization in EEG resulting in an *affected* and *unaffected* hemisphere. Fixel-based metrics fiber density (FD), fiber cross-section (FC), and fiber density and cross-section (FDC = FD · FC) were calculated to retrieve information about white matter integrity both on the micro- and the macroscale. As compared to healthy controls, patients with GAD-LE showed significantly (family-wise error-corrected, $p < 0.05$) lower FDC in the superior longitudinal fascicle bilaterally and in the isthmus of the corpus callosum. In CASPR2-LE, lower FDC in the superior longitudinal fascicle was only present in the *affected* hemisphere. In LGI1-LE, we did not find any white matter alteration of the superior longitudinal fascicle. In an explorative tract-based correlation analysis within the GAD-LE group, only a correlation between the left/right ratio of FC values of the superior longitudinal fascicle and verbal memory performance ($R = 0.64$, Holm-Bonferroni corrected $p < 0.048$) remained significant after correcting for multiple comparisons. Our results underscore the concept of LE as a disease comprising a broad and heterogeneous group of entities and contribute novel aspects to the pathomechanistic understanding of this disease that may strengthen the role of MRI in the diagnosis of LE.

1. Introduction

Limbic encephalitis (LE) is an autoimmune disease characterized by subacute short-term memory loss and psychiatric conspicuity. It often involves temporal lobe epilepsy (Bien and Elger, 2007; Graus et al., 2010; Dalmau and Graus, 2018). To date, a variety of autoantibodies related to different LE subtypes have been identified. Antibodies against the intracellular antigen glutamic acid decarboxylase 65 (GAD) and against the extracellular antigen voltage-gated potassium channel complex (VGKC) rank among the most common autoantibodies associated with LE (Dubey et al., 2018). Within the VGKC-complex, two components that are targeted by different autoantibodies have been found (Irani et al., 2010; Lai et al., 2010; van Sonderen et al., 2017; Binks et al., 2017): Leucine-rich glioma-inactivated 1 (LGI1) and contactin-associated protein-like 2 (CASPR2). Even though different LE subtypes share clinical features, they differ in relevant aspects such as

Corresponding author.
* *E-mail address:* theodor.rueber@ukbonn.de (T. Rüber).
[1] Equal contribution.

https://doi.org/10.1016/j.nicl.2020.102289
Received 4 December 2019; Received in revised form 22 April 2020; Accepted 24 April 2020
Available online 26 May 2020

Table 1
Demographic- and clinical data of all patient- and control groups. All values are arithmetic group means (range). Verbal memory test: VLMT Helmstaedter et al. (2001), figural memory test: DCS-R Helmstaedter et al. (1991), memory parameters were standardized according to a conormalization sample of 488 healthy volunteers (mean = 100, standard deviation = 10), applying a correction for age. [a]one subject is included in both groups, [b]3 subjects are included in both groups, [c]4 subjects are included in both groups, [d]4 subjects are included in both groups, [e]2 subjects are included in both groups, NA: not applicable, y: years.

	LE			controls			HS			ANOVA
Group	GAD	LGI1	CASPR2	(GAD)	(LGI1)	(CASPR2)	(GAD)	(LGI1)	(CASPR2)	*p*
Number	19	4	5	19[a]	8[b]	10[a,b]	19[c,d]	4[c,e]	5[d,e]	NA
Female (%)	11 (58)	2 (50)	0 (0)	11 (58)	4 (50)	0 (0)	11 (58)	2 (50)	0 (0)	NA
Lateralization right (%)	5 (26)	2 (50)	1 (20)	NA	NA	NA	7 (37)	2 (50)	1 (20)	NA
Age (y)	35.9 (20–61)	63.3 (57–69)	57.4 (40–72)	34.6 (20–50)	57.0 (23–67)	57.2 (44–67)	35.1 (18–59)	52.6 (46–59)	42.7 (26–50)	<0.001
Age at onset (y)	31.2 (16–56)	61.4 (57–67)	54.4 (39–69)	NA	NA	NA	15.7 (0–34)	6.5 (0–14)	9.3 (0–30)	<0.001
Disease duration (y)	4.6 (0–22)	1.9 (0–5)	3.0 (1–5)	NA	NA	NA	19.3 (5–47)	46.0 (40–50)	33.5 (15–50)	<0.001
Verbal memory	96.7 (71–108)	83.6 (70–108)	88.8 (78–92)	NA	NA	NA	86.1 (63–100)	90.5 (80–99)	84.5 (77–91)	0.065
Figural memory	88.5 (65–108)	77.5 (61–99)	91.9 (81–107)	NA	NA	NA	84.1 (61–102)	84.3 (75–87)	80.8 (66–87)	0.595
Seizure-free (%)	4 (21)	3 (75)	2 (40)	NA	NA	NA	1 (5)	0 (0)	1 (20)	NA

comorbidities and, most relevant, their response to immunotherapy (Quek et al., 2012). As the presence of pathologic neuronal autoantibodies yet undiscovered may not be excluded by negative antibody testing, diagnostic weight is added on clinical examinations and magnetic resonance imaging (MRI) (Dalmau and Vincent, 2017). Recent research indicates that MRI features of LE depend on the type of autoantibody harbored by the patient. Mesiotemporal structures have been shown to be initially- and predominantly affected by LE; in particular amygdala and hippocampal swelling has been described (Ernst et al., 2019; Heine et al., 2015; Wagner et al., 2015; Fredriksen et al., 2018). Besides, there is growing evidence for serospecific structural alterations also in white matter regions caused by the disease. While a recent study investigating white matter features of LE by means of diffusion tensor imaging (DTI) found widespread alterations of diffusivity parameters in patients with GAD-autoantibody associated LE (GAD-LE), no white matter alterations in patients with VGKC-autoantibody associated LE have been observed (Wagner et al., 2016). However, the accuracy of conventional DTI-methods for reflecting the result of pathophysiological processes in white matter remains questionable. Conventional DTI relies on measures averaged across the volume of one voxel, despite the fact that roughly 90% of white matter voxels contain multiple fiber orientations (Jeurissen et al., 2013). To address this issue in the present study, we chose to apply fixel-based analysis, where metrics are derived from the specific estimated fiber orientation distribution for each white matter voxel (Raffelt et al., 2017). Here, two metrics are combined for each distinct fiber population within a voxel: Fiber cross-section (FC) provides information on a macroscale, while fiber density (FD) assesses microstructural properties. By combining information on both scales, we hypothesized fixel-based analysis to draw a more detailed picture of white matter alterations to enhance future diagnostics. Studies applying fixel-based analysis to patients with hippocampal sclerosis (HS) found tract-specific atrophy on both hemispheres (Vaughan et al., 2017). In this study, we aimed to compare GAD-LE, LGI1-associated LE (LGI1-LE), CASPR2-associated LE (CASPR2-LE), chronic temporal lobe epilepsy patients with HS and healthy controls to investigate the disturbed structure–function relationship, hoping to unmask structural underpinnings of clinical and neuropsychological alterations in LE patients.

2. Materials and methods

2.1. Study groups

This study comprised three experimental and two control groups: GAD-LE, LGI1-LE and CASPR2-LE formed three study groups. Patients with hippocampal sclerosis (HS) and healthy subjects constituted two control groups. First, we prospectively ascertained 19 patients with GAD-LE (mean age = 35.9 years, 11 females), 4 patients with LGI1-LE (mean age = 63.3, 2 females) and 5 patients with CASPR2-LE (mean age = 57.4, 0 females) who presented at the Department of Epileptology at the University Hospital Bonn between April 2008 and November 2016. All patients included in this study were diagnosed with autoimmune limbic encephalitis according to the widely acknowledged diagnostic criteria set forth by Graus et al. (2016). Results of conventional DTI-analysis of a partly overlapping study group were previously published by Wagner et al. (2016). Moreover, autoantibodies against either GAD, LGI1 or CASPR2 were serologically proven in all patients included in this study (see below). Disease onset was defined as the onset of the first LE-associated symptoms. Second, we included 20 matched patients (mean age = 34.1, 11 females) with histologically confirmed HS and no suspicion of LE who presented for presurgical evaluation at our department between May 2008 and October 2013. This additional control group was included since we aimed to specifically detect autoimmune-mediated structural alterations caused by the respective autoantibodies and not those alterations that occur due to persistent temporal lobe epilepsy. HS subjects were individually matched to GAD-, LGI1- and CASPR2-LE with respect to the age at study, gender and the affected hemisphere. Subjects with dual pathologies were excluded from the study. Third, we composed three age- and gender-matched groups of healthy subjects with no history of neurological or psychiatric disorders from a pre-existing in-house database to be contrasted to GAD-LE, LGI1-LE and CASPR2-LE, respectively (GAD-LE healthy controls: mean age = 34.6 years, 11 females; LGI1-LE healthy controls: mean age = 57.0 years, 4 females; CASPR2-LE healthy controls: mean age = 57.2 years, 0 females). For the LGI1-LE and CASPR2-LE healthy control groups, two healthy subjects were matched to each patient to increase statistical power. Clinical data of all patients including memory performance (Verbal memory: VLMT; Helmstaedter et al. (2001), figural memory: DCS-R; Helmstaedter et al. (1991)) were retrieved from our in-house database. See Table 1 for groups characteristics (further details are provided in Supplementary Tables S1–S4). The study was approved by the Internal Review Board of the University Hospital Bonn and all participants provided written informed consent.

2.2. Antibody testing

From 2014 on, screening for onco-neuronal antibodies was performed using semiquantitative immunoblots (EUROLINE PNS 12, Euroimmun, DL 1111–1601-7 G) coated with recombinant antigen or antigen fragments (dilution: serum 1:100, cerebrospinal fluid: 1:1). Moreover, immunocytochemistry was performed using HEK293-cells (Human Embryonic Kidney 293) with expression of antigens on the cell surface (IIFT: Autoimmune-Enzephalitis-Mosaik1, Euroimmun, FA

1120–1005-1; GAD65-IIFT, Euroimmun, FA 1022–1005-50) for NMDAR-, CASPR, LGI1, GABAA-, GABAB-, AMPAR- and GAD65-autoantibodies (dilution: serum 1:10, cerebrospinal fluid: 1:1). Before 2014, detection of GAD antibodies in serum was performed by using an Anti-125 I-GAD-radioimmunoprecipitation assay (normal values ≤1 U/ml; Weatherall Institute, Oxford, UK, or Euroimmun, Lübeck, Germany). VGKC-complex antibodies were detected by radioimmunoprecipitation assay (normal values < 100 pM; Weatherall Institute or Euroimmun). Antibodies against LGI1 and CASPR2 were examined by indirect immunofluorescence using formalin fixed HEK293 cells containing membrane bound LGI1 or CASPR2 (normal values <1 : 10; all tests performed by Euroimmun).

2.3. Neuropsychological assessment

Neuropsychological testing was performed within 100 days of the scan. Abilities in figural learning and the overall memory performance were assessed using the revised *Diagnosticum fuer Cerebralschaedigung* (DCR-R; Helmstaedter et al. (1991)). Abilities in verbal learning and the overall memory performance were assessed using the verbal learning and memory test (VLMT; Helmstaedter et al. (2001)). Memory parameters were standardized according to a conormalization sample of 488 healthy volunteers (mean = 100, standard deviation = 10), applying a correction for age.

2.4. MRI examinations

Diffusion Tensor Imaging (DTI) for all subjects was performed at the Life & Brain Center in Bonn using a 3 Tesla MRI-Scanner (Magnetom Trio, Siemens Healthineers, Erlangen, Germany). Diffusion-weighted data were acquired using single shot spin-echo echo-planar imaging. Due to a scanner update in early 2014, two different acquisition protocols were used. Parameters before the update were TR = 12 s, TE = 100 ms using an eight channel headcoil, parameters after the update were TR = 9 s, TE = 87 ms using a 32 channel headcoil. Both protocols acquired 72 axial slices, matrix 128 × 128, voxel size 1.72 mm × 1.72 mm × 1.7 mm and in both protocols, diffusion weighting was isotropically distributed along 60 directions at b = 1000 s · mm^{-2}. Six images with $b = 0$ were acquired initially and following each series of ten diffusion-weighted images. Healthy control groups were matched with regard to sequences before and after the scanner update.

2.5. Reorientation of images

Cortical reconstruction and volumetric segmentation of T1-weighted images was performed using FreeSurfer (version 6.0; Fischl et al. (2002); http://surfer.nmr.mgh.harvard.edu). As it remains unclear whether LE is a predominantly unihemispheric process (Navarro et al., 2016), we defined either the right, the left or both hemispheres as *affected* hemispheres using a two-step classification scheme according to Ernst et al. (2019). Interictal EEG data acquired during the same hospital stay as the MRI examination were used as primary criterion: The hemispheres presenting pathological interictal EEG potentials were classified as the *affected* hemisphere. If EEG data were not available, we used the right/left amygdala volumetric ratio, calculated as $2(V_R - V_L)/(V_R + V_L)$, as a secondary criterion: If the amygdala volumetric ratio was in the upper quartile as compared to controls, the right hemisphere was defined as *affected* hemisphere. If the amygdala volumetric ratio was in the lower quartile as compared to controls, the left hemisphere was defined as *affected* hemisphere. In between, we regarded both hemispheres as *affected*. For whole-brain fixel-based analysis and subsequent group-wise comparisons, we flipped all LE and HS patients with affected right hemispheres along the left–right axis. For ROI-wise correlation analysis with neuropsychological tests, we used the native (unflipped) image orientation.

2.6. Fixel-based preprocessing

Fixel-based analysis was performed using the MRtrix3 toolbox (The Florey Institute, Melbourne, Australia; http://mrtrix.readthedocs.io). The principle behind this approach is to use constrained spherical deconvolution and probabilistic tractography to compute metrics on anatomically plausible fiber populations. Preprocessing of diffusion-weighted images included denoising (Veraart et al., 2016), motion and eddy current distortion correction (Andersson et al., 2003; Andersson and Sotiropoulos, 2016) using the FMRIB software library (FSL, Version 5.0; Jenkinson et al. (2012); http://www.fmrib.ox.ac.uk/fsl) and N4 bias field correction (Tustison et al., 2011). Next, we performed group intensity normalization to the median white matter b = 0 signal and upsampled images to (1.3 mm)^3 voxel size in order to improve downstream spatial normalization statistics. We computed a group average single-shell white matter response function (Tournier et al., 2013), performed constrained spherical deconvolution (Jeurissen et al., 2014) in order to estimate the fiber orientation distribution function (FOD) for all subjects and generated a study-specific group FOD template from a representative subgroup comprising 45 images. FOD template and subject FOD images were segmented to discrete fixels (Smith et al., 2013). Subject FOD and all subsequent images were then registered to the group template. Subsequently, we calculated values for FD (Raffelt et al., 2012), and FC (Raffelt et al., 2017) for all subject fixel images. Furthermore, we computed fiber density and cross-section as FDC = FD · FC and ln(FC) images. ln(FC) images were computed to ensure data were normally distributed and centered around zero for downstream statistical analysis. We performed whole-brain probabilistic tractography on the FOD template selecting 20 · 10^6 streamlines with a length between 10 and 250 mm and a maximum angle of 22.5°. To correct for tractography biases, we performed spherical deconvolution informed filtering (Smith et al., 2013) and reduced the number of streamlines to 2 · 10^6. See Fig. 1 for an overview on the processing pipeline. We tested for differences in FD and FC fixel values between both MRI acquisition setups used and did not find any differences within the healthy control group.

2.7. Statistical analysis

Analysis was conducted following a two-tier strategy: First, fixel-wise analysis was conducted and, second, mean fixel values of resulting clusters were used for ROI-wise group comparisons or correlation analysis with neuropsychological assessment metrics. Cross-sectional statistical analysis of fixel-based metrics was performed using connectivity-based fixel enhancement (Raffelt et al., 2015, parameters: $C = 0.75$, $E = 3.5$, $H = 4$) and fixel-wise non-parametric permutation testing (5000 permutations) with the MRtrix3 toolbox. By smoothing and enhancing fixels along the template streamlines, this method puts additional weight on local fixel-fixel connectivity and determines significant fixels that are structurally connected. Second, fixels from resulting clusters were extracted, averaged, and subjected to ROI-wise comparisons and correlation analysis: For comparison of means of independent numerical data across more than two groups, we used one-way analysis of variance and post-hoc Tukey-Kramer test for pair-wise comparisons including a correction for multiple comparisons. Correlation analysis was carried out using Pearson correlation and Steiger's *Z*-test. The Holm-Bonferroni procedure was applied to adjust *p*-values for multiple testing (Holm, 1979). ROI-wise statistical analyses were performed using Stata 14 (Stata Statistical Software: Release 14, StataCorp LP, College Station, TX, USA). In this study, we regard a probability value $p < 0.05$ as statistically significant.

3. Results

3.1. Clinical group differences

All study groups were compared using one-way analysis of variance

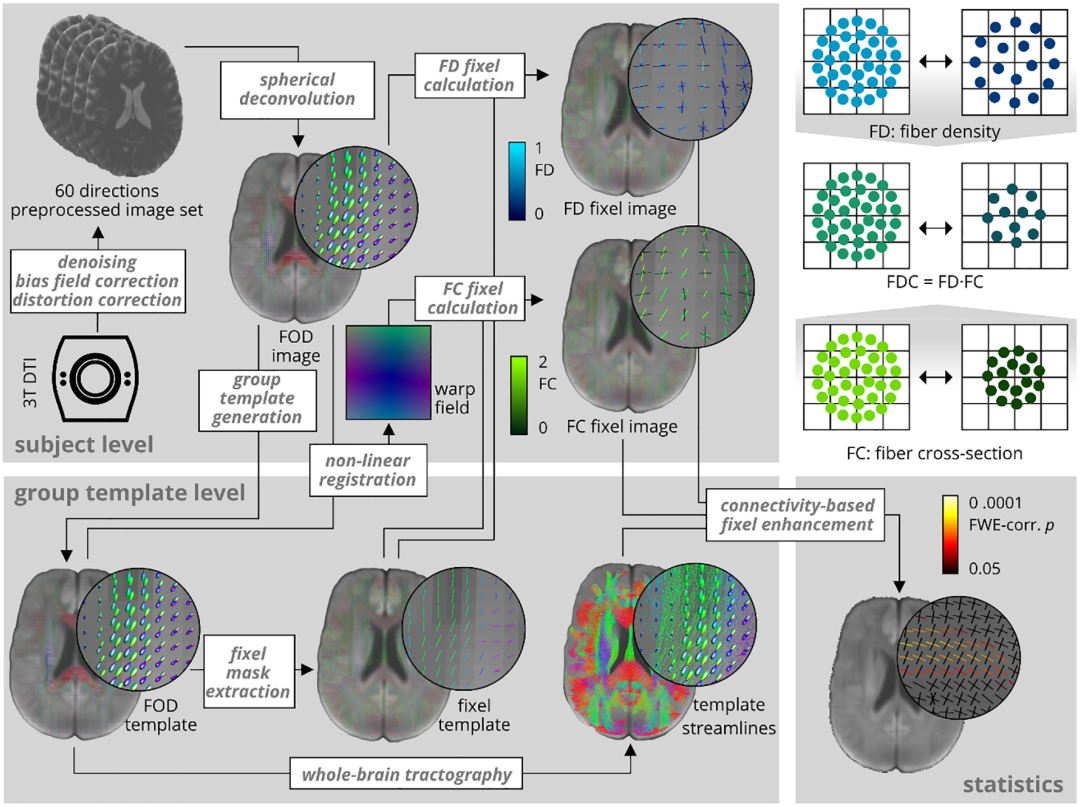

Fig. 1. Overview over the processing pipeline. Fixel-based analysis was performed using the MRtrix3 toolbox. It was conducted as proposed by Raffelt et al. (2017). FC: fiber cross-section, FD: fiber density, FOD: Fiber orientation distribution.

with Tukey-Kramer post-hoc pairwise testing. Between LE groups, we found a significantly lower age at study and age at disease onset in GAD-LE as compared to LGI1-LE (age at study: Tukey-Kramer $p < 0.001$, age at disease onset: Tukey-Kramer $p < 0.001$) and CASPR2-LE (age at study: Tukey-Kramer $p < 0.001$, age at disease onset: Tukey-Kramer $p < 0.001$). Disease duration did not differ significantly neither between GAD-LE and LGI-LE (Tukey-Kramer $p = 0.994$) nor between GAD-LE and CASPR2-LE (Tukey-Kramer $p = 0.999$). Between LE groups and the matched HS groups, in all LE groups the age at disease onset was significantly higher and disease duration was significantly shorter as compared to the matched HS group (all Tukey-Kramer $p < 0.001$). LE groups and HS control groups did not differ significantly in verbal memory performance ($F(5,50) = 2.23$, $p = 0.065$) or figural memory performance ($F(5,50) = 0.74$, $p = 0.595$).

3.2. Fixel values group differences between GAD-LE and control groups

Fixel-wise group comparisons revealed three clusters with significantly lower FDC in GAD-LE versus controls: First and second, we found a significant reduction of FDC in fibers associated to the superior longitudinal fascicle (SLF) on both the *affected* (1) and *unaffected* (2) hemispheres with an average reduction of −5.4% in the *affected* ($t_{max} = 4.57$, $p_{min} = 0.036$, FWE-corrected) and −5.0% in the *unaffected* hemisphere ($t_{max} = 5.25$, $p_{min} = 0.002$, FWE-corrected). Third, we found a significant reduction of FDC in crossing fibers (3) located in the isthmus of the corpus callosum ($t_{max} = 4.88$, $p_{min} = 0.012$, FWE-corrected; see Fig. 2A). FDC reduction was driven by a reduction of both FD and FC (see Supplementary Table S5). In a second step, we projected the (more extensive) SLF-cluster in the *unaffected* hemisphere cluster to the contralateral/*affected* hemisphere, extracted and averaged fixels from both clusters and computed whole-brain-corrected FDC fixel values within the SLF on both hemispheres. Consecutive ROI-wise analysis of covariance adjusting for age and post-hoc pairwise testing confirmed significantly lower bihemispheric FDC values in GAD-LE patients ($F(9,152) = 6.57$, $\eta^2 = 0.28$, $p < 0.001$; see Fig. 2B and Supplementary Table S6) as compared to healthy controls (Tukey-Kramer, *affected* hemisphere: $p < 0.001$, *unaffected* hemisphere: $p = 0.029$). ROI-wise analysis of control patients with HS showed unilaterally lower FDC values only in the *affected* hemisphere as compared to healthy controls (Tukey-Kramer, $p < 0.001$). ROI-wise analysis of CASPR2-LE patients also revealed unilaterally lower FDC values only in the *affected* hemisphere as compared to healthy controls (Tukey-Kramer, $p = 0.003$), the *unaffected* hemisphere in LGI1-LE (Tukey-Kramer, $p = 0.015$) and the *unaffected* hemisphere in HS (Tukey-Kramer, $p = 0.042$). In a second analysis of covariance adjusting all LE and HS groups for age and seizure freedom ($F(9,86) = 2.71$, $\eta^2 = 0.22$, $p = 0.008$; see Supplementary Table S7), lower FDC values in the *affected* hemisphere in CASPR2-LE than in the *unaffected* hemisphere in LGI1-LE remained significant (Tukey-Kramer, $p = 0.013$), whereas the *affected* hemisphere in CASPR2-LE did no longer show significantly lower FDC values than the *unaffected* hemisphere in HS (Tukey-Kramer, $p = 0.211$). After adjusting for seizure freedom, we found significantly lower FDC values in the *affected* hemisphere in HS patients than in the *unaffected* hemisphere in LGI1-LE (Tukey-Kramer, $p = 0.035$).

3.3. Fixel values group differences between LGI1-LE and control groups

Fixel-wise group comparison did not reveal any cluster with significantly different FD, ln(FC) or FDC neither between LGI1-LE and healthy controls ($p_{min} > 0.05$, FWE-corrected) nor between LGI1-LE and HS ($p_{min} > 0.05$, FWE-corrected).

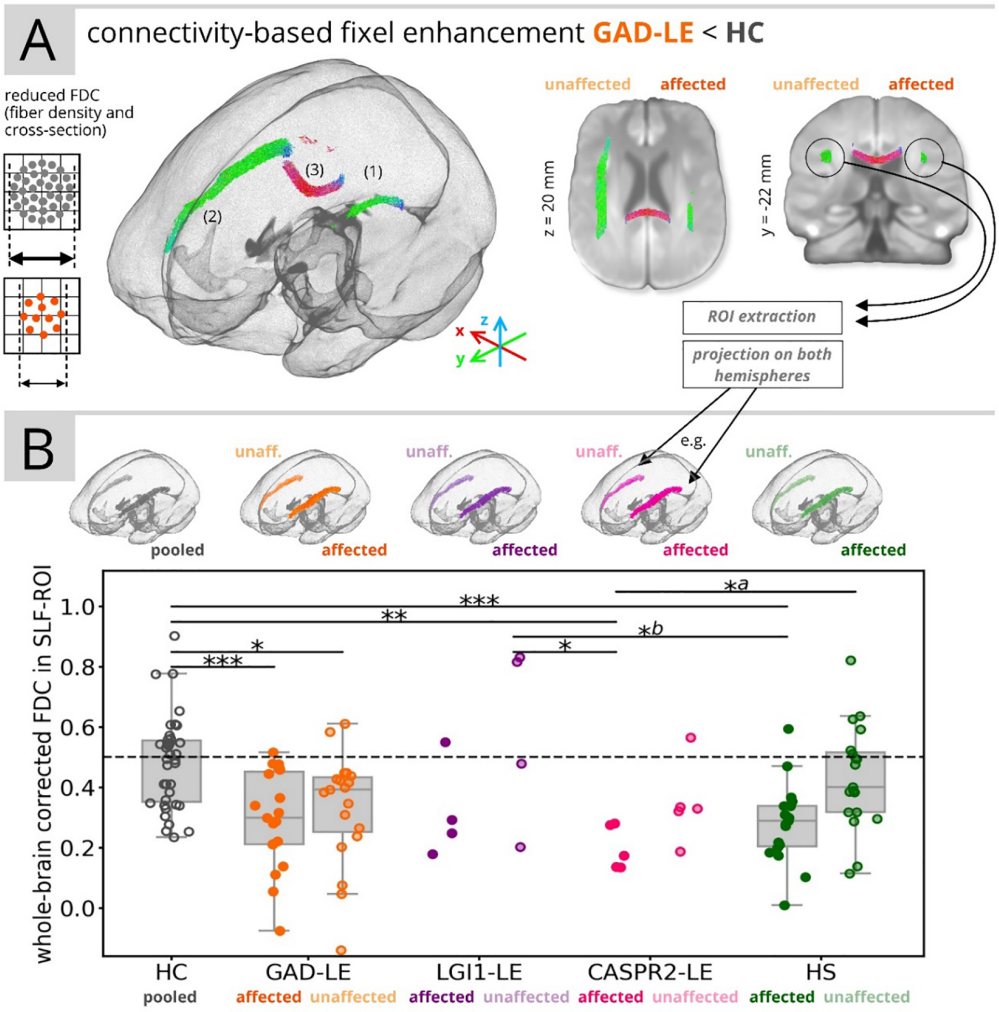

Fig. 2. Summary of fixel-based analysis results. (A) Display of streamlines associated to fixels with significant ($p < 0.05$, FWE-corrected) reduction of FDC in GAD-LE versus controls. (B) Whole-brain corrected mean FDC values in the extracted superior-longitudinal-fascicle-ROI for all groups are shown. [a]Results did not remain significant after adjusting for seizure freedom. [b]Results was only significant after adjusting for seizure freedom. HC: healthy controls; HS: control patients with hippocampal sclerosis; unaff.: unaffeceted; *: $p < 0.05$, **: $p < 0.01$, ***: $p < 0.001$.

3.4. Fixel values group differences between CASPR2-LE and control groups

Fixel-wise group comparison did not reveal any cluster with significantly different FD, ln(FC) or FDC between CASPR2-LE and healthy controls ($p_{min} > 0.05$, FWE-corrected). While FD did not differ significantly between CASPR2-LE and HS, we found a small cluster of significantly higher ln(FC) and FDC in the cerebellar peduncle on CASPR2-LE versus HS ($t_{max} = 10.16$, $p_{min} = 0.01$, FWE-corrected).

3.5. Correlation between ROI-wise fixel values and neuropsychological test results

Moreover, we performed correlation analysis in an explorative design between fixel values extracted from the SLF-ROI found in cross-sectional analysis and neuropsychological scores within the GAD-LE group (see Fig. 3 and Supplementary Table S8). For this analysis, as memory is known to be lateralized, we used a "native" left/right orientation in addition to the orientation according to the hemisphere affected by the disease. We found a significant correlation ($R = 0.64$, Holm-Bonferroni corrected $p < 0.048$) between the left/right ratio of whole brain corrected FC values in the SLF and the assessed verbal memory score. We did not find any correlation between hippocampal volumes and figural or verbal memory performance (uncorrected $p > 0.05$).

3.6. Regression of ROI-wise fixel values by clinical features

We performed regression analysis in order to link our finding of lower FDC in the SLF-ROI with clinical features. Within the HS group, FDC values in the SLF in the affected hemisphere were predicted by a linear regression model ($F(2,17) = 5.23$, $p = 0.017$, $R^2 = 0.38$) including disease duration and age at onset as covariates (see Fig. 4). While we found a significant effect of the disease duration ($t = -3.22$, $p = 0.004$), the contribution of age at onset was not significant ($t = -1.55$, $p = 0.140$). Within the GAD-LE group, the same model did not significantly predict FDC values in the SLF neither of the affected hemisphere ($F(2,16) = 0.48$, $p = 0.628$) nor pooled across both hemispheres ($F(2,16) = 0.82$, $p = 0.451$).

4. Discussion

Using the novel approach of fixel-based analysis, our study reveals distinct fiber tract alteration patterns in patients with LE that can be related to the associated antibody. GAD-LE showed bilaterally lower

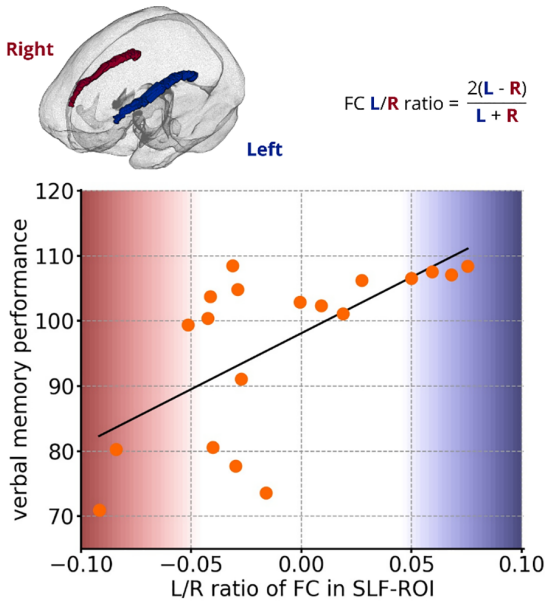

Fig. 3. Results of explorative ROI-wise correlation analysis with neuropsychological performance in the GAD-LE group. Correlation between Left/Right ratio of fiber cross-section values in the extracted SLF-ROI and verbal memory performance (R = 0.64, Holm-Bonferroni corrected p = 0.048; FC: fiber cross-section; SLF: superior longitudinal fascicle; L: left; R: right.

fiber density and cross-section (FDC) in the SLF as compared to healthy controls, while this reduction was present only in the *affected* hemisphere in CASPR2-LE and was not present at all in LGI1-LE. Correlation analysis finally draws a link between the altered SLF and memory performance further suggesting the functional relevance of our findings.

4.1. Clinical group differences

Analyses of clinical features confirm serogroup characteristics previously described in several studies (Malter et al., 2010; Bien et al., 2007; Graus et al., 2016; Dalmau and Graus, 2018): GAD-LE were significantly younger at the onset of the disease than LGI1-LE and CASPR2-LE patients. Also, there were more female patients in the group of GAD-LE (Graus et al., 2016). The disease onset of all LE-groups was much later than in the HS patient control groups, where first symptoms appeared in childhood. As expected, all LE and HS patients equally showed impaired figural and verbal memory performance.

4.2. Fixel-based analysis reflects serostatus

In GAD-LE, widespread reductions of fractional anisotropy have been observed by means of conventional DTI (Wagner et al., 2016). Using fixel-based analysis, this finding could be narrowed down to two fiber tracts affected by significant FDC reduction: Crossing fibers in the isthmus of the corpus callosum and in the SLF in both hemispheres. Reduction of diffusivity parameters in the corpus callosum have been repeatedly observed and discussed (Whelan et al., 2015; Caligiuri et al., 2016). It is subject to an ongoing debate whether they are a consequence of seizures, a part of the underlying pathology, or a contribution of genetics (Vaughan et al., 2017). Structural affection of the *affected* SLF is also known to occur in temporal lobe epilepsy: Reduced FDC of the SLF (Raffelt et al., 2017; Vaughan et al., 2017) and FA reduction (Otte et al., 2012) could be shown by previous studies and is now confirmed by findings in our HS patient control group. The bilateral affection of the SLF found in GAD-LE, however, is novel and may be interpreted as bilateral axonal damage caused by persisting seizures involving a network not limited to the *affected* hemisphere (Ahmadi et al., 2009; Otte et al., 2012; Campos et al., 2015) or as part of the pathologic process in autoimmune encephalitis. In LGI1-LE, a unilateral disease onset is discussed (Navarro et al., 2016; Ernst et al., 2019). Our results, in contrast, failed to reveal any asymmetrical white matter alteration patterns in this group. This might be due to the fact that not all LGI1-LE patients are identified in the early disease stage or due to the very small sample size. Notably, despite small sample sizes, CASPR2-LE showed reduced FDC in the SLF limited to the *affected* hemisphere. Considering the older age at disease onset of LE patients in comparison to HS control patients, it remains open which amount of FDC reduction in the SLF is purely grounded in the autoimmune pathology of LE or simply a consequence of persisting seizures, as it is the case in HS where FDC reduction in the SLF is significantly associated with disease duration. Based on our data, such a link cannot be drawn for LE, especially GAD-LE. Notably, different age at disease onset has been shown to influence the vulnerability of the brain to seizures and the potential for neuroplasticity (Berg et al., 2012; Ben-Ari & Holmes, 2006), which is why the direct comparison between LE subgroups and HS has to be made with caution.

4.3. Functional relevance of structural alterations

We discuss our finding of lower FDC in GAD-LE versus controls located within the SLF in the light of verbal memory performance, a cognitive domain most commonly impaired in temporal lobe epilepsy (Helmstaedter, 2001; Hermann et al., 2006). It is widely recognized that both affected SLF subdivisions, the SLF II and SLFIII, are key components of the dorsal language processing stream and involved in mediating between language functions and working memory (Baddeley, 2000; Bernal and Ardila, 2009; Maldonado et al., 2011; Smits et al., 2014). Our data, showing a positive correlation between the left-greater-than-right asymmetry of FC values within the SLF and verbal memory, is in line with previous studies applying DTI based measures (Vernooij et al., 2007; Catani et al., 2007; Thiebaut de Schotten et al., 2011). This underlines the concept that integrity of superordinated organizational properties of the language processing system rather than isolated damage to one component predicts verbal memory performance (Catani et al., 2007).

4.4. Limitations and outlook

There are three major limitations to the current study. The first limitation lies in the study design: Transversal study designs like the current one are challenged by therapeutic interventions. GAD-LE has been described to be less responsive to immunotherapy as compared to LGI1-LE and CASPR2-LE (Graus et al., 2016). It is, therefore, difficult to discriminate whether differences observed between groups reflect the response to differing treatments or the natural course of the disease. Second, small sample sizes and heterogeneity especially of the LGI1-LE and CASPR2-LE groups limit the ability of the present study to reveal distinct serospecific properties. Notably, because of this limitation, this study did not reveal any significant group differences when comparing LE subgroups against each other. Third, the interpretation of fixel-based measures, mostly in analogy to DTI measures, remains speculative. Yet, in order to increase the value of those metrics as meaningful imaging biomarkers offering pathomechanistic insight, a more detailed understanding of the histopathological underpinnings is essential. Therefore, future studies investigating histolopathological correlates of imaging measures are needed.

5. Conclusion

Imaging research in LE has recently been focused on mesiotemporal gray matter structures. However, in DTI studies it became evident that white matter structures also undergo pathological changes. In the current study, fixel-based analysis has proven to be a useful tool for the

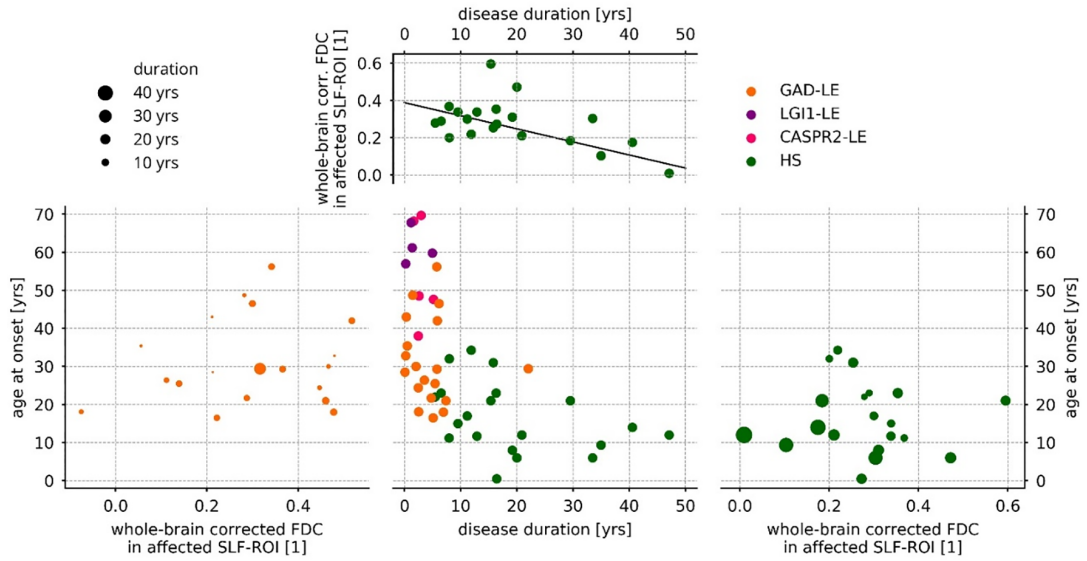

Fig. 4. Results of regression analysis of FDC in the affected superior longitudinal fascicle. Within the hippocampal sclerosis group (right and top), FDC values were predicted ($F(2,17) = 5.23, p = 0.017, R^2 = 0.38$) by disease duration ($t = -3.22, p = 0.004$) and age at onset($t = -1.55, p = 0.140$) , while only the contribution of disease duration was significant (top). Within the GAD-LE group, the same model failed ($F(2,16) = 0.48, p = 0.628$) to predict FDC values in the affected superior longitudinal fascicle (left). FDC: fiber density and cross-section; SLF: superior longitudinal fascicle; yrs: years.

detection of distinct microstructural white matter alterations and could show their functional relevance. It is our hope that the current study, as well as future studies, will help in unveiling the pathomechanism of LE, thereby, strengthening the role of MRI in the diagnosis of LE patients.

Declaration of competing interest

C.E.E. received fees as speaker or consultant from UCB Pharma, Desitin, BIAL and Eisai. R.S. has received fees as speaker or consultant from Bial, Cyberonics, Desitin, Eisai, LivaNova, Novartis, and UCB Pharma.

Acknowledgements

T.B. and L.E. received support from the “BonnNi Promotionskolleg Neuroimmunology” of the University of Bonn and the “Else Kröner-Fresenius-Stiftung” (Grants Nr. 2018-S2-01 and 2016-S2-05). T.R. was supported by the BONFOR research commission of the medical faculty of the University of Bonn. This work was supported by the “Verein zur Förderung der Epilepsieforschung”.

Appendix A. Supplementary data

Supplementary data to this article can be found online at https://doi.org/10.1016/j.nicl.2020.102289.

References

Ahmadi, M.E., Hagler, D.J., McDonald, C.R., Tecoma, E.S., Iragui, V.J., Dale, A.M., Halgren, E., 2009. Side matters: Diffusion tensor imaging tractography in left and right temporal lobe epilepsy. Am. J. Neuroradiol. 30, 1740–1747. https://doi.org/10.3174/ajnr.A1650.

Andersson, J.L., Sotiropoulos, S.N., 2016. An integrated approach to correction for off-resonance effects and subject movement in diffusion MR imaging. Neuroimage 125, 1063–1078. https://doi.org/10.1016/j.neuroimage.2015.10.019.

Andersson, J.L.R., Skare, S., Ashburner, J., 2003. How to correct susceptibility distortions in spin-echo echo-planar images: Application to diffusion tensor imaging. Neuroimage 20, 870–888. https://doi.org/10.1016/S1053-8119(03)00336–7.

Baddeley, A., 2000. The episodic buffer: A new component of working memory? Trends Cogn Sci. 4 417 (423). https://doi.org/10.1016/S1364-6613(00)01538–2.

Ben-Ari, Y., Holmes, G.L., 2006. Effects of seizures on developmental processes in the immature brain. Lancet Neurol. 5 (12), 1055–1063. https://doi.org/10.1016/s1474-4422(06)70626-3.

Berg, A.T., Zelko, F.A., Levy, S.R., Testa, F.M., 2012. Age at onset of epilepsy, pharmacoresistance, and cognitive outcomes. A prospective cohort study. Neurology 79 (13), 1384–1391. https://doi.org/10.1212/WNL.0b013e31826c1b55.

Bernal, B., Ardila, A., 2009. The role of the arcuate fasciculus in conduction aphasia. Brain 132, 2309–2316. https://doi.org/10.1093/brain/awp206.

Bien, C.G., Elger, C.E., 2007. Limbic encephalitis: A cause of temporal lobe epilepsy with onset in adult life. Epilepsy Behav. 10, 529–538. https://doi.org/10.1016/j.yebeh.2007.03.011.

Bien, C.G., Urbach, H., Schramm, J., Soeder, B.M., Becker, A.J., Voltz, R., Vincent, A., Elger, C.E., 2007. Limbic encephalitis as a precipitating event in adult-onset temporal lobe epilepsy. Neurology 69 (1236), 1244. https://doi.org/10.1212/01.wnl.0000276946.08412.ef.

Binks, S.N.M., Klein, C.J., Waters, P., Pittock, S.J., Irani, S.R., 2017. LGI1, CASPR2 and related antibodies: a molecular evolution of the phenotypes. J. Neurol. Neurosurg. Psychiatry 89, 526–534. https://doi.org/10.1136/jnnp-2017-315720.

Caligiuri, M.E., Labate, A., Cherubini, A., Mumoli, L., Ferlazzo, E., Aguglia, U., Quattrone, A., Gambardella, A., 2016. Integrity of the corpus callosum in patients with benign temporal lobe epilepsy. Epilepsia 57, 590–596. https://doi.org/10.1111/epi.13339.

Campos, B.M., Coan, A.C., Beltramini, G.C., Liu, M., Yassuda, C.L., Ghizoni, E., Beaulieu, C., Gross, D.W., Cendes, F., 2015. White matter abnormalities associate with type and localization of focal epileptogenic lesions. Epilepsia 56, 125–132. https://doi.org/10.1111/epi.12871.

Catani, M., Allin, M.P.G., Husain, M., Pugliese, L., Mesulam, M.M., Murray, R.M., Jones, D.K., 2007. Symmetries in human brain language pathways correlate with verbal recall. Proc. Natl. Acad. Sci. 104, 17163–17168. https://doi.org/10.1073/pnas.0702116104.

Dalmau, J., Graus, F., 2018. Antibody-mediated encephalitis. N. Engl. J. Med. 378, 840–851. https://doi.org/10.1056/NEJMra1708712.

Dalmau, J., Vincent, A., 2017. Do we need to measure specific antibodies in patients with limbic encephalitis? Neurology 88, 508–509. https://doi.org/10.1212/WNL.0000000000003592.

Dubey, D., Pittock, S.J., Kelly, C.R., McKeon, A., Lopez-Chiriboga, A.S., Lennon, V.A., Gadoth, A., Smith, C.Y., Bryant, S.C., Klein, C.J., Aksamit, A.J., Toledano, M., Boeve, B.F., Tillema, J.M., Flanagan, E.P., 2018. Autoimmune encephalitis epidemiology and a comparison to infectious encephalitis. Ann. Neurol. 83, 166–177. https://doi.org/10.1002/ana.25131.

Ernst, L., David, B., Gaubatz, J., Elger, C.E., Rüber, T., 2019. Volumetry of Mesiotemporal Structures Reflects Serostatus in Patients with Limbic Encephalitis. Am. J. Neuroradiol. doi:10.3174/ajnr.A6289 [in press].

Fischl, B., Salat, D., Busa, E., Albert, M., Dieterich, M., Haselgrove, C., Van der Kouwe, A., Killiany, R., Kennedy, D., Klaveness, S., Montillo, A., Makris, N., Rosen, B., Dale, A., 2002. Whole brain segmentation: Automated labeling of neuroanatomical structures in the human brain. Neuron 33 (3), 341–355. https://doi.org/10.1016/s0896-6273(02)00569-x.

Fredriksen, J.R., Carr, C.M., Koeller, K.K., Verdoorn, J.T., Gadoth, A., Pittock, S.J., Kotsenas, A.L., 2018. MRI findings in glutamic acid decarboxylase associated autoimmune epilepsy. Neuroradiology 60, 239–245. https://doi.org/10.1007/s00234-018-1976-6.

Graus, F., Saiz, A., Dalmau, J., 2010. Antibodies and neuronal autoimmune disorders of the CNS. J. Neurol. 257, 509–517. https://doi.org/10.1007/s00415-009-5431-9.

Graus, F., Titulaer, M.J., Balu, R., Benseler, S., Bien, C.G., Cellucci, T., Cortese, I., Dale, R.C., Gelfand, J.M., Geschwind, M., Glaser, C.A., Honnorat, J., Höftberger, R., Iizuka, T., Irani, S.R., Lancaster, E., Leypoldt, F., Prüss, H., Rae-Grant, A., Reindl, M.,

Rosenfeld, M.R., Rostásy, K., Saiz, A., Venkatesan, A., Vincent, A., Wandinger, K.P., Waters, P., Dalmau, J., 2016. A clinical approach to diagnosis of autoimmune encephalitis. Lancet Neurol. 15, 391–404. https://doi.org/10.1016/S1474-4422(15)00401-9.

Heine, J., Prüss, H., Bartsch, T., Ploner, C.J., Paul, F., Finke, C., 2015. Imaging of autoimmune encephalitis - Relevance for clinical practice and hippocampal function. Neuroscience 309, 68–83. https://doi.org/10.1016/j.neuroscience.2015.05.037.

Helmstaedter, C., 2001. Neuropsychological complaints, deficits, and difficulties in everyday, in: Fäfflin, M., Fraser, R., Thorbecke, R., Specht, U., Wolf, P. (Eds.), Compr. Care People With Epilepsy, pp. 293–306.

Helmstaedter, C., Lendt, M., Lux, S., 2001. VLMT Verbaler Lern- und Merkfaehigkeitstest. Beltz Test GmbH, Goettingen.

Helmstaedter, C., Pohl, C., Hufnagel, A., Elger, C., 1991. visual learning deficits in non-resected patients with right temporal lobe epilepsy. Cortex 27, 547–555. https://doi.org/10.1016/S0010-9452(13)80004-4.

Hermann, B.P., Seidenberg, M., Dow, C., Jones, J., Rutecki, P., Bhattacharya, A., Bell, B., 2006. Cognitive prognosis in chronic temporal lobe epilepsy. Ann. Neurol. 60, 80–87. https://doi.org/10.1002/ana.20872.

Holm, S., 1979. A simple sequentially rejective multiple test procedure. Scandinavian J. Stat. 6 (2), 65–70.

Irani, S.R., Alexander, S., Waters, P., Kleopa, K.A., Pettingill, P., Zuliani, L., Peles, E., Buckley, C., Lang, B., Vincent, A., 2010. Antibodies to Kv1 potassium channel-complex proteins leucine-rich, glioma inactivated 1 protein and contactin-associated protein-2 in limbic encephalitis Morvan's syndrome and acquired neuromyotonia. Brain 133 (9), 2734–2748. https://doi.org/10.1093/brain/awq213.

Jenkinson, M., Beckmann, C.F., Behrens, T.E., Woolrich, M.W., Smith, S.M., 2012. FSL. Neuroimage 62, 782–790. https://doi.org/10.1016/J.NEUROIMAGE.2011.09.015.

Jeurissen, B., Leemans, A., Tournier, J.D., Jones, D.K., Sijbers, J., 2013. Investigating the prevalence of complex fiber configurations in white matter tissue with diffusion magnetic resonance imaging. Hum. Brain Mapp. 34, 2747–2766. https://doi.org/10.1002/hbm.22099.

Jeurissen, B., Tournier, J.D., Dhollander, T., Connelly, A., Sijbers, J., 2014. Multi-tissue constrained spherical deconvolution for improved analysis of multi-shell diffusion MRI data. Neuroimage 103, 411–426. https://doi.org/10.1016/j.neuroimage.2014.07.061.

Lai, M., Huijbers, M.G., Lancaster, E., Graus, F., Bataller, L., Balice-Gordon, R., Cowell, J.K., Dalmau, J., 2010. Investigation of LGI1 as the antigen in limbic encephalitis previously attributed to potassium channels: A case series. Lancet. Neurol. 9 (8), 776–785. https://doi.org/10.1016/S1474-4422(10)70137-X.

Maldonado, I.L., Moritz-Gasser, S., Duffau, H., 2011. Does the left superior longitudinal fascicle subserve language semantics? A brain electrostimulation study. Brain Struct. Funct. 216, 263–274. https://doi.org/10.1007/s00429-011-0309-x.

Malter, M.P., Helmstaedter, C., Urbach, H., Vincent, A., Bien, C.G., 2010. Antibodies to glutamic acid decarboxylase define a form of limbic encephalitis. Ann. Neurol. 67, 470–478. https://doi.org/10.1002/ana.21917.

Navarro, V., Kas, A., Apartis, E., Chami, L., Rogemond, V., Levy, P., Psimaras, D., Habert, M.O., Baulac, M., Delattre, J.Y., Honnorat, J., Collaborators,, 2016. Motor cortex and hippocampus are the two main cortical targets in LGI1-antibody encephalitis. Brain 139, 1079–1093.

Otte, W.M., Van Eijsden, P., Sander, J.W., Duncan, J.S., Dijkhuizen, R.M., Braun, K.P., 2012. A meta-analysis of white matter changes in temporal lobe epilepsy as studied with diffusion tensor imaging. Epilepsia 53, 659–667. https://doi.org/10.1111/j.1528-1167.2012.03426.x.

Quek, A.M.L., Britton, J.W., McKeon, A., So, E., Lennon, V.A., Shin, C., Klein, C., Watson, R.E., Kotsenas, A.L., Lagerlund, T.D., Cascino, G.D., Worrell, G.A., Wirrell, E.C., Nickels, K.C., Aksamit, A.J., Noe, K.H., Pittock, S.J., 2012. Autoimmune epilepsy: clinical characteristics and response to immunotherapy. Arch. Neurol. 69, 582–593. https://doi.org/10.1001/archneurol.2011.2985.

Raffelt, D.A., Smith, R.E., Ridgway, G.R., Tournier, J.D., Vaughan, D.N., Rose, S., Henderson, R., Connelly, A., 2015. Connectivity-based fixel enhancement: Whole-brain statistical analysis of diffusion MRI measures in the presence of crossingfibres. Neuroimage 117, 40–55. https://doi.org/10.1016/j.neuroimage.2015.05.039.

Raffelt, D.A., Tournier, J.D., Rose, S., Ridgway, G.R., Henderson, R., Crozier, S., Salvado, O., Connelly, A., 2012. Apparent Fibre Density: A novel measure for the analysis of diffusion-weighted magnetic resonance images. Neuroimage 59, 3976–3994. https://doi.org/10.1016/j.neuroimage.2011.10.045.

Raffelt, D.A., Tournier, J.D., Smith, R.E., Vaughan, D.N., Jackson, G., Ridgway, G.R., Connelly, A., 2017. Investigating white matter fibre density and morphology using fixel-based analysis. Neuroimage 144, 58–73. https://doi.org/10.1016/j.neuroimage.2016.09.029.

Smith, R.E., Tournier, J.D., Calamante, F., Connelly, A., 2013. SIFT: Spherical-deconvolution informed filtering of tractograms. Neuroimage 67, 298–312. https://doi.org/10.1016/j.neuroimage.2012.11.049.

Smits, M., Jiskoot, L.C., Papma, J.M., 2014. White Matter Tracts of Speech and Language. Semin. Ultrasound, CT MRI 35, 504–516. https://doi.org/10.1053/J.SULT.2014.06.008.

van Sonderen, A., Petit-Pedrol, M., Dalmau, J., Titulaer, M.J., 2017. The value of LGI1, Caspr2 and voltage-gated potassium channel antibodies in encephalitis. Nat. Rev. Neurol. 13, 290.

Thiebaut de Schotten, M., Ffytche, D.H., Bizzi, A., Dell'Acqua, F., Allin, M., Walshe, M., Murray, R., Williams, S.C., Murphy, D.G., Catani, M., 2011. Atlasing location, asymmetry and inter-subject variability of white matter tracts in the human brain with MR diffusion tractography. Neuroimage 54, 49–59. https://doi.org/10.1016/J.NEUROIMAGE.2010.07.055.

Tournier, J.D., Calamante, F., Connelly, A., 2013. Determination of the appropriate b value and number of gradient directions for high-angular-resolution diffusion-weighted imaging. NMR Biomed. 26, 1775–1786. https://doi.org/10.1002/nbm.3017.

Tustison, N.J., Cook, P.A., Gee, J.C., 2011. N4ITK: Improved N3 Bias Correction. IEEE Trans Med Imaging 29, 1310–1320. https://doi.org/10.1109/TMI.2010.2046908.N4ITK.

Vaughan, D.N., Raffelt, D., Curwood, E., Tsai, M.H., Tournier, J.D., Connelly, A., Jackson, G.D., 2017. Tract-specific atrophy in focal epilepsy: Disease, genetics, or seizures? Ann. Neurol. 81, 240–250. https://doi.org/10.1002/ana.24848.

Veraart, J., Fieremans, E., Novikov, D.S., 2016. Diffusion MRI noise mapping using random matrix theory. Magn. Reson. Med. 76, 1582–1593. https://doi.org/10.1002/mrm.26059.

Vernooij, M.W., Smits, M., Wielopolski, P.A., Houston, G.C., Krestin, G.P., van der Lugt, A., 2007. Fiber density asymmetry of the arcuate fasciculus in relation to functional hemispheric language lateralization in both right- and left-handed healthy subjects: A combined fMRI and DTI study. Neuroimage 35, 1064–1076. https://doi.org/10.1016/j.neuroimage.2006.12.041.

Wagner, J., Schoene-Bake, J.C., Witt, J.A., Helmstaedter, C., Malter, M.P., Stoecker, W., Probst, C., Weber, B., Elger, C.E., 2016. Distinct white matter integrity in glutamic acid decarboxylase and voltage-gated potassium channel-complexantibody-associated limbic encephalitis. Epilepsia 57, 475–483. https://doi.org/10.1111/epi.13297.

Wagner, J., Weber, B., Elger, C.E., 2015. Early and chronic gray matter volume changes in limbic encephalitis revealed by voxel-based morphometry. Epilepsia 56, 754–761. https://doi.org/10.1111/epi.12968.

Whelan, C.D., Alhusaini, S., O'Hanlon, E., Cheung, M., Iyer, P.M., Meaney, J.F., Fagan, A.J., Boyle, G., Delanty, N., Doherty, C.P., Cavalleri, G.L., 2015. White matter alterations in patients with MRI-negative temporal lobe epilepsy and their asymptomatic siblings. Epilepsia 56, 1551–1561. https://doi.org/10.1111/epi.13103.

2.2 Supplementary Material zur Originalpublikation in *Neuroimage:Clinical*

Table S1. Clinical characteristics of GAD-LE patients.

Patient	Gender	Laterali-zation	Age at onset, yrs	Age at 1st visit, yrs	Age at study, yrs	# of AEDs at study	Ab at 1st visit	Ab at study	Initial IT	IT at study	Verbal memory at study	Figural memory at study	Clinical MRI at 1st visit	Clinical MRI at study
1	F	L	46.4	48.4	52.6	2	>1000U/ml	NA	MPR pulse	None	88	92	uWML	uWML
2	F	R + L	16.5	18.0	21.6	2	>1000U/ml	>1000U/ml	MPR pulse	MMF	105	73	HI AMR+HCR + claustrum bilateral	HI+A HCR
3	M	R + L	26.4	26.7	29.9	2	>1000U/ml	>1000U/ml	MPR pulse	None	100	104	HI AML	Normal
4	F	R	30.0	32.0	32.1	2	>1000U/ml	>1000U/ml	IVIG	None	103	102	Normal	Normal
5	F	R + L	21.0	25.7	28.4	2	>1000U/ml	>1000U/ml	IVIG	PR oral	109	97	HI+A HCL	HI+A HCL
6	F	R	18.1	18.2	20.6	2	>1000U/ml	0U/ml	MPR pulse	None	85	66	HI+VI AMR+HCR, HI biparietal+ thalamus bilateral	HI HCR
7	M	L	29.3	35.0	35.0	2	>1000U/ml	>1000U/ml	AZA	None	107	108	Normal	Normal
8	M	L	43.0	43.3	43.5	1	>1000U/ml	>1000U/ml	PR oral	MPR pulse+ PR oral	92	106	HI AML+HCL	HI AML+HCL
9	F	L	48.7	49.1	50.1	1	>1000U/ml	>1000U/ml	MPR pulse	None	107	84	HI+VI AMR	HI AMR
10	F	L	28.5	28.6	28.6	1	>1000U/ml	>1000U/ml	MPR pulse	MPR pulse	108	104	Normal	Normal
11	M	R	21.7	26.4	26.4	2	>1000U/ml	>1000U/ml	MPR pulse	MPR pulse	101	92	HI+A HCL	HI+A HCL
12	M	L	32.7	32.9	32.9	1	>1000U/ml	>1000U/ml	PR oral	None	107	101	HI HCR	HI HCR
13	M	L	35.4	35.9	35.9	0	>1000U/ml	>1000U/ml	MPR pulse	None	103	84	HI AML+HCL	HI AML+HCL
14	F	R + L	55.3	60.9	61.9	1	>1000U/ml	>1000U/ml	MPR pulse	None	102	67	HI AMR+HCR, uWML	HI AMR+HCR, uWML
15	M	R	29.4	49.4	51.4	2	>1000U/ml	>1000U/ml	MPR pulse	MMF	71	104	HI AMR, uWML	uWML
16	F	L	24.4	24.8	26.8	2	>1000U/ml	>1000U/ml	MPR pulse	MMF	109	77	HI+VI AML+HCL	HI+VI AML+HCL
17	M	R	18.0	21.1	24.9	3	>1000U/ml	NA	MPR pulse	MPR pulse + BAS	80	67	Normal	Normal
18	F	L	42.0	47.4	47.9	2	>1000U/ml	>1000U/ml	MPR pulse	None	74	67	HI AML+HCL, uWML	HI AML+HCL, uWML
19	F	L	25.5	30.6	30.9	2	>1000U/ml	0U/ml	MPR pulse	MPR pulse	101	77	HI AML	HI AML

M: male, F: female, R: right, L: left, NA: not available, yrs: years, AEDs: antiepileptic drugs, Ab: serum antibody concentration, IT: immunotherapy, MPR:methylprednisolone, IVIG: intravenous immunoglobulin, PR: prednisolone, AZA: azathioprine, MMF: mycophenolate-mofetil, BAS: Basiliximab, uWML: unspecific white matter lesions, HI: hyperintensity, A: atrophy, VI: volume increase, AMR: right amygdala, AML: left amygdala, HCR: right hippocampus, HCL: left hippocampus.

Table S2. Clinical characteristics of LGI1-LE patients.

Patient	Gender	Laterali-zation	Age at onset, yrs	Age at 1st visit, yrs	Age at study, yrs	# of AEDs at study	Ab at 1st visit	Ab at study	Initial IT	IT at study	Verbal memory at study	Figural memory at study	Clinical MRI at 1st visit	Clinical MRI at study
1	M	R	67.8	67.8	69	2	VGKC > 100 pM LGI1 1:10 CASPR2 <1:10	VGKC NA LGI1 NA CASPR2 NA	MPR pulse	None	71	76	HI+VI AMR+AML	VI AMR A HCL+HCR
2	M	L	59.7	60.0	64.7	1	VGKC >7655pM LGI1 1:100 CASPR2 <1:10	VGKC NA LGI1 NA CASPR2 NA	MPR pulse	None	96	83	HI AMR+ AML+HCR	HI+A AMR+AML+ HCR+HCL
3	F	L	61.1	61.2	63.4	1	VGKC 679pM LGI1 1:100 CASPR2 <1:10	VGKC 0pM LGI1 <1:10 CASPR2 <1:10	MPR pulse	None	64	59	HI+VI HCR	HI+A HCR+HCL
4	F	R	57.0	57.1	57.2	2	VGKC 558pM LGI1 1:10 CASPR2 <1:10	VGKC 558pM LGI1 1:10 CASPR2 <1:10	PR oral	MPR pulse	86	73	Normal	Normal

M: male, F: female, R: right, L: left, NA: not available, yrs: years, AEDs: antiepileptic drugs, Ab: serum antibody concentration, IT: immunotherapy, MPR: methylprednisolone, IVIG: intravenous immunoglobulin, PR: prednisolone, AZA: azathioprine, MMF: mycophenolate-mofetil, IA: immunoadsorption, uWML: unspecific white matter lesions, HI: hyperintensity, A: atrophy, VI: volume increase, AMR: right amygdala, AML: left amygdala, HCR: right hippocampus, HCL: left hippocampus.

Table S3. Clinical characteristics of CASPR2-LE patients.

Patient	Gender	Laterali-zation	Age at onset, yrs	Age at 1st visit, yrs	Age at study, yrs	# of AEDs at study	Ab at 1st visit	Ab at study	Initial IT	IT at study	Verbal memory at study	Figural memory at study	Clinical MRI at 1st visit	Clinical MRI at study
1	M	L	69.7	70.2	75.6	1	VGKC 1419pM LGI1 <1:10 CASPR2 1:1000	VGKC NA LGI1 NA CASPR2 NA	MPR pulse	None	93	82	HI+VI AML	A HCR+HCL
2	M	L	38.0	38.5	40.4	2	VGKC 475pM LGI1 <1:10 CASPR2 1:1000	VGKC 1929pM LGI1 <1:10 CASPR2 1:1000	MPR pulse	PR oral+ MMF	92	107	HI AMR	Normal
3	M	R	68.1	69.1	72.6	1	VGKC 556pM LGI1 <1:10 CASPR2 1:100	VGKC 46pM LGI1 <1:10 CASPR2 <1:10	MPR pulse	None	81	96	Normal	A HCR+HCL
4	M	R + L	47.6	47.9	52.7	1	VGKC 1336pM LGI1 <1:10 CASPR2 1:3200	VGKC 502pM LGI1 <1:10 CASPR2 1:3200	MPR pulse	None	93	87	HI+VI AMR+AML, HI HCR+HCL	HI AMR+AML
5	M	L	48.4	51.0	51.0	2	VGKC 1203pM LGI1 <1:10 CASPR2 1:3200	VGKC 1203pM LGI1 <1:10 CASPR2 1:3200	MPR pulse	MPR pulse	90	84	Normal	Normal

M: male, F: female, R: right, L: left, NA: not available, yrs: years, AEDs: antiepileptic drugs, Ab: serum antibody concentration, IT: immunotherapy, MPR: methylprednisolone, IVIG: intravenous immunoglobulin, PR: prednisolone, AZA: azathioprine, MMF: mycophenolate-mofetil, IA: immunoadsorption, uWML: unspecific white matter lesions, HI: hyperintensity, A: atrophy, VI: volume increase, AMR: right amygdala, AML: left amygdala, HCR: right hippocampus, HCL: left hippocampus.

Table S4. Clinical characteristics of HS patients.

Patient	**Sex**	**Side of HS**	**Age at onset ,yrs**	**Age at study, yrs**	**# of AEDs at study**
1	M	R	6.0	26.0	3
2	F	L + R	22.0	27.5	1
3	F	L	23.0	39.3	2
4	F	R	0.5	18.9	1
5	M	R	11.2	19.1	2
6	F	R	21.0	36.4	2
7	M	L	12.0	32.9	2
8	M	L	9.4	44.3	2
9	M	L	8.0	27.2	1
10	F	L	15.0	24.5	2
11	F	L	14.0	54.6	2
12	F	L	17.0	28.2	3
13	M	L	6.0	39.5	3
14	F	L	23.0	29.5	2
15	F	R	11.7	24.6	2
16	F	L	32.0	40.0	2
17	F	R	12.0	59.1	3
18	M	R	21.0	50.5	2
19	M	L + R	34.3	46.1	1
20	M	L	30.8	46.8	2

M: male, F: female, R: right, L: left, yrs: years, AEDs: antiepileptic drugs, NA: not available

Table S5. Statistical values of all two-tailed t-tests using connectivity-based fixel enhancement conducted in this study.

Contrast	Metric	min *p*-value	max *t*-value	number of voxels containing fixels with fwe-corrected $p < 0.05$	location of fixels with fwe-corrected $p < 0.05$
GAD-LE < HC	FD	0.017 *	6.02	102	BL SLF
	ln(FC)	0.035*	5.38	58	Isthmus CC
	FDC	0.002 **	5.58	829	BL SLF, isthmus CC
GAD-LE > HC	FD	0.924	4.64	0	
	ln(FC)	0.616	4.22	0	
	FDC	0.652	5.04	0	
GAD-LE < HS	FD	0.101	6.78	0	
	ln(FC)	0.651	5.41	0	
	FDC	0.596	6.28	0	
GAD-LE > HS	FD	0.082	8.33	0	
	ln(FC)	0.012 *	6.99	92	Anterior commisure
	FDC	0.139	6.28	0	
LGI1-LE < HC	FD	0.14	7.08	0	
	ln(FC)	0.21	6.72	0	
	FDC	0.22	7.59	0	
LGI1-LE > HC	FD	0.96	7.11	0	
	ln(FC)	0.80	4.96	0	
	FDC	0.95	8.32	0	
LGI1-LE < HS	FD	0.65	7.31	0	
	ln(FC)	0.64	5.36	0	
	FDC	0.52	8.11	0	
LGI1-LE > HS	FD	0.11	7.30	0	
	ln(FC)	0.14	3.49	0	
	FDC	0.07	7.76	0	
CASPR2-LE < HC	FD	0.33	7.32	0	
	ln(FC)	0.09	5.87	0	
	FDC	0.07	6.54	0	

CASPR2-LE > HC	FD	0.64	7.78	0	
	ln(FC)	0.97	5.69	0	
	FDC	0.59	6.11	0	
CASPR2-LE < HS	FD	0.47	6.85	0	
	ln(FC)	0.91	3.02	0	
	FDC	0.70	6.47	0	
CASPR2-LE > HS	FD	0.11	8.08	0	
	ln(FC)	0.01 *	10.16	218	cerebellar peduncle + splenium of CC
	FDC	0.03 *	11.19	56	cerebellar peduncle
LGI1-LE < GAD-LE	FD	0.95	6.20	0	
	ln(FC)	0.55	3.67	0	
	FDC	0.93	6.06	0	
LGI1-LE > GAD-LE	FD	0.06	6.49	0	
	ln(FC)	0.37	3.14	0	
	FDC	0.34	5.78	0	
CASPR2-LE < GAD-LE	FD	0.92	5.27	0	
	ln(FC)	0.51	4.18	0	
	FDC	0.65	5.96	0	
CASPR2-LE > GAD-LE	FD	0.25	5.10	0	
	ln(FC)	0.42	3.65	0	
	FDC	0.12	4.61	0	
CASPR2-LE < LGI1-LE	FD	0.24	18.08	0	
	ln(FC)	0.79	10.63	0	
	FDC	0.83	13.67	0	
CASPR2-LE > LGI1-LE	FD	0.42	18.30	0	
	ln(FC)	0.12	15.09	0	
	FDC	0.22	14.58	0	

BL: bilateral, FD: fiber density, FC: fiber cross-section, FDC: fiber density and cross-section, SLF: superior longitudinal fascicle, CC: corpus callosum

Table S6. Analysis of variance and Tukey-Kramer post-hoc pairwise comparison of extracted superior longitudinal fascicle FDC fixel metrics across all groups adjusting for age.

ANCOVA	Post-hoc tests (Tukey-Kramer)	*t*-value	*p*-value
$F(9,152)=6.57$ $p<0.001$ $\eta^2=0.28$	HC <> GAD-LE aff.	4.25	< 0.001 ***
	HC <> GAD-LE not aff.	3.34	0.029 *
	HC <> LGI1-LE aff.	2.29	0.353
	HC <> LGI1-LE not aff.	0.89	0.993
	HC <> CASPR2-LE aff.	4.04	0.003 **
	HC <> CASPR2-LE aff.	2.06	0.506
	HC <> HS aff.	4.74	< 0.001 ***
	HC <> HS not aff.	0.96	0.989
	GAD-LE aff. <> GAD-LE not aff.	-0.74	0.998
	GAD-LE aff. <> LGI1-LE aff.	0.17	1.000
	GAD-LE aff. <> LGI1-LE not aff.	-2.77	0.132
	GAD-LE aff. <> CASPR2-LE aff.	1.52	0.847
	GAD-LE aff. <> CASPR2-LE not aff.	-0.28	1.000
	GAD-LE aff. <> HS aff.	0.33	1.000
	GAD-LE aff <> HS not aff.	-2.72	0.149
	GAD-LE not aff. <> LGI1-LE aff.	0.59	1.000
	GAD-LE not aff. <> LGI1-LE not aff.	-2.35	0.318
	GAD-LE not aff. <> CASPR2-LE aff.	1.98	0.560
	GAD-LE not aff. <> CASPR2-LE not aff.	0.18	1.000
	GAD-LE not aff. <> HS aff.	1.08	0.976
	GAD-LE not aff. <> HS not aff.	-1.97	0.566
	LGI1-LE aff. <> LGI1-LE not aff.	-2.39	0.297
	LGI1-LE aff <> CASPR2-LE aff.	1.03	0.982
	LGI1-LE aff <> CASPR2-LE not aff.	-0.36	1.000
	LGI1-LE aff. <> HS aff.	0.02	1.000
	LGI1-LE aff. <> HS not aff.	-1.69	0.753
	LGI1-LE not aff <> CASPR2-LE aff.	3.35	0.015 *
	LGI1-LE not aff <> CASPR2-LE not aff.	2.15	0.441
	LGI1-LE not aff. <> HS aff.	2.95	0.082
	LGI1-LE not aff <> HS not aff	1.26	0.941
	CASPR2-LE aff. <> CASPR2-LE not aff.	-1.48	0.864
	CASPR2-LE aff. <>HS aff.	-1.32	0.925
	CASPR2-LE aff. <> HS not aff.	-3.21	0.042 *
	CASPR2-LE not aff. <> HS aff.	0.49	1.000
	CASPR2-LE not aff. <> HS not aff.	-1.40	0.896
	HS aff. <> HS not aff.	-3.09	0.058

aff.: affected hemisphere, FDC: fiber density and cross-section

Table S7. Analysis of variance and Tukey-Kramer post-hoc pairwise comparison of extracted superior longitudinal fascicle FDC fixel metrics across all groups adjusting for age and seizure freedom.

ANCOVA	Post-hoc tests (Tukey-Kramer)	*t*-value	*p*-value
$F(9,86)=2.71$	GAD-LE aff. <> GAD-LE not aff.	-0.71	0.997
$P=0.008$	GAD-LE aff. <> LGI1-LE aff.	-0.39	1.000
$\eta^2=0.22$	GAD-LE aff. <> LGI1-LE not aff.	-3.02	0.063
	GAD-LE aff. <> CASPR2-LE aff.	1.08	0.960
	GAD-LE aff. <> CASPR2-LE not aff.	-0.58	0.999
	GAD-LE aff. <> HS aff.	0.50	1.000
	GAD-LE aff <> HS not aff.	-2.38	0.265
	GAD-LE not aff. <> LGI1-LE aff.	-0.01	1.000
	GAD-LE not aff. <> LGI1-LE not aff.	-2.64	0.155
	GAD-LE not aff. <> CASPR2-LE aff.	1.50	0.805
	GAD-LE not aff. <> CASPR2-LE not aff.	-0.15	1.000
	GAD-LE not aff. <> HS aff.	1.21	0.927
	GAD-LE not aff. <> HS not aff	-1.67	0.707
	LGI1-LE aff. <> LGI1-LE not aff.	-2.28	0.317
	LGI1-LE aff <> CASPR2-LE aff.	1.20	0.929
	LGI1-LE aff <> CASPR2-LE not aff.	-0.11	1.000
	LGI1-LE aff. <> HS aff.	0.64	0.998
	LGI1-LE aff. <> HS not aff.	-0.86	0.989
	LGI1-LE not aff <> CASPR2-LE aff.	3.58	0.013 *
	LGI1-LE not aff <> CASPR2-LE not aff.	2.26	0.325
	LGI1-LE not aff. <> HS aff.	3.24	0.035 *
	LGI1-LE not aff <> HS not aff.	1.74	0.663
	CASPR2-LE aff. <> CASPR2-LE not aff.	-1.41	0.851
	CASPR2-LE aff. <>HS aff.	-0.77	0.994
	CASPR2-LE aff. <> HS not aff.	-2.50	0.211
	CASPR2-LE not aff. <> HS aff.	0.87	0.988
	CASPR2-LE not aff. <> HS not aff.	-0.85	0.990
	HS aff. <> HS not aff.	-2.95	0.076

aff.: affected hemisphere, FDC: fiber density and cross-section

Table S8. Statistical values of all correlation analyses between ROI-wise fixel metrics and memory performance. P-values are reported uncorrected and after applying a Holm-Bonferroni procedure to correct p-values for multiple comparisons.

ROI	hemisphere	metric	Verbal memory			Figural Memory		
			Pearson *R*	*p*	H.-B.-corr. *p*	Pearson *R*	*p*	H.-B.-corr. *p*
SLF	Affected	FD	-0.047	0.847	1.000	-0.092	0.707	1.000
		FC	-0.128	0.601	1.000	0.169	0.489	1.000
		FDC	0.013	0.958	1.000	0.112	0.649	1.000
	Unaffected	FD	0.009	0.971	1.000	0.159	0.516	1.000
		FC	-0.084	0.731	1.000	-0.090	0.715	1.000
		FDC	0.038	0.878	1.000	0.108	0.660	1.000
	L	FD	-0.268	0.267	1.000	0.026	0.917	1.000
		FC	0.213	0.380	1.000	0.215	0.377	1.000
		FDC	0.088	0.719	1.000	0.170	0.487	1.000
	R	FD	0.162	0.505	1.000	0.073	0.765	1.000
		FC	-0.418	0.075	1.000	-0.106	0.665	1.000
		FDC	-0.028	0.908	1.000	0.057	0.817	1.000
	2(L-R)/(L+R)	FD	-0.348	0.144	1.000	-0.032	0.898	1.000
		FC	0.684	0.001	0.048 *	0.301	0.210	1.000
		FDC	0.197	0.419	1.000	0.188	0.441	1.000
	(L+R)/2	FD	-0.011	0.971	1.000	0.064	0.515	1.000
		FC	-0.126	0.601	1.000	0.058	0.810	1.000
		FDC	0.029	0.906	1.000	0.117	0.632	1.000
Hippo-campus	affected		-0.136	0.577	1.000	0.363	0.126	1.000
	unaffected		-0.008	0.972	1.000	0.430	0.066	1.000
	L		-0.135	0.580	1.000	-0.228	0.347	1.000
	R		-0.116	0.638	1.000	0.018	0.943	1.000
	2(L-R)/(L+R)		<0.001	1.000	1.000	-0.212	0.383	1.000
	(L+R)/2		-0.150	0.539	1.000	-0.124	0.611	1.000

SLF: superior longitudinal fascicle, R: right, L: left, H.-B.-corr.: Holm-Bonferroni correceted values.

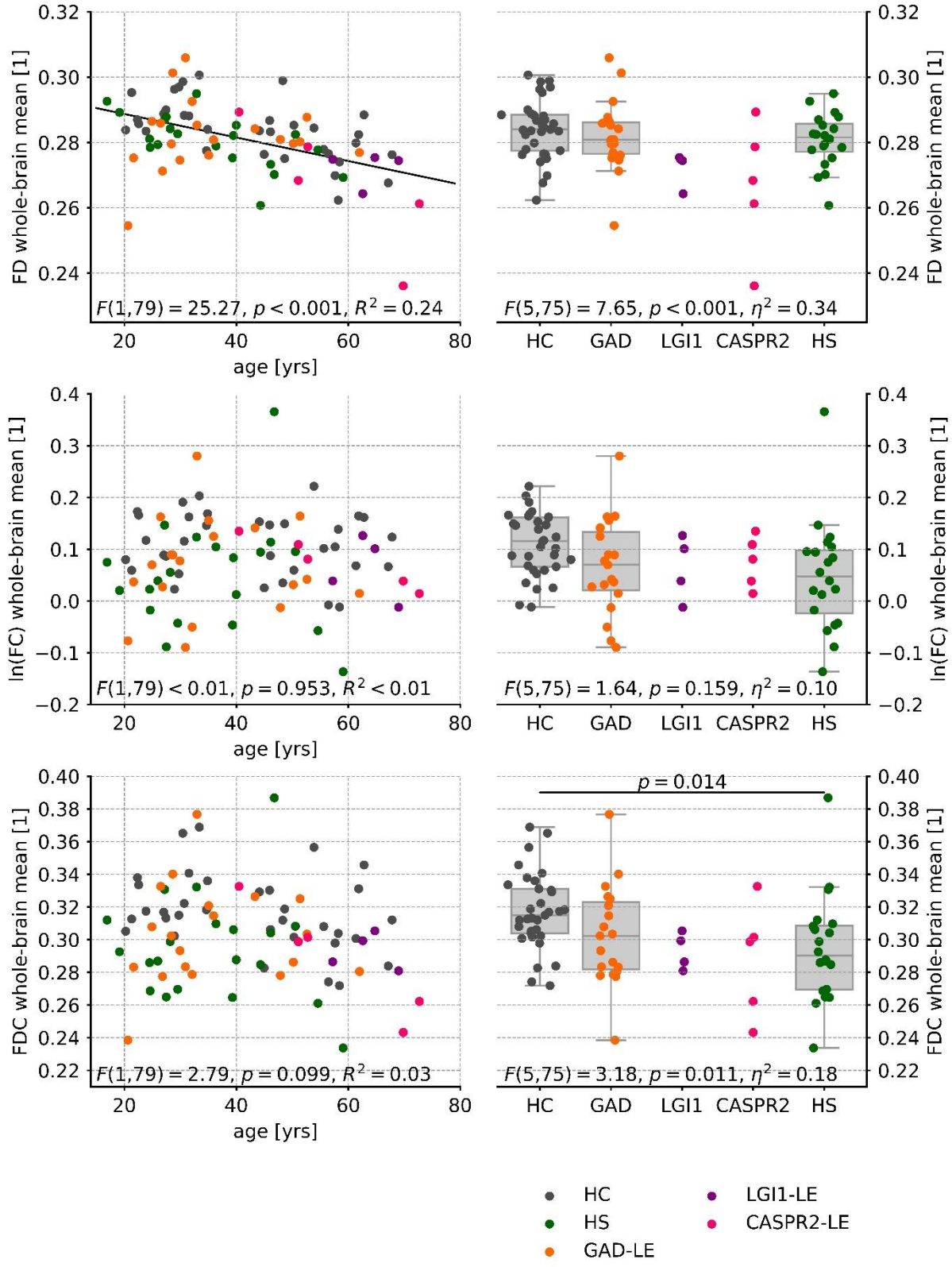

Figure S1. Whole-brain average ln(FC), FD and FDC values of all subjects over age including results of regression analysis (left) and grouped with results of ANCOVAs adjusting for age (right).

FD: fiber density, FC: fiber cross-section, FDC: fiber density and cross-section, yrs: years

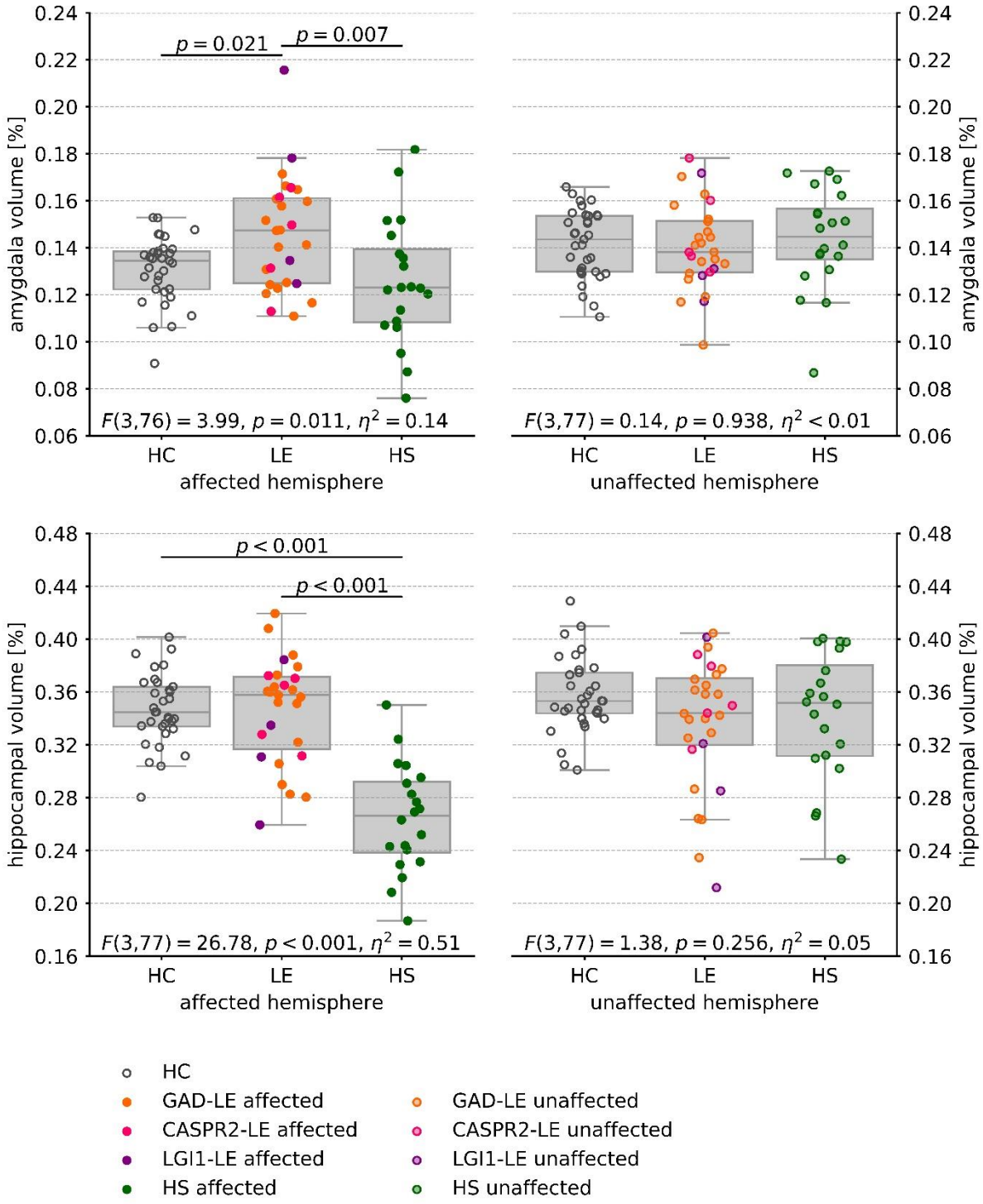

Figure S2. Whole-brain corrected amygdala (top) and hippocampal (bottom) volumes on the affected (left) and unaffected (right) hemisphere including results of ANCOVAs adjusting for age.

2.3 Originalpublikation in *Epilepsia*

Received: 29 June 2020 | Revised: 14 August 2020 | Accepted: 19 August 2020

DOI: 10.1111/epi.16691

BRIEF COMMUNICATION

Epilepsia®

Structural network topology in limbic encephalitis is associated with amygdala enlargement, memory performance and serostatus

Tobias Bauer[1] | **Bastian David**[1] | **Leon Ernst**[1] | **Albert J. Becker**[2] | **Juri-Alexander Witt**[1] | **Christoph Helmstaedter**[1] | **Jan Wagner**[3] | **Bernd Weber**[4] | **Christian E. Elger**[1] | **Rainer Surges**[1] | **Theodor Rüber**[1,5,6]

[1]Department of Epileptology, University Hospital Bonn, Germany

[2]Department of Neuropathology, University Hospital Bonn, Bonn, Germany

[3]Department of Neurology, University of Ulm and Universitäts- and Rehabilitationskliniken, Ulm, Germany

[4]Institute of Experimental Epileptology and Cognition Research, University Hospital Bonn, Bonn, Germany

[5]Department of Neurology, Epilepsy Center Frankfurt Rhine-Main, Goethe University Frankfurt, Frankfurt am Main, Germany

[6]Center for Personalized Translational Epilepsy Research, Goethe University Frankfurt, Frankfurt am Main, Germany

Correspondence
Theodor Rüber, Department of Epileptology, University Hospital Bonn, Venusberg-Campus 1, 53127 Bonn, Germany.
Email: theodor.rueber@ukbonn.de

Funding information
BONFOR research commission of the medical faculty of the University of Bonn: 2019-4-07; Verein zur Förderung der Epilepsieforschung; Else Kröner-Fresenius-Stiftung, Grant/Award Number: 2016-S2-05 and 2018-S2-01; "BonnNi Promotionskolleg Neuroimmunology" of the University of Bonn: 2016-S2-05 and 2018-S2-01

Abstract

Limbic encephalitis (LE) forms a spectrum of autoimmune diseases involving temporal lobe epilepsy and memory impairment. Imaging features of LE are known to depend on the associated antibody and to occur on the brain network level. However, first studies investigating brain networks in LE have either focused on one distinct antibody subgroup or on distinct anatomical regions. In this study, brain graphs of 17 LE patients with autoantibodies against glutamic acid decarboxylase 65 (GAD-LE), four LE patients with autoantibodies against leucine-rich glioma-inactivated 1, five LE patients with autoantibodies against contactin-associated protein-like 2, 26 age- and gender-matched healthy control subjects, and 20 epilepsy control patients with hippocampal sclerosis were constructed based on T1-weighted structural magnetic resonance imaging scans and diffusion tensor imaging. GAD-LE showed significantly altered global network topology in terms of integration and segregation as compared to healthy controls and patients with hippocampal sclerosis ($P < .01$, analysis of variance with Tukey-Kramer post hoc tests). Linear regression linked global network measures with amygdala volume and verbal memory performance ($P < .05$). Alterations of local network topology show serotype dependence in hippocampus, amygdala, insula, and various cortical regions. Our findings reveal serotype-dependent patterns of structural connectivity and prove the relevance of in silico network measures on clinical grounds.

KEYWORDS

brain graph, limbic encephalitis, structural connectivity, temporal lobe epilepsy

1 | INTRODUCTION

Limbic encephalitis (LE) comprises a spectrum of autoimmune brain diseases characterized by temporal lobe epilepsy and memory impairment.[1] Growing evidence suggests that the clinical picture of LE patients including their magnetic resonance imaging (MRI) signature largely depends on the associated antibody.[2,3] Antibodies against glutamic acid decarboxylase 65 (GAD), leucine-rich glioma-inactivated 1 (LGI1), and contactin-associated protein-like 2 (CASPR2) are most commonly found in LE patients.[1] Previous imaging research in the field of LE has mostly focused on identifying structural alterations of either mesiotemporal gray matter regions or white matter tracts.[2,3] Nevertheless, these approaches are limited in their ability to gain insights into pathological processes at a larger scale. To integrate previous findings into a global and functionally relevant framework, we chose to apply a structural connectivity network model.[8] In this framework, we investigated alterations of network topology across multiple scales and serogroups. Moreover, we aimed to establish a link between in silico measures of network topology and well-established clinical parameters in the field of LE, in particular mesiotemporal volumetry and memory performance. To discriminate structural network topology between LE patients and other patients with focal epilepsy, we include epilepsy patients with hippocampal sclerosis (HS) as a clinical control group. To draw a complete picture, we opted to retain LE patient groups with only few subjects, although this requires a less powerful nonparametric approach for group-level statistical comparisons.

2 | MATERIALS AND METHODS

2.1 | Study group

Three experimental and two control groups were contrasted. For the experimental groups, we prospectively included 17 patients with GAD-autoantibody–associated LE (GAD-LE), four patients with LGI1-autoantibody–associated LE (LGI1-LE), and five patients with CASPR2-autoantibody–associated LE (CASPR2-LE). All LE patients were diagnosed according to widely acknowledged diagnostic criteria and harbored serologically proven autoantibodies.[9] As it remains unclear whether LE is a predominantly unihemispheric process, we defined either one hemisphere as the predominantly affected hemisphere or both hemispheres as affected hemispheres according to a two-step classification scheme based on electroencephalographic data and mesiotemporal volumetry described elsewhere.[2,3,10] Twenty-six healthy control subjects from a preexisting in-house database were individually age- and gender-matched to the LE patients. Moreover, presurgical scans of 20 epilepsy patients with histologically confirmed HS who underwent selective amygdalohippocampectomy were included. In all patients, figural and verbal memory performance was assessed.[11,12] Memory parameters were standardized according to a conormalization sample of 488 healthy volunteers (mean = 100, SD = 10), applying a correction for age. See Table 1 and Supplementary material S1 for details. The study was approved by the internal review board of the University Hospital Bonn. All participants provided written informed consent.

TABLE 1 Demographic and clinical data of all patient and control groups

Group	GAD-LE	LGI1-LE	CASPR2-LE	HS	Controls	ANOVA, *P*
n	17	4	5	20	26	NA
Female, n (%)	10 (58.8)	2 (50.0)	0	11 (55.0)	12 (46.2)	.47
Lateralization, right/bilateral/left	4/5/8	2/1/1	1/2/2	4/0/16	NA	.25
Age, y	35.50 ± 11.72	63.37 ± 4.90	57.35 ± 13.57	38.84 ± 13.22	44.63 ± 15.62	<.001
Age at onset, y	31.75 ± 11.89	61.44 ± 4.60	54.39 ± 2.96	14.49 ± 11.86	NA	<.001
Disease duration, y	3.75 ± 2.56	1.92 ± 2.09	2.96 ± 1.31	24.35 ± 14.27	NA	<.001
Verbal memory	98.04 ± 11.35	80.31 ± 11.68	88.81 ± 6.00	84.26 ± 10.28	NA	.002
Figural memory	87.04 ± 14.97	74.33 ± 7.66	91.89 ± 11.06	83.42 ± 61.81	NA	.23
Seizure-free at study, n (%)	5 (29.4)	3 (75.0)	2 (40.0)	1 (5.0)	NA	.014

Note: Continuous data are given as arithmetic group means ± standard deviation. *P* values correspond to analyses of variance for continuous data or Pearson chi-square tests for categorical data. Verbal memory test: Verbal Learning and Memory Test[12]; figural memory test: *Diagnosticum für Cerebralschädigung*, revised[11]; memory parameters were standardized according to a conormalization sample of 488 healthy volunteers (mean = 100, standard deviation = 10), applying a correction for age. ANOVA, analysis of variance; CASPR2-LE, CASPR2-autoantibody–associated LE; GAD-LE, GAD-autoantibody–associated LE; HS, hippocampal sclerosis; LE, limbic encephalitis; LGI1-LE, LGI1-autoantibody–associated LE; NA, not applicable.

2.2 | Image acquisition

All subjects underwent diffusion tensor imaging with 60 directions and T1-weighted structural imaging in Bonn using a 3T MRI scanner (Magnetom Trio, Siemens Healthineers). Due to a scanner update in 2014, two different acquisition protocols and head coils were used. Details on acquisition parameters can be found in Supplementary Data S2. We accounted for this factor by introducing *scanner update* as an independent variable in the statistical models.

2.3 | Image preprocessing and network construction

Surface reconstruction and volumetric segmentation of T1 structural images were performed using FreeSurfer (v6.0, https://surfer.nmr.mgh.harvard.edu/); 84 cortical and subcortical regions of interest (ROIs) of the Desikan-Killiany atlas were used as nodes in the structural connectivity graph. Preprocessing of diffusion-weighted images was performed as described elsewhere[3]; streamline and network reconstruction was performed using the MRtrix3 toolbox (http://www.mrtrix.org). Edge weights were derived as the streamline count between each pair of ROIs and normalized to [0,1] on an intrasubject level.

2.4 | Global network analysis

Using the Brain Connectivity Toolbox, the clustering coefficient as a measure of segregation and the characteristic path length as a measure of integration were calculated for all individuals.[8] Statistical comparisons between groups were performed in two steps. First, we tested for differences between GAD-LE, HS, and healthy controls using a one-way analysis of variance adjusting for age and scanner update with post hoc Tukey-Kramer pairwise tests. Second, to include LGI1-LE and CASPR2-LE groups, we tested for differences across all groups using a Kruskal-Wallis test with post hoc Dunn pairwise tests. A Benjamini-Hochberg procedure was applied to correct for multiple comparisons. Furthermore, regression analyses to predict amygdala volumes and memory performance based on global network measures across all LE serogroups were performed using linear regression including scanner update and individual intercepts for each serogroup as independent variables.

2.5 | Local network analysis

Differences in node strength were tested for every node across all groups using Kruskal-Wallis tests with post hoc Dunn pairwise tests and Benjamini-Hochberg correction for multiple comparisons. In the healthy control group, node strengths were pooled across both hemispheres. Unpaired *t* tests adjusting for age and scanner update were used to test for differences of connection weights between groups by means of network-based statistics including nonparametric permutation testing with 5000 permutations to correct for familywise error rate (FWE).[13]

3 | RESULTS

3.1 | Global network topology

An analysis of variance revealed significant group differences between GAD-LE, HS patients, and healthy controls in clustering coefficient ($F_{4, 58} = 4.98$, $P = .002$) and characteristic path length ($F_{4, 58} = 3.66$, $P = .010$). A Kruskal-Wallis test confirmed significant group differences across all groups in clustering coefficient ($\chi^2_4 = 15.78$, $P = .003$) and characteristic path length ($\chi^2_4 = 10.83$, $P = .03$). Post hoc pairwise tests revealed significantly lower clustering and a higher characteristic path length in GAD-LE as compared to HS patients and healthy controls at $P < .01$. Post hoc tests involving LGI1-LE and CASPR2-LE did not reveal any significant group differences at $P < .05$. By means of linear regression, the amygdala volume on the predominantly affected hemisphere ($F_{4, 21} = 3.09$, $P = .038$, $R^2 = .31$) and verbal memory performance ($F_{4, 21} = 4.39$, $P = .010$, $R^2 = .45$) were predicted by the clustering coefficient. The amygdala volume on the unaffected hemisphere, the amygdala volume averaged across both hemispheres, and figural memory performance were not significantly predicted by either clustering coefficient or characteristic path length at $P < .05$ (see Figure 1A,B and Figure S3).

3.2 | Local network topology

Comparing connection weights between GAD-LE and healthy controls, the network-based statistics approach detected 11 connections with significantly (FWE-corrected $P < .05$) lower weights across both hemispheres. When contrasting HS patients and healthy controls, only the connection between both lateral orbitofrontal gyri showed significantly lower weight in HS patients than healthy controls. All other contrasts did not reveal any significantly altered connections at FWE-corrected $P < .05$ (see Figure 1B and Figure S3B). Comparing node strengths across all groups, global Kruskal-Wallis tests revealed significant (false discovery rate–corrected $P < .05$) group differences for 18 nodes, including hippocampus, amygdala, and insula (Figure 1C and Figure S4C).

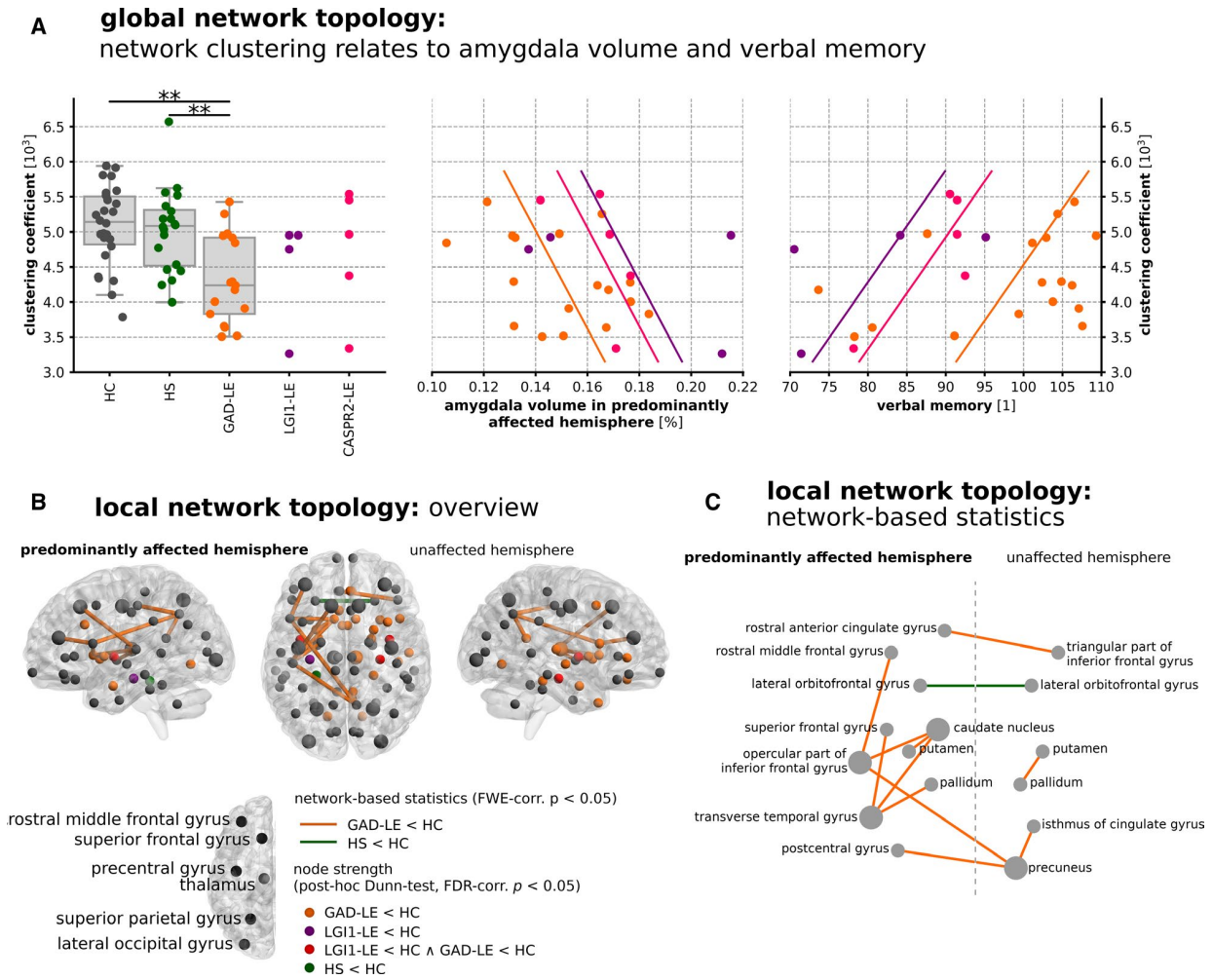

FIGURE 1 Overview of alterations of local and global network topology. A, Left: Group-level pairwise comparisons revealed a significantly lower clustering in GAD-autoantibody–associated limbic encephalitis (GAD-LE) as compared to healthy controls and patients with hippocampal sclerosis. Middle and right: Across all LE groups, amygdala volume in the predominantly affected hemisphere (middle) and verbal memory performance (right) are predicted by the clustering coefficient and individual group intercepts using linear regression. B, Overview of local network topology alterations. Colored edges denote significantly reduced connection weights by means of network-based statistics at FWE-corrected $P < .05$; colored nodes show significantly reduced node strength. Larger-appearing nodes are top 15% hubs according to node strength. C, The network-based statistics approach detected 11 connections with significantly (FWE-corrected $P < .05$) lower weights in GAD-LE as compared to controls (orange lines). When contrasting hippocampal sclerosis patients and healthy controls, only the connection between both lateral orbitofrontal gyri showed significantly lower connection weight (green line). $^{**}P < .01$ (Tukey-Kramer post hoc test). CASPR2-LE, CASPR2-autoantibody–associated LE; FWE, familywise error rate; HC, healthy controls; HS, hippocampal sclerosis; LGI1-LE, LGI1-autoantibody–associated LE

4 | DISCUSSION

In the present study, we describe altered network topology in three distinct LE serogroups and aim to relate our findings to their clinical and cognitive profiles. Although the interpretation of altered network topology in a clinical context remains challenging, mesiotemporal volumetry is a clinically recognized marker for diagnostics and follow-up monitoring in the field of autoimmune LE.[2,4] Here, we show that lower clustering in LE patients is associated with greater amygdala enlargement in the predominantly affected hemisphere. Beyond imaging characteristics, memory impairment ranks among the most relevant cognitive deficits associated with LE.[14] Although figural memory was independent of network topology, lower clustering was predictive for verbal memory impairment. This finding confirms a previously reported association between disease severity and verbal memory performance, which was related to structural integrity of the left hippocampus. This association was not found for figural memory performance.[14]

With regard to local network topology, our results reflect previously described reduced interhippocampal and hippocampocortical functional connectivity in LGI1-LE.[14,15] This

is further backed by our data regarding reduced hippocampal node centrality in LGI1-LE and GAD-LE. However, our finding of reduced insular node centrality in GAD-LE and LGI1-LE is novel and supports previous reports indicating a possible involvement of the insula in GAD-LE and LGI1-LE.[16,17] Nevertheless, the pathomechanism of this finding remains a topic for future study. In comparison to HS patients, GAD-LE shows more widespread alterations of local network topology. Whereas in HS patients reduced node strengths are restricted to the predominantly affected hippocampus and both parahippocampal gyri, we found 18 anatomical regions with reduced node strength across both hemispheres in GAD-LE. Notably, in 10 nodes this reduction is significant in comparison to HS patients. In contrast to HS patients, reduced node strengths as well as reduced connection weights in GAD-LE largely cover bilateral subcortical gray matter regions, which may be associated with previously reported basal ganglia hypermetabolism in these patients.[18]

Altogether, our findings underline the concept that GAD-LE is a disease entity involving a variety of anatomical structures across the entire brain and beyond the mesial temporal lobe.[3,5] With regard to LGI1-LE and as previously hypothesized, in contrast, our results point toward a less widespread pathology with a clear focus on mesiotemporal structures.[5,6] The absence of significant alterations of network topology in CASPR2-LE may be grounded in insufficient statistical power due to the small sample size on the one hand, and on the other hand, previous literature has reported only subtle MRI findings in CASPR2-LE.[6]

Three aspects limit the explanatory power of the present study. First, small sample sizes in the LGI1-LE and CASPR2-LE groups made the use of low-power nonparametric statistical approaches unavoidable. Moderate group-level effects might therefore become apparent with increasing statistical power in a larger study cohort. Second, transversal study designs like the present one are challenged by therapeutic interventions. Because different LE serogroups are known to differ in their response to immunotherapy, and patients may be captured at different disease stages, immunotherapy interaction with effects of pathology are unobserved in a transversal statistical approach. Third and last, the biological underpinnings of altered network topology remain speculative and require further investigation. Nonetheless, this study pioneers in linking observed network alterations across different scales and serological groups to well-established clinical parameters in the field of LE.

ACKNOWLEDGMENTS

T.B. and L.E. received support from the BonnNi Promotionskolleg Neuroimmunology of the University of Bonn and the Else-Kröner-Fresenius Stiftung (grants 2018-S2-01 and 2016-S2-05). T.R. and T.B. were supported by the BONFOR research commission of the medical faculty of the University of Bonn. This work was supported by the Verein zur Förderung der Epilepsieforschung. Open access funding enabled and organized by Projekt DEAL.

CONFLICT OF INTEREST

C.E.E. has received fees as a speaker or consultant from UCB Pharma, Desitin, Bial, and Eisai. R.S. has received fees as a speaker or consultant from Bial, Cyberonics, Desitin, Eisai, LivaNova, Novartis, and UCB Pharma. None of the other authors has any conflict of interest to disclose.

ETHICAL PUBLICATION STATEMENT

We confirm that we have read the Journal's position on issues involved in ethical publication and affirm that this report is consistent with those guidelines.

ORCID

Tobias Bauer https://orcid.org/0000-0002-0555-6214
Bastian David https://orcid.org/0000-0002-0146-0629
Leon Ernst https://orcid.org/0000-0001-8146-4234
Albert J. Becker https://orcid.org/0000-0003-2661-3705
Juri-Alexander Witt https://orcid.org/0000-0001-5640-2592
Christoph Helmstaedter https://orcid.org/0000-0002-6608-6244
Jan Wagner https://orcid.org/0000-0002-0459-8885
Bernd Weber https://orcid.org/0000-0002-7811-9605
Christian E. Elger https://orcid.org/0000-0002-2531-6701
Rainer Surges https://orcid.org/0000-0002-3177-8582
Theodor Rüber https://orcid.org/0000-0002-6180-7671

REFERENCES

1. Dubey D, Pittock SJ, Kelly CR, McKeon A, Lopez-Chiriboga AS, Lennon VA, et al. Autoimmune encephalitis epidemiology and a comparison to infectious encephalitis. Ann Neurol. 2018;83(1):166–77.
2. Ernst L, David B, Gaubatz J, Domínguez-Narciso I, Lüchters G, Becker AJ, et al. Volumetry of mesiotemporal structures reflects serostatus in patients with limbic encephalitis. Am J Neuroradiol. 2019;40(12):2081–9.
3. Bauer T, Ernst L, David B, Becker AJ, Wagner J, Witt J-A, et al. Fixel-based analysis links white matter characteristics, serostatus and clinical features in limbic encephalitis. Neuroimage Clin. 2020;27:102289.
4. Wagner J, Witt J-A, Helmstaedter C, Malter MP, Weber B, Elger CE. Automated volumetry of the mesiotemporal structures in antibody-associated limbic encephalitis. J Neurol Neurosurg Psychiatry. 2015;86(7):735–42.
5. Wagner J, Schoene-Bake JC, Witt JA, Helmstaedter C, Malter MP, Stoecker W, et al. Distinct white matter integrity in glutamic acid decarboxylase and voltage-gated potassium channel-complex antibody-associated limbic encephalitis. Epilepsia. 2016;57(3):475–83.

6. Heine J, Prüss H, Bartsch T, Ploner CJ, Paul F, Finke C. Imaging of autoimmune encephalitis—relevance for clinical practice and hippocampal function. Neuroscience. 2015;309:68–83.
7. Bien CG, Bien CI, Dogan Onugoren M, De Simoni D, Eigler V, Haensch C-A, et al. Routine diagnostics for neural antibodies, clinical correlates, treatment and functional outcome. J Neurol. 2020;267(7):2101–14.
8. Rubinov M, Sporns O. Complex network measures of brain connectivity: uses and interpretations. Neuroimage. 2010;52(3):1059–69.
9. Graus F, Titulaer MJ, Balu R, Benseler S, Bien CG, Cellucci T, et al. A clinical approach to diagnosis of autoimmune encephalitis. Lancet Neurol. 2016;15(4):391–404.
10. Navarro V, Kas A, Apartis E, Chami L, Rogemond V, Levy P, et al. Motor cortex and hippocampus are the two main cortical targets in LGI1-antibody encephalitis. Brain. 2016;139(4):1079–93.
11. Helmstaedter C, Pohl C, Hufnagel A, Elger CE. Visual learning deficits in nonresected patients with right temporal lobe epilepsy. Cortex. 1991;27(4):547–55.
12. Helmstaedter C, Durwen HF. The Verbal Learning and Retention Test. A useful and differentiated tool in evaluating verbal memory performance. Schweiz Arch Neurol Psychiatr (1985). 1990;141(1):21–30. [in German].
13. Zalesky A, Fornito A, Bullmore ET. Network-based statistic: identifying differences in brain networks. Neuroimage. 2010;53(4):1197–207.
14. Loane C, Argyropoulos GPD, Roca-Fernández A, Lage C, Sheerin F, Ahmed S, et al. Hippocampal network abnormalities explain amnesia after VGKCC-Ab related autoimmune limbic encephalitis. J Neurol Neurosurg Psychiatry. 2019;90:965–74.
15. Heine J, Prüss H, Kopp UA, Wegner F, Then Bergh F, Münte T, et al. Beyond the limbic system: disruption and functional compensation of large-scale brain networks in patients with anti-LGI1 encephalitis. J Neurol Neurosurg Psychiatry. 2018;89(11):1191–9.
16. Bose G, Zwicker JC, Sitwell LD, Osman N, Fantaneanu TA. Anti-LGI1 limbic encephalitis presenting as an expanding insular lesion. Can J Neurol Sci. 2019;46(6):770–2.
17. Falip M, Rodriguez-Bel L, Castañer S, Sala-Padró J, Miro J, Jaraba S, et al. Hippocampus and insula are targets in epileptic patients with glutamic acid decarboxylase antibodies. Front Neurol. 2019;9:1143.
18. Tripathi M, Tripathi M, Roy SG, Parida GK, Ihtisham K, Dash D, et al. Metabolic topography of autoimmune non-paraneoplastic encephalitis. Neuroradiology. 2018;60(2):189–98.

SUPPORTING INFORMATION

Additional supporting information may be found online in the Supporting Information section.

How to cite this article: Bauer T, David B, Ernst L, et al. Structural network topology in limbic encephalitis is associated with amygdala enlargement, memory performance and serostatus. *Epilepsia*. 2020;61:e140–e145. https://doi.org/10.1111/epi.16691

2.4 Supplementary Material zur Originalpublikation in *Epilepsia*

SUPPLEMENTARY MATERIAL

S1 Patient characteristics

Table S1A. Clinical data of all GAD-LE patients.

ID	Sex	Lateral-ization	Age at onset, yrs	Age at study, yrs	Ab at study, U/ml	Initial IT	IT at study	Verbal memory at study	Figural memory at study
1	F	L	45-50	50-55	NA	MPR pulse	None	88	92
2	F	R + L	15-20	20-25	>1000	MPR pulse	MMF	105	73
3	M	R + L	25-30	25-30	>1000	MPR pulse	None	100	104
4	F	R	30-35	30-35	>1000	IVIG	None	103	102
5	F	R + L	20-25	25-30	>1000	IVIG	PR oral	109	97
6	F	R	15-20	20-30	0	MPR pulse	None	85	66
7	M	L	25-30	35-40	>1000	AZA	None	107	108
8	M	L	40-45	40-45	>1000	PR oral	MPR pulse+ PR oral	92	106
9	F	L	45-50	50-55	>1000	MPR pulse	None	107	84
10	F	L	25-30	25-30	>1000	MPR pulse	MPR pulse	108	104
11	M	R	20-25	20-25	>1000	MPR pulse	MPR pulse	101	92
12	M	L	30-35	30-35	>1000	PR oral	None	107	101
13	M	L	35-40	35-40	>1000	MPR pulse	None	103	84
14	F	R + L	55-60	60-65	>1000	MPR pulse	None	102	67
15	M	R	15-20	20-25	NA	MPR pulse	MPR Pulse + BAS	80	67
16	F	L	40-45	45-50	>1000	MPR pulse	None	74	67
17	F	L	25-30	30-35	0	MPR pulse	MPR pulse	101	77

M: male, F: female, R: right, L: left, NA: not available, yrs: years, Ab: serum antibody concentration, IT: immunotherapy, MPR: methylprednisolone, IVIG: intravenous immunoglobulin, PR: prednisolone, AZA: azathioprine, MMF: mycophenolate-mofetil, BAS: Basiliximab

Table S1B. Clinical data of all LGI1-LE patients.

ID	Sex	Lateral-ization	Age at onset, yrs	Age at study, yrs	Ab at study	Initial IT	IT at study	Verbal memory at study	Figural memory at study
1	M	R	65-70	65-70	NA	MPR pulse	None	71	76
2	M	L	55-60	60-65	NA	MPR pulse	None	96	83
3	F	L	60-65	60-65	<1:10	MPR pulse	None	64	59
4	F	R	55-60	55-60	1:10	PR oral	MPR pulse	86	73

M: male, F: female, R: right, L: left, NA: not available, yrs: years, Ab: serum antibody concentration, IT: immunotherapy, MPR: methylprednisolone, PR: prednisolone

Table S1C. Clinical data of all CASPR2-LE patients.

ID	Sex	Lateral-ization	Age at onset, yrs	Age at study, yrs	Ab at study	Initial IT	IT at study	Verbal memory at study	Figural memory at study
1	M	L	65-70	75-80	NA	MPR pulse	None	93	82
2	M	L	35-40	40-45	1:1000	MPR pulse	PR oral+ MMF	92	107
3	M	R	65-70	70-75	<1:10	MPR pulse	None	81	96
4	M	R + L	45-50	50-55	1:3200	MPR pulse	None	93	87
5	M	L	45-50	50-55	1:3200	MPR pulse	MPR pulse	90	84

M: male, F: female, R: right, L: left, NA: not available, yrs: years, Ab: serum antibody concentration, IT: immunotherapy, MPR: methylprednisolone, PR: prednisolone, MMF: mycophenolate-mofetil

Table S1D. Clinical data of all hippocampal sclerosis patients.

ID	Sex	Side of HS	Age at onset ,yrs	Age at study, yrs
1	M	R	5-10	25-30
2	F	L + R	20-25	25-30
3	F	L	20-25	35-40
4	F	R	<5	15-20
5	M	R	10-15	15-20
6	F	R	20-25	35-40
7	M	L	10-15	30-35
8	M	L	5-10	40-45
9	M	L	5-10	25-30
10	F	L	15-20	20-25
11	F	L	10-15	50-55
12	F	L	15-20	25-30
13	M	L	5-10	35-40
14	F	L	20-25	25-30
15	F	R	10-15	20-25
16	F	L	30-35	40-45
17	F	R	10-15	55-60
18	M	R	20-25	50-55
19	M	L + R	30-35	45-50
20	M	L	30-35	45-60

M: male, F: female, R: right, L: left, HS: hippocampal sclerosis

S2 Image acquisition parameters

T1-weighted structural imaging and diffusion tensor imaging (DTI) for all subjects was performed at the Life & Brain Center in Bonn using a 3 Tesla MRI-Scanner (Magnetom Trio, Siemens Healthineers, Erlangen, Germany). Diffusion-weighted data were acquired using single shot spin-echo echo-planar imaging. Due to a scanner update in early 2014, two different acquisition protocols were used. DTI Parameters before the update were TR = 12 s, TE = 100 ms using an eight channel headcoil, parameters after the update were TR = 9 s, TE = 87 ms using a 32 channel headcoil. Both protocols acquired 72 axial slices, matrix 128 × 128 pixel, voxel size 1.72 mm × 1.72 mm × 1.7 mm and in both protocols, diffusion weighting was isotropically distributed along 60 directions at b = 1000 s · mm^{-2}. Six images with b = 0 were acquired initially and following each series of ten diffusion-weighted images. T1-weighted images were acquired using MPRAGE sequences. Scanning parameter before the update were TR = 1570 ms, TE = 3.42 ms, flip angle 15°, matrix 256 × 256 pixel, .voxel size 1.0 mm × 1.0 mm × 1.0 mm, parameters after the update were TR = 1660 ms, TE = 2.54 ms, flip angle 9°, matrix 320 × 320 pixel, voxel size 0.8 mm × 0.8 mm× 0.8 mm.

S3 Overview over alterations of global network topology

(A) Left: Group-level pairwise comparisons revealed a significantly lower clustering in GAD-LE as compared to healthy controls and patients with hippocampal sclerosis. Middle and right: Across all LE groups, amygdala volume on the affected hemisphere (middle) and verbal memory performance (right) are predicted by the clustering coefficient and individual group intercepts using linear regression. (B) Group-level pairwise comparisons revealed a significantly lower local efficiency and transitivity, two alternative measures of network segregation, in GAD-LE as compared to healthy controls and patients with hippocampal sclerosis. (C) Group-level pairwise comparisons revealed a significantly higher characteristic path length in GAD-LE as compared to healthy controls and patients with hippocampal sclerosis. Global efficiency did not differ significantly between groups.

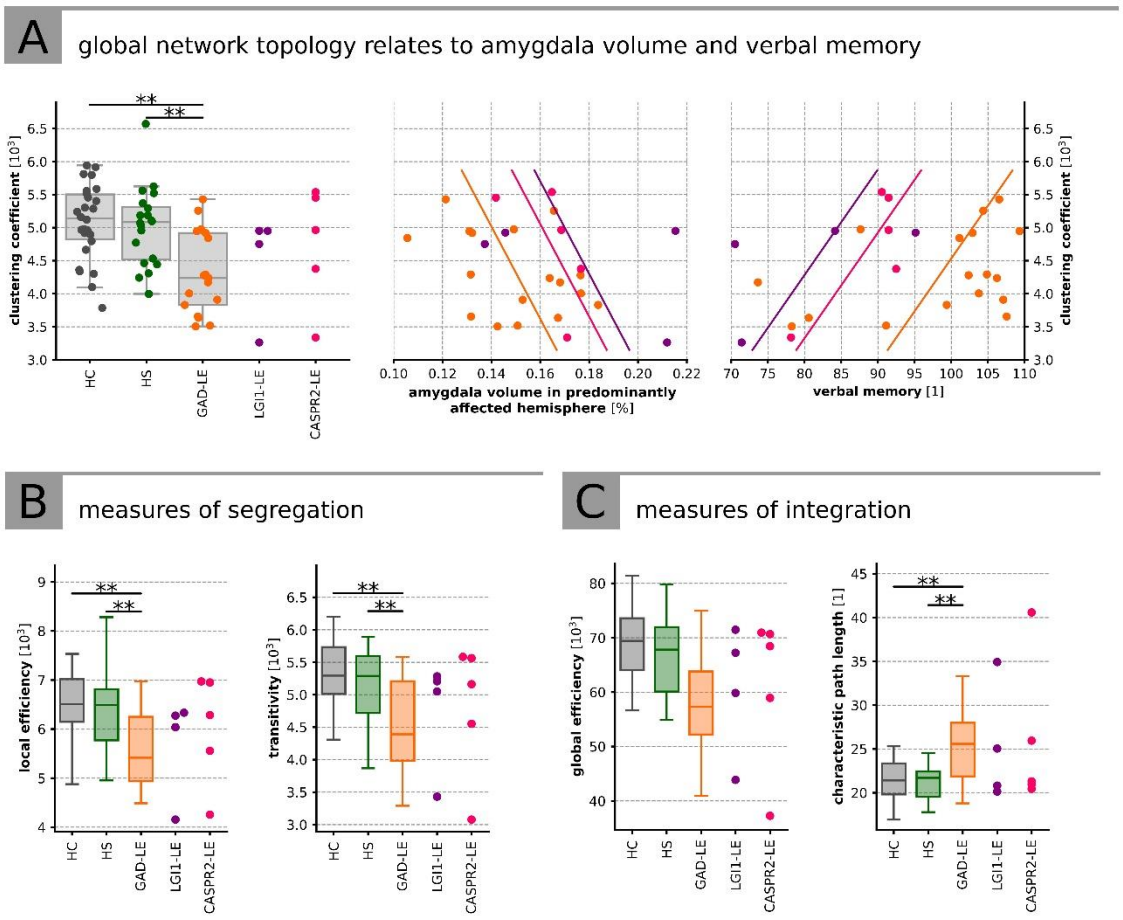

S4 Overview over alterations of local network topology

(A) Overview over alterations of local network topology in terms of nodal strength and connection weights. (B) The network-based statistics approach detected 11 connections with significantly (FWE-corrected $p < 0.05$) lower weights in GAD-LE as compared to controls (orange lines). When contrasting hippocampal sclerosis patients and healthy controls, only the connection between both lateral orbitofrontal gyri showed significantly lower connection weight (green line). (C) Comparing node strengths across all groups, global Kruskal-Wallis tests revealed significant (FDR-corrected $p < 0.05$) group differences for 18 nodes.

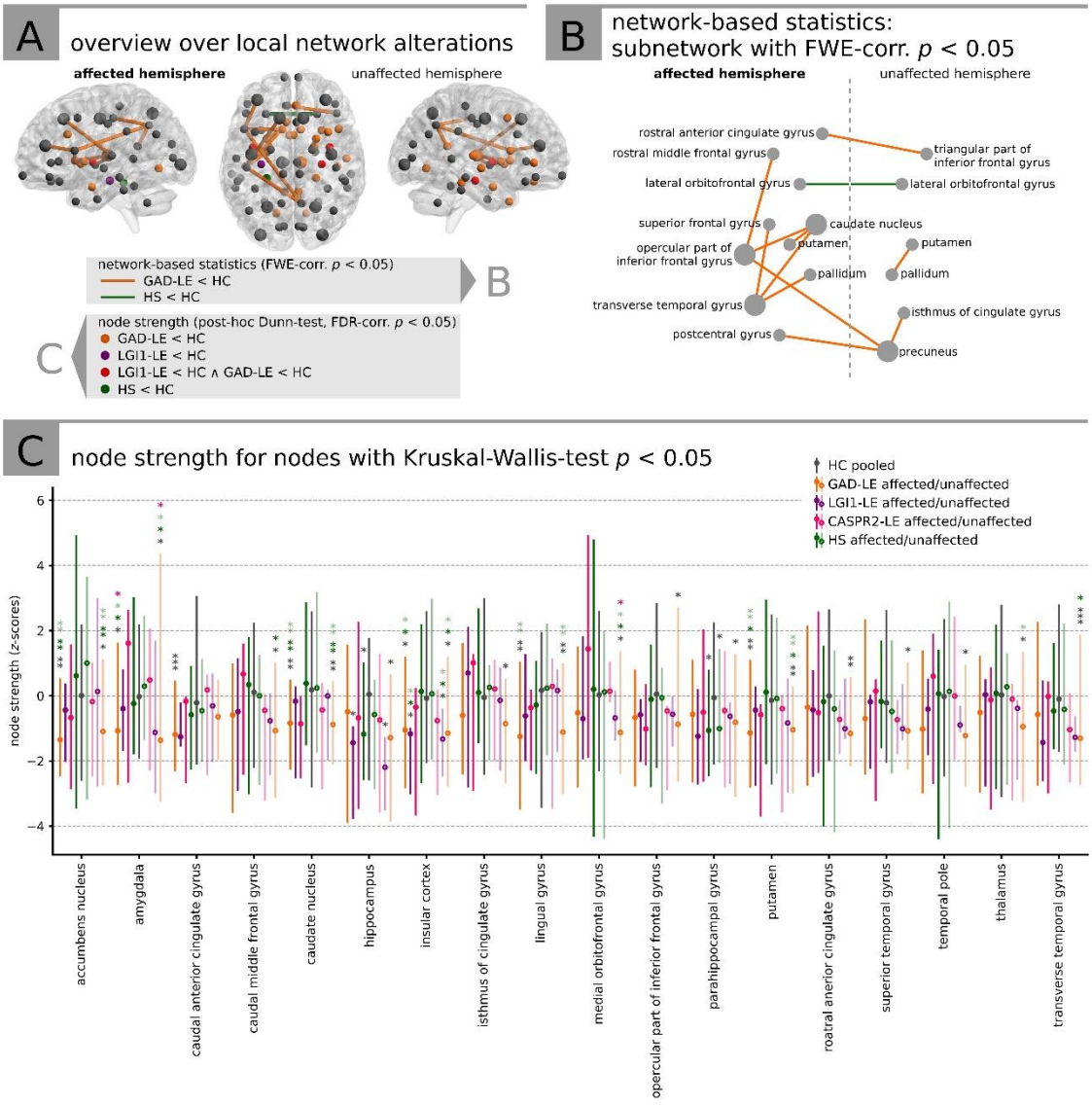

3. Danksagung

Mein erster Dank gilt meinem Doktorvater, Herrn Priv.-Doz. Dr. Theodor Rüber. Ich bin ihm sehr dankbar für die Chancen, die er mir eröffnet hat sowie für das Wissen über die Forschungswelt, das er mir vermittelte und welches es mir ermöglicht, diese Chancen zu nutzen. Seine ansteckende Begeisterung für unsere gemeinsame Forschung, sein vorausschauendes Mitdenken meines Weges und seine freundschaftliche Supervision machen mich ihm sehr verbunden.

Für die stetige Förderung und mentorielle Begleitung meiner wissenschaftlichen Arbeit danke ich Herrn Prof. Dr. Rainer Surges, Herrn Prof. em. Dr. Christian Elger und Herrn Prof. Dr. Albert Becker. Ihre Begleitung auf dem Einstieg in die akademische Welt weiß ich sehr zu schätzen.

Meinen aktuellen und ehemaligen Kolleg:innen in der Arbeitsgruppe für translationale Neurobildgebung, Felix Bitzer, Dr. Bastian David, Dr. Leon Ernst, Laura Fischbach, Antonia Harms, Johannes Reiter, Dr. Martin Schidlowski, Freya Schulte und Lennart Walger, danke ich für das konstruktive Miteinander. Der freundschaftliche Austausch war mir stets Inspiration und Motivation.

Den Referent:innen der Bischöflichen Studienförderung Cusanuswerk danke ich für die finanziellen Freiräume und die ideelle Förderung, wie sie eine Universität nicht zu leisten vermag.

Meiner Familie gilt mein größter Dank. Durch ihre liebevolle und unermüdliche Förderung, gepaart mit maximalen Freiräumen und größtmöglichem Vertrauen, haben insbesondere meine Eltern meinen bisherigen Werdegang entscheidend getragen. Meiner Frau Franziska danke ich von Herzen für ihre bedingungslose Unterstützung in allen Lebenslagen.